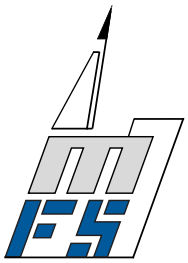

UNIVERSITE DE STRASBOURG

Ecole Doctorale Mathématiques, Sciences de l'Information et de l'Ingénieur

Institut de Mécanique des Fluides et des Solides

THESE

Présentée pour obtenir le grade de:

Docteur de l'Université de Strasbourg

Spécialité: Mécanique des matériaux

Par

MOSSI IDRISSA Abdoul Kader

Modeling and simulation of the mechanical behavior under finite strains of filled elastomers as function of their microstructure

Soutenue le 20 Juin 2011

Membres du jury:

Rapporteur:	**Pr Moussa NAÏT-ABDELAZIZ**	**Polytech Lille**
Rapporteur:	**Dr Laurent GORNET**	**Ecole centrale de Nantes**
Examinateur:	**Pr Jean Louis HALARY**	**ESPCI ParisTech**
Examinateur:	**Dr David RUCH**	**CRP Henri Tudor, Luxembourg**
Examinateur:	**Pr Stanislav PATLAZHAN**	**SICP, Moscou, Russie**
Co-directeur de thèse:	**Pr Yves REMOND**	**Université de Strasbourg**
Directeur de thèse:	**Pr Saïd AHZI**	**Université de Strasbourg**

For a wonderful woman, my grandmother Zeinabou Issa.

Remerciements

Cette thèse de doctorat a été réalisée à l'Institut de Mécanique des Fluides et des Solides (IMFS) de l'université de Strasbourg avec un financement du Ministère de l'Education Nationale, de l'Enseignement Supérieur et de la Recherche. Je tiens alors à remercier son directeur, professeur Yves REMOND pour son accueille chaleureux au sein du laboratoire.

Je tiens à exprimer ma profonde gratitude à mes directeurs de thèse les professeurs Saïd AHZI et Yves REMOND pour leur disponibilité et leurs nombreux précieux conseils tout au long de cette thèse, qui ont permit la concrétisation de ce travail.

J'adresse un grand merci au professeur Stanislav PATLAZHAN de Semenov Institute of Chemical Physics de Moscou pour sa disponibilité et ses conseils scientifiques.

J'adresse toute ma reconnaissance aux professeurs Laurent GORNET, Moussa NAÏT-ABDELAZIZ pour avoir accepté de rapporter ce travail, ainsi qu'aux examinateurs, professeur Jean Louis HALARY, professeur Stanislav PATLAZHAN et au docteur David RUCH.

Je remercie l'ensemble des membres de l'équipe lois de comportement et microstructure: Siham M'GUIL, Nadia BAHLOULI, Joao Pedro CORREIA DE MAGALHAES, Ahmed MAKRADI, Rodrigue MATADI BOUMBIMBA, Amin MIKDAM, Lyazib BOUHALA, Muhammad Ali SIDDIQUI, Kamel HIZOUM, Olivier GUEGEN, Zhor NIBENNAOUNE, Kui WANG, Wei WEN, Rania ABDEL RAHMAN MAHMOUD, Safa LHADI, Nicolas BHART, Mathieu NIERENBERGER; ainsi que le personnel administratif et technique de l'IMFS, Catherine HELMERINGER, Sylvie VILAIN, Daniel BITINGER, ESSA Michael, Abdelkrim AZIZI, et Johary RASAMMANANA.

Enfin, à ma famille, mes amis et à l'ensemble de la communauté nigérienne à Strasbourg pour leur soutien moral et tout ceux qui ont participé de près ou de loin à la réalisation de ce travail; qu'ils trouvent ici ma gratitude.

Résumé

Aujourd'hui, notre quotidien fait intervenir l'usage d'innombrables matériaux performants et adaptés à nos besoins, comme les alliages de fer, les céramiques, les polymères. Les élastomères qui sont des matériaux caoutchouteux synthétiques ou naturels appartiennent à cette dernière famille. Au fil des temps, le caoutchouc a connu plusieurs révolutions dans sa fabrication, dont la principale est celle de 1839 avec Charles Goodyear. Il a mit au point le procédé de vulcanisation qui consiste en un branchement des chaînes par des liaisons covalentes.

La mise sous contrainte d'un élastomère provoque des changements mécaniques et optiques. Les changements mécaniques sont en général formulés par une relation entre la contrainte et la déformation. Ceux optiques sont dus à l'anisotropie, ils se caractérisent par la différence de propagation de la lumière dans les différentes directions du matériau. Cette anisotropie peut être mesurée par la biréfringence qui est la différence entre deux indices de réfraction de deux directions principales.

Plusieurs travaux ont été effectués en se basant généralement sur des méthodes Gaussiennes et non Gaussiennes pour déterminer les variations de la contrainte et de la biréfringence dans les polymères en fonction de la déformation. Elles permettent aussi d'obtenir une relation entre la contrainte et la biréfringence comme formulé par **Treloar (1947)** pour le cas Gaussien et **Arruda et Przybylo (1995)** pour le modèle non Gaussien à huit-chaînes. Le second est mieux adapté aux cas expérimentaux car il prend en compte l'effet de la non linéarité pour les grandes déformations. Quant au premier, il n'est valable que dans les cas de déformation modérée ($\varepsilon < 1$).

Actuellement, deux modèles sont très utilisés pour prédire le comportement mécanique des élastomères en fonction de la déformation: le modèle de Gent et celui de huit-chaînes d'Arruda et Boyce. Par contre, seul le second a été étendu à la biréfringence pour avoir une relation entre la biréfringence et la contrainte tout au long de la déformation dans les élastomères. Raison pour laquelle dans cette étude, nous avons formulé une relation entre la différence de deux contraintes principales quelconques du modèle de Gent en trois dimensions avec la biréfringence sous la forme Gaussienne. Ensuite, les résultats numériques de cette relation sont comparés avec ceux expérimentaux et du modèle non Gaussien à huit-chaînes. Les résultats montrent que les prédictions de ce modèle concordent avec les résultats expérimentaux en grande déformation comme celui basé sur le modèle de huit-chaînes.

Plusieurs autres phénomènes physiques caractérisent les élastomères dont l'élasticité non linéaire, la viscoélasticité, l'hyperélasticité, et principalement une température de transition vitreuse inférieure à la température ambiante, ceci implique un état caoutchouteux des élastomères à la température ambiante. L'effet Mullins est un phénomène d'adoucissement qui se produit particulièrement dans les élastomères chargés. En effet, pour améliorer leurs propriétés chimiques ou mécaniques, les élastomères sont renforcés par des nodules de noir de carbone ou d'autres particules. **Mullins et Tobin (1957,1965)** considèrent un élastomère renforcé comme un matériau composite à deux domaines, dont un domaine mou et un domaine dur. D'après leur concept, l'effet Mullins n'est autre que la transformation d'une partie du domaine dur en domaine mou lorsque le composite est sollicité en contrainte.

Dans nos travaux, pour modéliser le comportement mécanique d'élastomères chargés en fonction de leur microstructure, on a considéré un matériau composite à base d'élastomère constitué par une matrice en élastomère, une partie de matrice occluse par les renforts et les

renforts qui sont des nodules de noir de carbone comme dans l'industrie pneumatique. Ainsi, la matrice constitue le domaine mou considéré par Mullins et Tobin tandis que les deux autres constituent le domaine dur c'est-à-dire la fraction volumique effective des renforts (incluant la matrice occluse). L'estimation du domaine dur en fonction du type de nodule de noir de carbone et de sa fraction volumique est obtenue à partir des mesures de microscopie électronique de **Medalia (1970)**. D'où on peut quantifier le domaine dur de notre composite.

En se basant sur les équations de la mécanique des milieux continus, on établit la relation entre la contrainte et la déformation tout au long du chargement du composite, en tenant compte de l'évolution de sa microstructure. Cette évolution de la microstructure se caractérise principalement par la libération des portions inactives de la matrice qui se trouvent emprisonnées entre les particules, provoquant ainsi une augmentation de la fraction volumique du domaine mou dans le composite. Cette transformation est modélisée par la théorie proposée par **Oshmyan et al (2006)**. Ensuite, l'énergie de déformation de **Gent (1996)** pour les matériaux caoutchouteux non chargés a été reformulée pour tenir compte de l'effet des particules de renforts dans le composite. Le principal fondement de cette reformulation est d'admettre que la déformation du composite se produit uniquement au sein du domaine mou. Ainsi, l'énergie de déformation se réduit à celle du domaine mou, impliquant la connaissance de l'évolution de sa fraction volumique durant la déformation. La modélisation du comportement mécanique avec l'effet Mullins spécifique à chaque type de nodules de noir de carbone est ainsi établie avec la mise en relation de l'évolution de la microstructure et la loi de comportement reformulée utilisant la théorie de Gent.

Le modèle obtenu donne des résultats numériques du comportement mécanique des élastomères chargés avec l'effet Mullins en tenant compte du type de nodules de carbone, la

fraction volumique des renforts et les modes de déformation (uni-axial, bi-axial ou en déformation plane). Ces résultats concordent aussi avec des résultats expérimentaux trouvés dans la littérature. Ce modèle est ensuite étendu au cas de l'élastomère thermoplastique polyuréthane dont le comportement mécanique introduit de la viscoplasticité.

INTRODUCTION

For their properties, elastomers are very useful materials for many applications like pneumatic, cable jacketing for electrical or electronic industries, shaft seals, shock absorbers and power-transmission flexible joints used for automotive, rail, aerospace and other engineering industries. These examples show how elastomeric materials become more and more important for industries which aim to improve our life conditions. The current advances made on elastomeric materials properties knowledge explain the increase in their performance and process for different industries applications. However, a deeper understanding of these materials behavior could provide a useful tool for higher performance elastomers production. Elastomeric materials are usually classified as function of their origin, their ability to vulcanization or their composition. Hence, we have natural or synthetic elastomers, vulcanizable or thermoplastic elastomers and filled or unfilled elastomers.

Filled or unfilled elastomers mechanical behaviors are predicted by physical or phenomenological models but their optical anisotropy behavior is given by a physical Gaussian or non-Gaussian model. In physical models, the behavior involves two essential scales which are the treatment for a single macromolecule long-chain structure and the application of this treatment to the material network. Thus, the contribution of all chains in the network corresponds to the material behavior. Some model applications may present limitations like for the well known Gaussian model which is adapted for moderate strains. However, for high strains, a Gaussian model may become inadequate. In this case, one can use a more elaborate non-Gaussian model developed by **Kuhn and Grun (1942)** and **James and Guth (1943)** for small strain to full extended length. A phenomenological model is a

purely mathematical approach. The aim of such method is essentially to find the most general way to describe material properties.

Here, we investigate modeling optical anisotropy behavior for unfilled elastomers under stress and also Mullins effect or softening produced in filled elastomers during cyclic loading-unloading-reloading. Modeling of thermoplastic elastomers behavior is also investigated. This work will be subdivided into four chapters. In the first chapter, we introduce a general presentation of elastomeric materials. It presents a summary of the origin of elastomers and a short history on the material evolution. We also discuss, in this chapter, the elastomeric materials chemical and mechanical properties like the macromolecule structure obtained from the monomers, vulcanization process, viscoelasticity or hyperelasticity behavior. Different physical and phenomenological models are presented for unfilled and filled elastomers. The second chapter is on the modeling and prediction of the mechanical and optical property of unfilled elastomers where the Gaussian theory for optical anisotropy and the corresponding stress-optical law is utilized. We show how **Gent (1996)** model can be extended to optical anisotropy prediction during stretching. The proposed approach is compared to **Arruda and Przybylo (1995)** model and to experimental data from literature. In the third chapter, a constitutive model is built to predict mechanical behavior of filled elastomers based on the consideration of microstructure evolution using hard-to-soft domains transformations. In the last chapter, the elastic-viscoplastic behavior is introduced in the constitutive model in order to predict thermoplastic elastomers behavior (stress-strain response), with particular application to thermoplastic polyurethane. The obtained model is validated by experimental data from literature.

Finally, this thesis is concluded by a general conclusion and remarks. Some suggestions on future research are also exposed.

CHAPTER I

WHAT IS AN ELASTOMER?

The term elastomer is often used interchangeably with the term rubber. Elastomers are amorphous polymer materials which have the ability to recover their shape after a large deformation. They are normally used at temperatures above their glass transition temperature so that considerable molecular segmental motion is possible. Thus, elastomers are soft and deformable. However, hard plastics normally exist either below their glass transition temperature, they are called thermoplastics at room temperature. They are different from other polymers because of their special properties such as flexibility, extensibility, resilience and durability. Elastomers are used in a wide range of applications because of their unusual physical properties.

The first known elastomer was natural rubber. It was originally derived from milky colloidal suspension, or latex found in the sap of some plants such as Para rubber tree which present the major commercial source of natural latex. The purified natural rubber corresponds to the chemical polyisoprene which can also be produced synthetically. Mentioned by Spanish and Portuguese writers in the 16^{th} century, pre-Columbian people of South and Central America like Maya used non-vulcanized natural rubber to make balls, containers, shoes and waterproofing fabrics. Charles Marie de la Condamine is credited of introducing samples of rubber in 1736 to the French Academy of Sciences. He called this material by the name used by natives, *caoutchouc*. In 1751, it was presented a paper on rubber by François Fresneau at

the same Academy. He described many properties of rubber in a paper which was published in 1755. This paper has been referred as the first scientific paper on rubber. Before 1800, natural rubber was used only for elastic bands and erasers. Joseph Priestley is credited the discovery of its use as an eraser and also the name rubber for this material. In 1823, Charles Macintosh found a process using rubber to make waterproof. In 1839, the industry of rubber was revolutionized with the discovery of vulcanization process by Charles Goodyear. His process consists to heat natural rubber with sulfur. It was first used in Springfield, Massachusetts, in 1841. During the latter half of the 19th century, rubber was demanded for its insulating property by the electrical industry. After, the pneumatic tire increased this demand.

I.1. MOLECULAR STRUCTURE

Elastomers like other polymers are obtained by polymerization process which can be illustrated by monomers conversion to macromolecular structures. Example, ethylene molecules are converted into polyethylene which is the most widely produced thermoplastic in the word. The ethylene molecule (In **Figure I.1**) which is unsaturated must be transformed under appropriate conditions of heating and pressure with the presence of catalyst. Then, the double bond between the two carbon atoms can be broken and replaced by a single saturated bond. After, a long macromolecular chain is obtained from monomers combination (See **Figure I.2**).

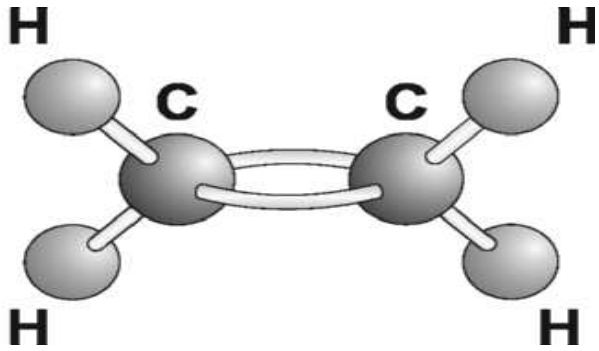

Figure I.1: Ethylene molecule.

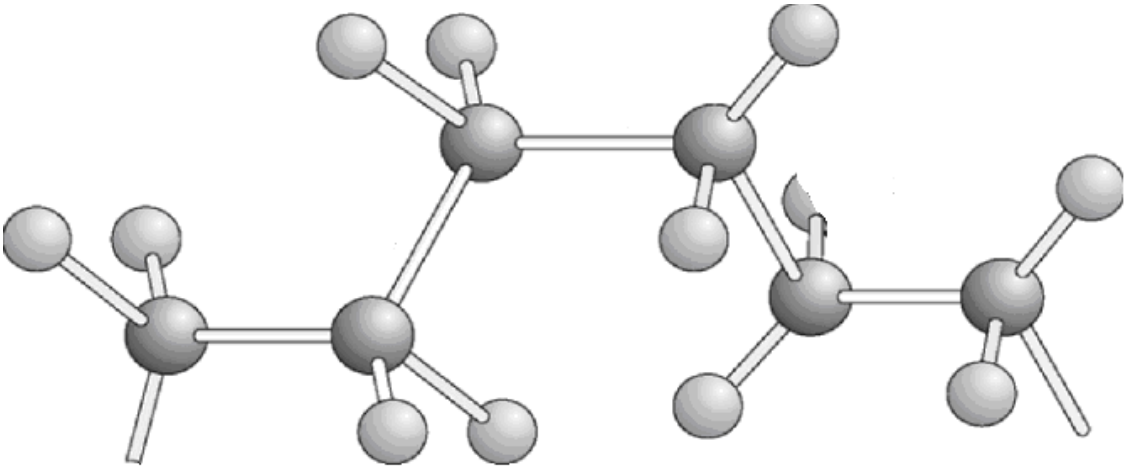

Figure I.2: Polyethylene macromolecule.

I.2. VULCANIZITION

Vulcanization is a process applied to some elastomeric materials in order to improve their retraction to approximately original shape after large mechanical imposed deformation. Vulcanization can be defined as a process that increases the retractile forces and decreases the permanent deformation remaining after unloading. Hence, vulcanization increases elasticity in rubber. Vulcanization chemically produces network junctions by the insertion of cross-links between polymer chains like in **Figure I.3**. The process is usually carried out by heating elastomeric materials with vulcanizing agents. The cross linking element may be a group of sulfur atoms in a short chain, a single sulfur atom, a carbon to carbon bond, a polyvalent organic radical, an ionic cluster or a polyvalent metal ion. The increase of junctions generates supporting chains. This supporting chain is a linear chain in the network between two junctions. The retractile force needed to resist to a permanent deformation is proportional to the number of supporting chains in the network per volume of elastomeric materials.

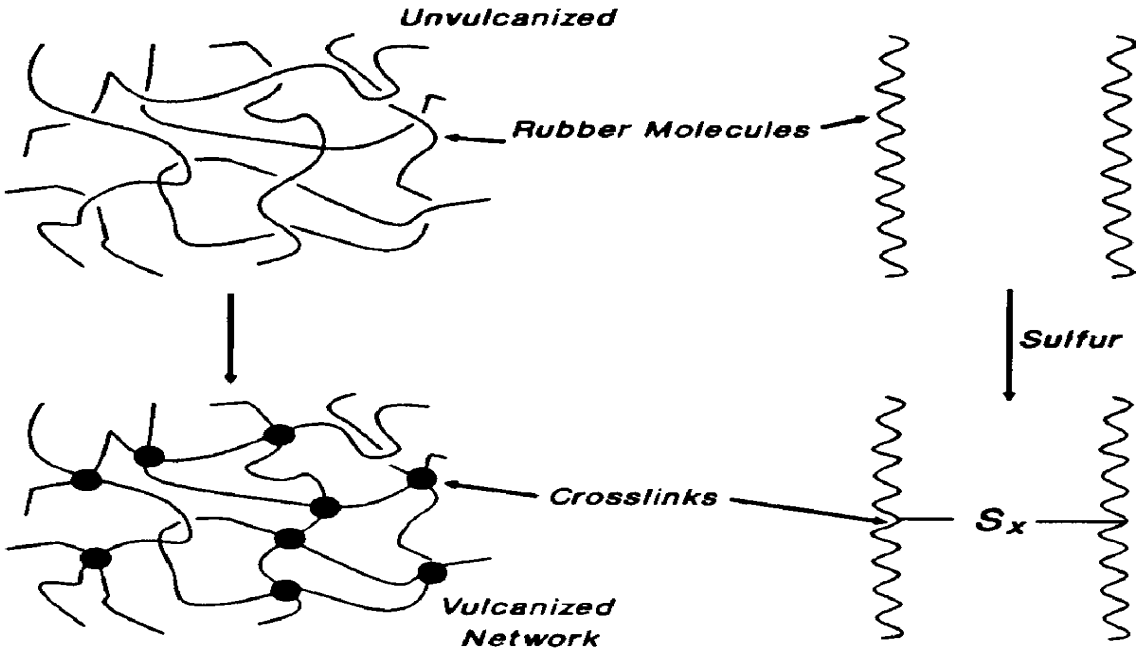

Figure I.3: Vulcanized network formation.

The network formation by vulcanization implies significant effect on elastomer properties like hysteresis whose effect decrease with an increasing cross-linking in the network. At the same time, the ability of elastomer for elastic recovery and stiffness becomes high. For tear strength, fatigue life and toughness, these properties increase with small amount of cross-linking but they are decreased by further cross-linking formation. (See **Figure I.4**).

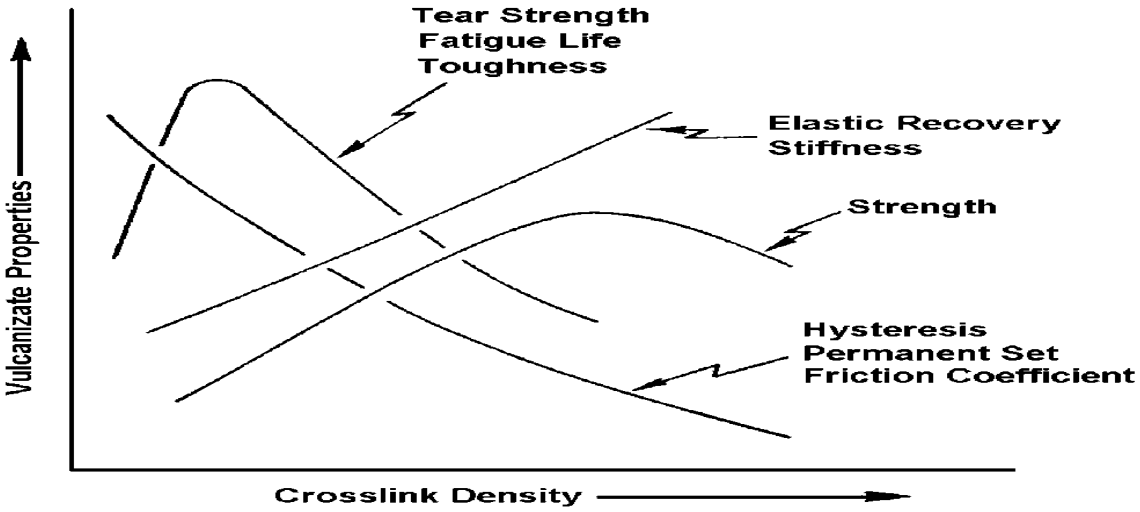

Figure I.4: Elastomer properties as functions of the extent of vulcanization.

I.3. HYPERELASTICITY AND VISCOELASTICITY

Elastomers are well known to exhibit non linear hyper-elastic deformation during uniaxial stretching at room temperature. This property is a principal characteristic of these kinds of polymers. Elastomers are also viscoelastic materials; it can be shown by relaxation or creep test. The simply rheological models use for hyperelasticity and viscoelasticity are respectively spring and dashpot based Maxwell model (**Figure.I.5**) or Kelvin model (**Figure.I.6**).

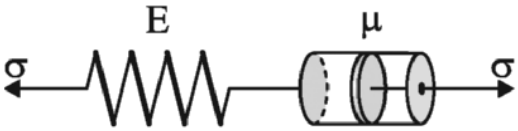

Figure I.5: Maxwell model.

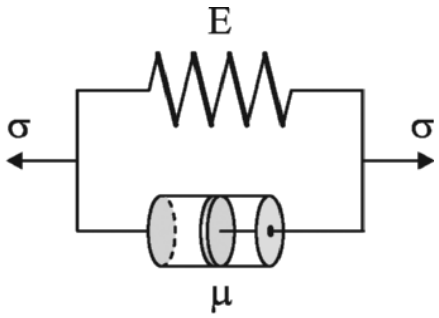

Figure I.6: Kelvin model.

I.4. CARBON BLACK

I.4.1. FILLERS

Elastomers are usually filled with much kind of inorganic or organic fillers in order to improve their properties or to control their processing characteristics. Sometime, particles are used to reduce their overall cost. Particles like carbon black or silica are stiffer and stronger than elastomer matrix and play an important role in materials mechanical properties improvement. They are reinforcing fillers. Basing on reinforcing assertion, fillers can be class in three types: non-reinforcing, semi-reinforcing and reinforcing. Filler effect in polymer composites is function of: their incorporation methods, their characteristics including geometry structures such aspect ratio, surface area, filler shape like in **Figure I.7** (plate, cylindrical, spherical or irregular), filler size (centimeter, millimeter or nanometer), their distribution (random or arrange) and their physical, mechanical, chemical, thermal, optical,

electrical properties. The interaction type or adhesion between filler and matrix also affect filled rubber on stress transfers from the elastomer matrix to the filler.

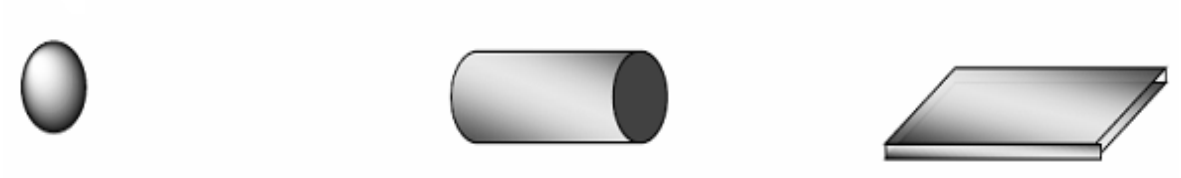

Spherical **Cylindrical** **Plate**

Figure I.7: Types of fillers shape.

I.4.2. CARBON BLACK

Carbon black has been used in rubber compounds for many years. At first, it was used as black pigment. In 1910, channel carbon blacks obtained by exposing an iron plate to a natural gas flame and collecting the deposited soot were used as reinforcing filler. In fact, furnace blacks were produced industrially from petroleum oil in a furnace by an incomplete combustion. After, thermal blacks were produced from natural gas in preheated chambers without air but their effect on composite reinforcement is low. The size of carbon black primary particles is generally expressed in specific surface area/weight (m^2/g).

In filled elastomers microstructure, carbon black primary particles with size between 20-50nm are dispersed separately or cluster in aggregates (100-200nm) (See **Figure I.8.a**). Aggregates are formed by chemical and physical interactions. These aggregates can also cluster. Hence, agglomerate structure is obtained with a size between 10^4-10^6nm (See **Figure I.8.a** and **Figure I.8.b)**. The aggregate structure is low or high in function of primary particles geometrical arrangements. The structure is low for linear arrangement and high for grape arrangement. The primary particles arrangement can be shown by transmission electron micrographs (TEMs) (See **Figure.I.8.c**). For the characterization of low and high structure, dibutyl phthalate (DBP) absorption method can be used. Hence, small amounts of DBP are

added to dry fillers until saturation. The DBP absorption is expressed in cm^3 of DBP per 100g filler (cm^3/100g) for each type of filler.

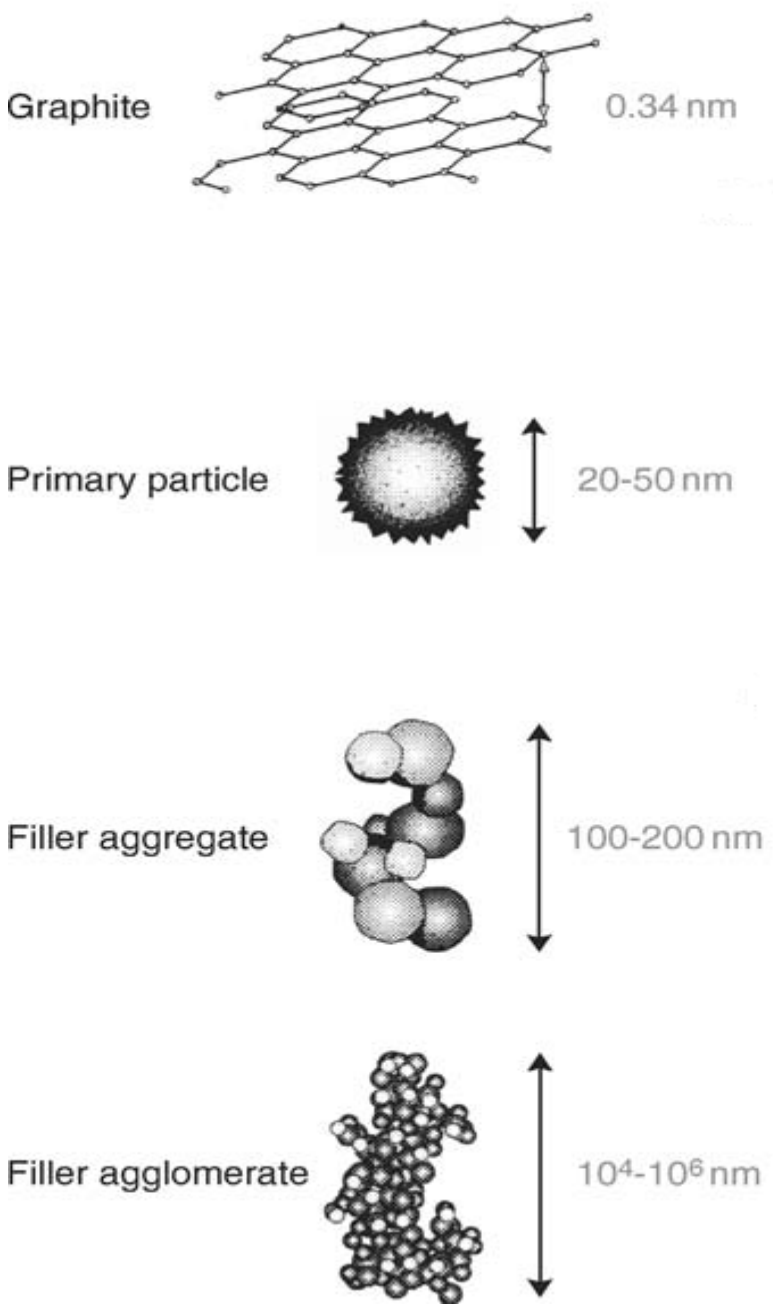

Figure I.8.a: The different length scales of carbon black. (Vilgis et al., 2009)

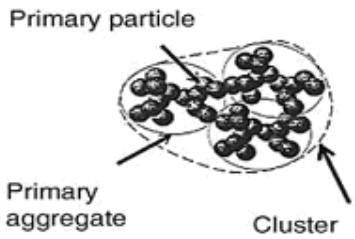

Figure I.8.b: Filler agglomerate structure.

Carbon black particles can be designated using the ASTM International nomenclature where the first letter indicates the type of cure rate applied on particles; N: for normal cure rate and S: for slow cure rate.

Where the first digit indicates particle size range as follows:

1: for 10 to 19 nm, 2: for 20 to 25 nm, 3: for 26 to 30 nm, 4: for 31 to 39 nm, 5: for 40 to 48 nm, 6: for 49 to 60 nm, 7: 61 to 100 nm, 8: for 101 to 200 nm, 9: for 201 to 500 nm.

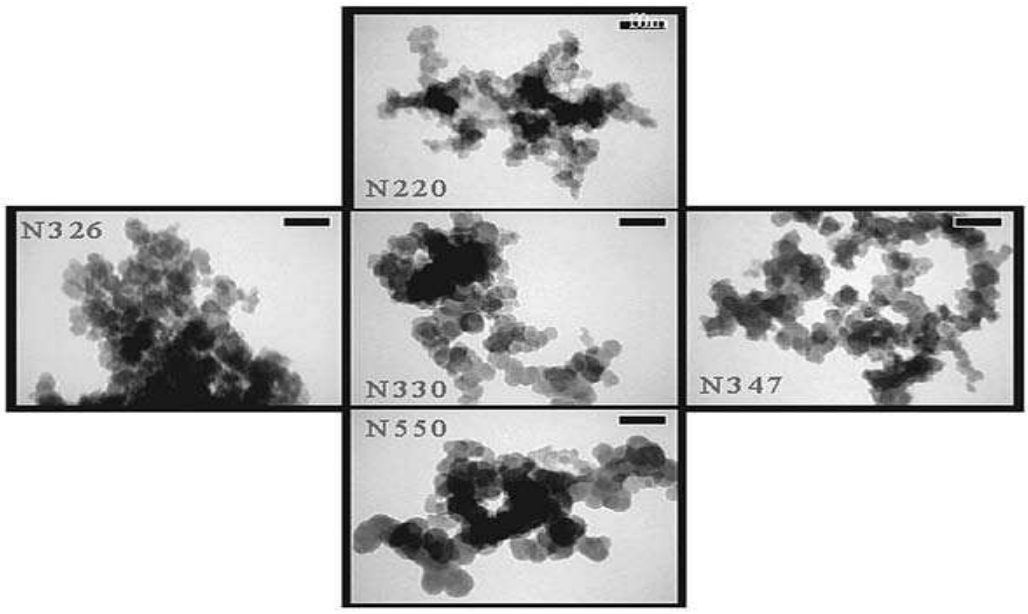

Figure I.8.c: TEMs of five types of carbon black particles. Their specific surface increases from top to bottom and their corresponding aggregate structure. (Vilgis et al., 2009)

I.5. UNFILLED ELASTOMERS MECHANICAL BEHAVIOR AND OPTICAL ANISOTROPY

I.5.1. PHYSICAL THEORY

I.5.1.1. SINGLE LONG-CHAIN TO ELASTOMER NETWORK BY GAUSSIAN THEORY

For the development of the statistical theory in mathematical terms, it is convenient to use an idealized simplest model which does not correspond directly to a real macromolecular structure. This model is consisting of a chain of N links of equal length l, in which the direction in space of any link is entirely random. Some assumptions have also been done. Hence, one end *A* of the single chain is considered to be fixed at the origin of a Cartesian coordinate system *Ox*, *Oy*, *and Oz*, and allow the other end *B* to move in random manner throughout the available space (See **Figure I.9**). The motion is random and all positions of *B* are not equally probable; and for any particular position *P* with coordinates *(x, y, z)* which will be an associated probability that the end *B* will be located at the position of the point *P*.

Kuhn (1934, 1936) and **Guth and Mark (1934)** give solution for this probability function *P(x, y, z)* in the following equation:

$$p(x,y,z)=\frac{b^3}{\pi^{3/2}}\exp\left[-b^2\left(x^2+y^2+z^2\right)\right] \qquad \textbf{I.1}$$

where $b^2=3/2Nl^2$

Equation **I.1** can also be written in this form:

$$p(r)=\frac{b^3}{\pi^{3/2}}\exp\left(-b^2r^2\right) \qquad \textbf{I.2}$$

where $r^2=x^2+y^2+z^2$

Equation **I.2** depends only on the vector r representing the end-to-end distance of the chain.

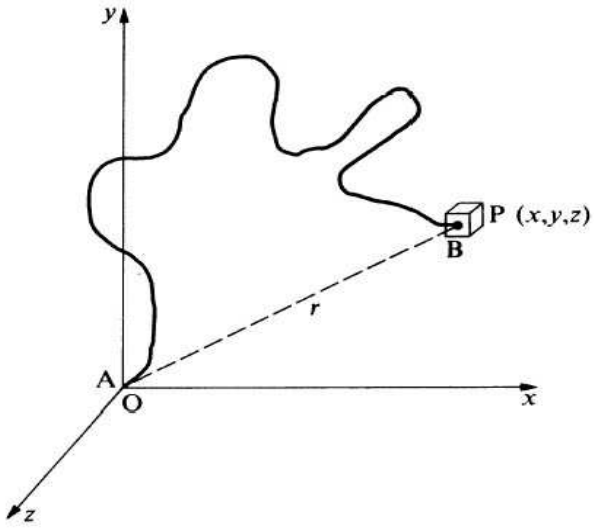

Figure I.9: The chain end-to-end distance vector.

All conformations of the chain described in this theory are purely entropic and the shape of the chain is driven purely by entropy. The entropy of the chain is given by Boltzmann formula as follows:

$$S = k_B \ln \Omega \qquad \textbf{I.3}$$

k_B is the Boltzmann constant and Ω is the number of conformations.

This fundamental equation can be rewritten in this form:

$$S(r) = k_B \ln p(r) = -k_B \left[b^2 r^2 + \ln\left(\frac{b^3}{\pi^{3/2}} \right) \right] \qquad \textbf{I.4}$$

It is convenient to use Helmholtz free energy

$$A = U - TS \qquad \textbf{I.5}$$

where U is the internal energy.

For change taking place at constant absolute temperature T, we have:

$$dA = dU - TdS \qquad \textbf{I.6}$$

Combining equation **I.6** with internal energy $(dU = dQ + dw)$ and entropy $(TdS = dQ)$ evolution which are respectively introduce by thermodynamic first and second laws. The following equivalence was obtained:

$$dA = (dQ + dw) - TdS = (TdS + dw) - TdS = dw \qquad \textbf{I.7}$$

Here, w is the work required to move one end of the chain. The internal energy U effect on the end-to-end distance is neglected. It obtained the tension f in single long-chain by using the relationship of work required to move one end of the chain from distance r to a distance $r + dr$, S is given in equation **I.4**, therefore:

$$f = \frac{dw}{dr} = \frac{dA}{dr} = -T\frac{dS}{dr} = 2k_B Tb^2 r = 3k_B T\frac{r}{Nl^2} \qquad \textbf{I.8}$$

Based on some fundamental assumptions generally originating from **Kuhn (1934, 1936)**, Gaussian theory can be extended to elastomeric materials and the network strain energy W equation is obtained as a function of I_1, the first invariant of the left Cauchy-Green stretch tensor B.

$$\begin{cases} I_1 = trB \\ I_2 = trB^{-1}\det B \\ I_3 = \det B \end{cases} \qquad \textbf{I.9}$$

I_2 and I_3 are respectively the second and the third invariant of the left Cauchy-Green stretch tensor B.

$$W = \frac{1}{2}k_B nT(I_1 - 3) \qquad \textbf{I.10}$$

where n is the number of chains per unit volume.

I.5.1.2 SINGLE LONG-CHAIN TO ELASTOMER NETWORK BY NON-GAUSSIAN THEORY

The aim of the non-Gaussian statistical treatment of the single chain is to take into account all finite extensibility in the chain. Thus, it leads a more realistic distribution function which has the ability to be valid for all range of extension until full extension. Then, the total chain length will be the sum of the x-components of each link, like show in **Figure I.10**. It is

important to known the x-components for all links in this case. Since a link inclined at an angle θ_i to the x-axis, it has a component of length $x_i = l\cos\theta_i$.

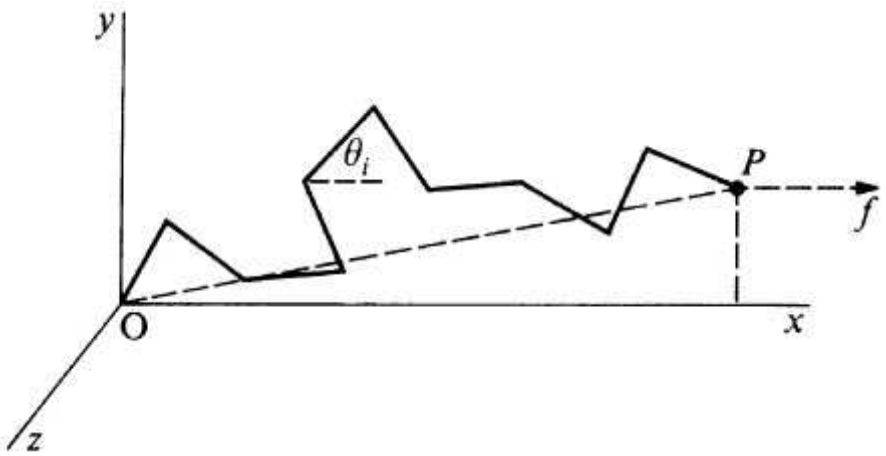

Figure I.10: Chain length by non-Gaussian theory.

Kuhn and Grün (1942) gave a method of solution for this problem by deriving the most probable distribution of link angles with respect to the vector length. The probability of a given vector length was taken to be the probability of this particular distribution of links angles. In this way, **Kuhn and Grün (1942)** obtained this probability in the logarithmic form:

$$\ln\left(p(r)\right) = C - N\left[\frac{r}{Nl}\beta + \ln\left(\frac{\beta}{\sinh\beta}\right)\right] \qquad \textbf{I.11}$$

where $\beta = L^{-1}\left(\frac{r}{\sqrt{Nl}}\right)$ and $L(x) = \coth(x) - \frac{1}{x}$

C and L are respectively a constant and Langevin function.

Entropy and tension for single chain in non-Gaussian theory were deduced like for Gaussian theory. Hence, we have the following equations respectively for entropy and tension:

$$S(r) = C - k_B N\left(\frac{r}{Nl}\beta + \frac{\beta}{\sinh\beta}\right) \qquad \textbf{I.12}$$

$$f = -T\frac{\partial S}{\partial r} = \frac{k_B T}{l}L^{-1}\left(\frac{r}{Nl}\right) \qquad \textbf{I.13}$$

The function Langevin $L^{-1}\left(\frac{r}{Nl}\right)$ written in form of series gives equation **I.13** in this form

$$f=\frac{k_BT}{l}\left[3\left(\frac{r}{Nl}\right)+\frac{9}{5}\left(\frac{r}{Nl}\right)^3+\frac{297}{175}\left(\frac{r}{Nl}\right)^5+\frac{1539}{875}\left(\frac{r}{Nl}\right)^7+\cdots\right] \qquad \textbf{I.14}$$

It is easy to observe that non-Gaussian tension expression's first term in the series corresponds to Gaussian expression given by equation **I.8**. For the network scale, models are generally presented in three-chain, four-chain, eight-chain or full network model by several authors.

I.5.1.2.1. Three-chain model

The three-chain model was suggested by **James and Guth (1943)** for rubber elasticity and assumes that the network n chains per unit volume may be equivalent to three independent sets of $n/3$ chains per unit volume parallel to the Eulerian principal axes system (See **Figure I.11**). According to this theory, the three principal stresses in principal axes have the following form:

$$\sigma_i=-p+\frac{1}{3}C_r\sqrt{N}\lambda_i L^{-1}\left(\frac{\lambda_i}{\sqrt{N}}\right) \qquad \textbf{I.15}$$

where $C_r=nk_BT$ is modulus and p is the hydrostatic pressure.

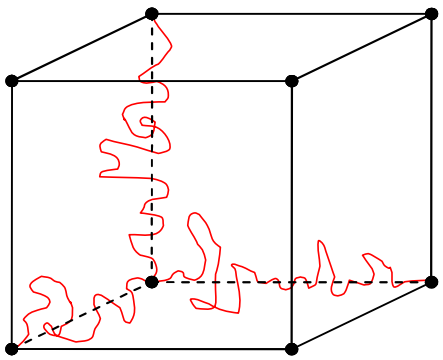

Figure I.11: Three-chain network model.

I.5.1.2.2. Four-chain model

This model is derived from **Flory and Rehner (1943)** development of four-chain model for Gaussian theory, and **Treloar (1946, 1954)** modified the model for non-Gaussian chains. The model considers that the network consists of four chains with a common junction point and all chains have the same contour length. Then, the average positions of their outer ends are at the four corners of a rectangular tetrahedron (See **Figure I.12**). This four-chain model does not exhibit the symmetry required for principal strain space, it is major inconvenience **(Arruda and Boyce, 1991).**

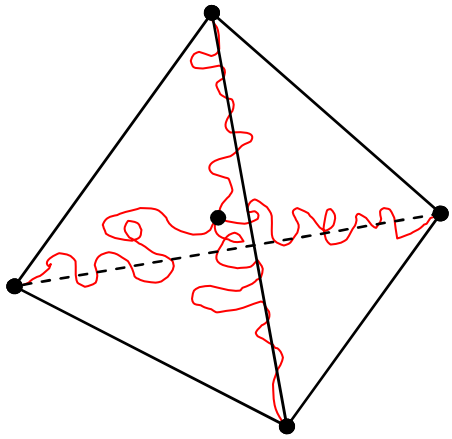

Figure I.12: Four-chain network model.

I.5.1.2.3. Eight-chain model

Arruda and Boyce (1993) proposed the eight-chain model for rubber elasticity. In this model, the network of elastomeric materials is considered to be equivalent to a set of eight chains connecting the central junction point and each of the eight corners of the unit cube like in **Figure I.13**. Cube edges are also taken to remain aligned with principal stretched space during deformation. The eight-chain model show ability to predict rubber materials mechanical behavior for large deformations in a good approximation with uniaxial or shear experimental data. In eight-chain model, strain energy is in the following form:

$$W = C_r \left[\sqrt{N}\lambda_{chain}\beta + N \ln \frac{\beta}{\sinh \beta} \right] \qquad \textbf{I.16}$$

where $\beta = L^{-1}\left(\frac{\lambda_{chain}}{\sqrt{N}}\right)$ and $\lambda_{chain} = \sqrt{I_1/3}$

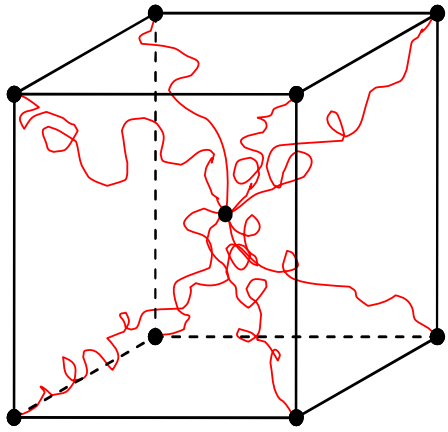

Figure I.13: Eight-chain network model.

I.5.1.2.4. Full Network Model

Treloar and Riding (1979) developed this theory based on a full network description but they limited their considerations to deformations with biaxial extension along fixed axes under plane stress conditions. **Wu and Van der Giessen (1992, 1993, 1995)** extended this model to a general three dimensional formulation where rubbers properties are obtained by the use of a full network of randomly chains connected at the center of a sphere. During material deformation, all chains are stretched and rotated at the same time. In the full network model, a single chain is considered with its end-to-end vector in unstrained or strained state with angular coordinates like in **Figure I.14**. The overall or macro-stress tensor of the network is obtained by simply averaging the individual chains micro-stress. The network stress components are given in this form:

$$\sigma_{ij} = -p\delta_{ij} + \frac{nk_BT}{4\pi}\sqrt{N}\int_0^{\pi}\int_0^{2\pi}\lambda_{chain}L^{-1}\left(\frac{\lambda_{chain}}{\sqrt{N}}\right)m_i m_j \sin\theta d\theta d\varphi \quad i,j = 1,2,3 \qquad \textbf{I.17}$$

where δ_{ij} is Kronecker symbol, λ_{chain} is the locking stretch chain and m_i are the components of unit direction vector.

$$\begin{cases} m_1 = \sin\theta\cos\varphi \\ m_2 = \sin\theta\sin\varphi \\ m_3 = \cos\theta \end{cases} \qquad \begin{cases} i = j \Rightarrow \delta_{ij} = 1 \\ i \neq j \Rightarrow \delta_{ij} = 0 \end{cases} \qquad \lambda_{chain} = \sqrt{m_1^2\lambda_1^2 + m_2^2\lambda_2^2 + m_3^2\lambda_3^2}$$

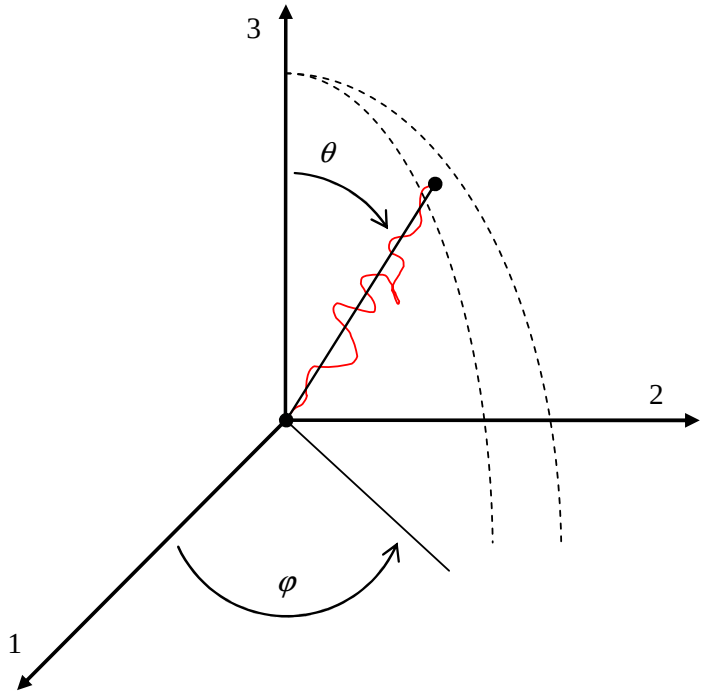

Figure I.14: Full network model.

I.5.2. PHENOMENOLOGICAL THEORY

The aim of such method is essentially to find the most mathematical reasoning way to describe the properties. However, this method is not usually able in itself to give molecular or physical structure explanation or interpretation. Various phenomenological theories have been developed to predict materials mechanical behavior. In this work, we will just present summaries on some well known phenomenological models used for elastomers.

I.5.2.1. Mooney's model (1940)

Based on the assumptions that rubber is incompressible and isotropic state and also obeys to Hooke's law in simple shear, **Mooney (1940)** developed this model with purely mathematical arguments. The strain-energy function of this model is presented in the following form:

$$W = C_1\left(I_1 - 3\right) + C_2\left(I_2 - 3\right) \qquad \textbf{I.18}$$

where C_1 and C_2 are two elastic constants. I_1 and I_2 are first and second invariants of left Cauchy-Green tensor B.

I.5.2.2. Mooney-Rivlin's model (1948)

Rivlin (1948) proposed strain-energy function as the sum of a series of terms $\left(I_1 - 3\right)$ and $\left(I_2 - 3\right)$. It is a general form of Mooney model and many other models from **Isihara et al. (1951)**, **Biderman (1958)**, **Tschoegl (1971)**, **James and Green (1975)**, **Haines and Wilson (1979)**, **Yeoh (1990)** are based on Mooney-Rivlin's model which has this form:

$$W = \sum_{i,j=0}^{\infty} C_{ij}\left(I_1 - 3\right)^i \left(I_2 - 3\right)^j \qquad \text{where } C_{00} = 0 \qquad \textbf{I.19}$$

I.5.2.3. Rivlin and Saunders's model (1951)

Rivlin and Saunders (1951) also proposed a general form for strain-energy after some observations on biaxial experimental data. They noted that $\frac{\partial W}{\partial I_1}$ is a constant independent of I_1 and I_2, while $\frac{\partial W}{\partial I_2}$ is function of I_2 but independent of I_1. They observed that $\frac{\partial W}{\partial I_1}$ is the major term for all states of deformation and that $\frac{\partial W}{\partial I_2}$ decreases when I_2 increases. Hence, they suggested this form for the strain-energy:

$$W = C_1\left(I_1 - 3\right) + F\left(I_2 - 3\right) \qquad \textbf{I.20}$$

I.5.2.4. Gent and Thomas model (1958)

A model which accounts to a fair degree of approximation for the general strain data of **Rivlin and Saunders (1951)** has been proposed by **Gent and Thomas (1958)**. In this model, the unknown function of Rivlin and Saunders is replaced by a logarithm one.

$$W = C_1\left(I_1 - 3\right) + k\ln\left(I_2/3\right) \qquad \textbf{I.21}$$

I.5.2.5. Ogden's model (1972)

A new departure was made by **Ogden (1972)** with a strain-energy function for incompressible rubbers in the form of series. Ogden's model strain energy is in this form:

$$W = \sum_n \frac{\mu_n}{\alpha_n}\left(\lambda_1^{\alpha_n} + \lambda_2^{\alpha_n} + \lambda_3^{\alpha_n} - 3\right) \qquad \textbf{I.22}$$

where α_n are positive or negative values and not necessarily integers and μ_n are constants. $\lambda_i \ \left(i = 1,2,3\right)$ is the stretch in the direction i.

I.5.2.6. Gent's model (1996)

Gent (1996) developed a new phenomenological model which is able to predict elastomers mechanical behavior at large deformation and can be reduced to the Neo-Hookean for small deformations. In this model, Gent introduced a parameter which presents a limiting state or fully stretched for a network of molecular chain. **Boyce (1996)** showed that the non-Gaussian eight-chain and Gent models are powerful three dimensional models to describe rubber behavior at large strain. Gent's strain energy is in this form:

$$W = -\frac{E}{6} J_m \ln\left[1 - \left(\frac{I_1 - 3}{J_m}\right)\right] \qquad \textbf{I.23}$$

where E and J_m are materials parameters corresponding respectively to modulus and maximum stretch.

I.5.3. ELASTOMERS OPTICAL ANISOTROPY

Optical anisotropy is characterized by different values of refractive index for different directions of light propagation through the material or precisely for different directions of polarization of the transmitted light. Based on the work of some authors like **Kuhn and Grün (1942)**, a close connection exists between the optical anisotropy and the mechanical behavior. Materials such as glasses and elastomers, whose structure is essentially irregular or amorphous, are normally isotropic in the unstrained state. But, during their deformation under loading, the amorphous network can have an arrangement distribution in some directions. Hence, the arrangement and amorphous distribution in the same network implies double refraction, it is a birefringence. This is an indicator of the structural anisotropy due to strain induced by stress. Optical anisotropic properties are represented by ellipsoid, whose axes, perpendicular one to them, represent the three principal refractive indices n_1, n_2 and n_3 (See **Figure I.15**). For optical anisotropy, we also have Gaussian and non-Gaussian conceptions, which are applied in material optical behavior. For the two concepts, mechanical and birefringence relationships have been introduced by some authors like **Treloar (1947a, 1947b)** for Gaussian network or **Arruda and Przybylo (1995)** for non-Gaussian. In an optically isotropic medium the relation between the polarizability β and the refractive n index is obtained by Lorentz-Lorenz formula in following form:

$$\frac{n^2-1}{n^2+2}=\frac{4\pi}{3}\beta \qquad \textbf{I.24}$$

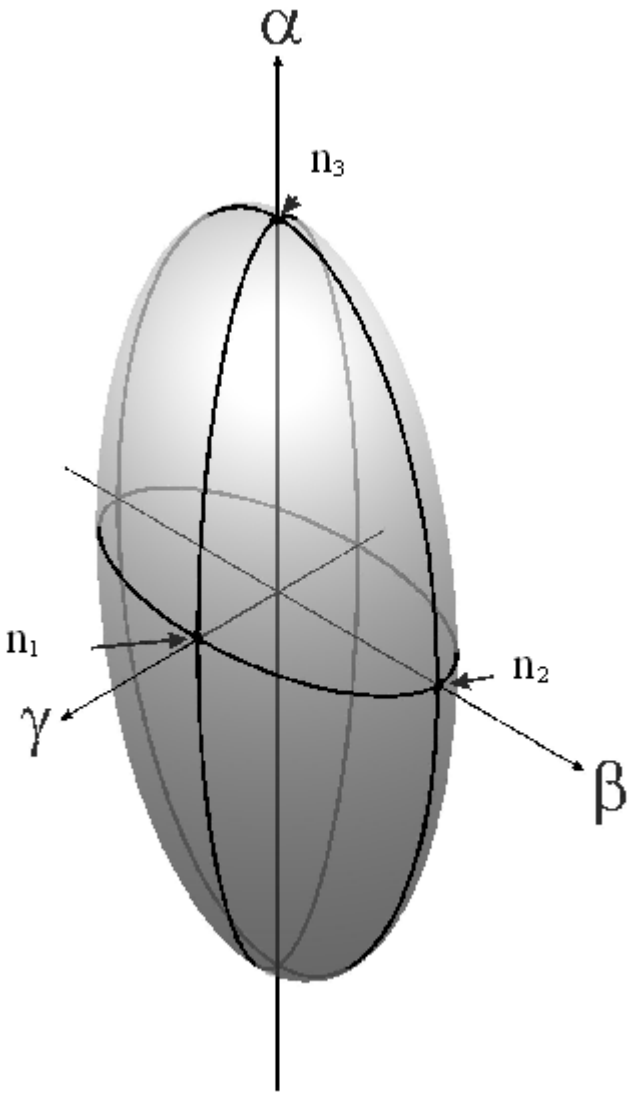

Figure I.15: The refractive index ellipsoid.

I.6. FILLED ELASTOMERS MECHANICAL BEHAVIOR

Filled elastomers are heterogeneous materials. They are composed by more than one phase. Defining the properties of these heterogeneous materials has always been a challenge for scientists. Hence, some authors like **Maxwell (1873)** developed model for electric and magnetic properties in heterogeneous materials containing spherical particles and **Rayleigh (1892)** for conductivity. In 1906, Einstein derived the increase in viscosity caused by a

suspension of spherical particles in a viscous fluid. After, several authors suggested many models to predict heterogeneous materials properties.

I.6.1. Voigt and Reuss models or upper and lower bounds

Voigt (1889) suggested a model for biphasic heterogeneous material where the two phases are parallel. After, **Reuss (1929)** gave another model for the same heterogeneous material where the phases are in series. The application of Voigt and Reuss models in mechanical elasticity implies respectively uniform strain or stress throughout all phases. From **Hill (1951)** works, the two models are also known as upper bound for Voigt and lower bound for Reuss. The biphasic heterogeneous material property is between the two approximations.

$$E^{Voigt} = \varphi_f E_f + \varphi_m E_m$$
$$E^{Reuss} = \left[\frac{\varphi_f}{E_f} + \frac{\varphi_m}{E_m} \right]^{-1} \qquad \textbf{I.25}$$

where $\varphi_m + \varphi_f = 1$

φ_f, φ_m are filler particles and matrix volume fraction and E_f, E_m their properties respectively.

I.6.2. Guth-Gold model (1938)

Guth and Gold (1938) also proposed Young's modulus for elastomers filled by spherical particles. This model includes the interaction between pairs of particles.

$$E = E_m \left(1 + 2.5\varphi_f + 14.1\varphi_f^2\right) \qquad \textbf{I.26}$$

I.6.3. Smallwood's model (1944)

From the work of **Einstein (1906)** on fluid viscosity with spherical particles, **Smallwood (1944)** applied the same approach on low concentrate particles for filled rubber to predict Young modulus.

$$E = E_m\left(1+2.5\varphi_f\right) \qquad \textbf{I.27}$$

Smallwood also showed that for low concentration of filler $\left(\varphi_f \leq 0.1\right)$, his model fitted the observed elastic behavior for lightly reinforced elastomers. But, serious departures occurred for highly reinforcing.

Guth (1945) found that the behavior of rubber containing spherical particles of carbon black is conformed to equation **I.27** up to volume concentrations around 0.3.

I.6.4. Guth model (1945)

Guth (1945) developed a model applicable to any shape of particles. He introduced a parameter k which characterizes aspect ratio of the particles, filler aggregate structures or cluster particles.

$$E = E_m\left[1+0.67k\varphi_f+1.62\left(k\varphi_f\right)^2\right] \qquad \textbf{I.28}$$

I.6.5. Mori-Tanaka model (1973)

Mori and Tanaka (1973) model is applied for spherical particles isotropically dispersed in an elastic matrix and can be written in this form:

$$K = K_m + \frac{\varphi_f\left(K_f-K_m\right)K_m}{K_m+3\varphi_m K_m\left(K_f-K_m\right)/\left(3K_m+4G_m\right)} \qquad \textbf{I.29.a}$$

$$G = G_m + \frac{\varphi_f\left(G_f-G_m\right)G_m}{G_m+6\varphi_m\left(K_f-K_m\right)\left(K_m+2G_m\right)/5\left(3K_m+4G_m\right)} \qquad \textbf{I.29.b}$$

where K K_m K_f are the bulk modulus and G G_m G_f are shear modulus respectively for the composite, the matrix and fillers. φ_m and φ_f are matrix and fillers volume fraction.

I.7. CONCLUSION

In this chapter, a general presentation is due on elastomers material. It includes their origin or their applications in many industries. Their macromolecule structure is introduced and also their well known mechanical behavior. Some physical and phenomenological models which have the ability to predict unfilled and filled elastomers mechanical behavior are presented. The fillers use for reinforced elastomers are also present, particularly carbon black. It is the most used in reinforced elastomers.

CHAPTER II

MODELING OF THE STRESS-BIREFRINGENCE-STRETCH BEHAVIOR IN RUBBERS USING THE GENT MODEL

Deformation of rubbers produces mechanical and optical changes of the polymer network. This mechanical behavior of the elastomeric materials is often given by a stress–strain relationship which can be obtained from assumed physical or phenomenological models. In the familiar works, the theory of rubber elasticity for single chain is treated by Gaussian statistics before to be applied on network. Hence, rubber properties are obtained from the contributions of the whole chains in network. **Kuhn and Grün (1942)** and **James and Guth (1943)** developed a non-Gaussian treatment for single chain which is extended to network. Based on these Gaussian and non-Gaussian theories, network stress-strain constitutive models were developed for rubber elasticity. These include: the four-chain Gaussian theory from **Flory and Rehner (1943)**, the four-chain non-Gaussian theory from **Treloar (1975)**, the three-chain non-Gaussian theory from **Wang and Guth (1952)**, the eight-chain non-Gaussian network theory from **Arruda and Boyce (1993)** and the full network non-Gaussian theory from **Wu and Van Der Geissen (1993, 1995)**. Phenomenological models have also been developed and used. These include models of **Mooney (1940)**, **Rivlin (1948)**, **Valanis and Landel (1976)**, **Ogden (1972)** and recently **Gent (1996)**, among many others.

The optical property like birefringence is characterized by the material anisotropy which is measured by the difference in the refractive indices in two orthogonal directions of the anisotropic medium. Optical anisotropy evolves with molecular orientation during

deformation. This implies, like for the stress, a relationship between birefringence and strain or stretch. This constitutive relation can also be expressed in terms of a birefringence-stress relationship. A statistical long-chain molecule optical property composed with anisotropic links has its foundation in the optical theory of **Kuhn and Grün (1942)**, **Treloar (1947a, 1947b)**. They also investigated the photo-elastic properties of rubbers.

Based on these works, several authors proposed models to simulate optical anisotropy and validated their modeling by comparison of the predicted birefringence-stretch and stress-stretch results to the experimental ones. For instance, **Wu and Van Der Giessen (1995)** simulated the birefringence evolution using the non-Gaussian full network model for rubbers. **Arruda and Przybylo (1995)** extended the non-Gaussian eight-chain model to the birefringence; they also compared their model to natural rubber and polydimethylsiloxane elastomers (PDMS) experimental results. **Von Lockette and Arruda (1999)** extended the eight-chain network model for stress-birefringence to derive Raman spectra evolution for elastomers.

Here, we propose to build birefringence-stress relationship with the Gent model in order to simulate the birefringence or optical refractive indices evolution in deformed rubbers under large strains. In this way, we combine Gent model with the Gaussian optic law. The results from our derived stress-optic model are compared to those from the non-Gaussian eight-chain stress-optic model and experimental data from the literature.

II.1. STRESS-OPTICAL LAW

II.1.1. GAUSSIAN MODEL

II.1.1.1. GAUSSIAN STRESS-STRETCH

The first theories based on the stress and optical responses of rubber network using Gaussian statistics were developed by several authors like **Kuhn and Grün (1942)**; **Flory and Rehner, (1943)**; **Wang and Guth (1952)**; **Treloar (1975)**. From the Gaussian strain energy in equation **I.10**, we can deduce stress-stretch response of the network between any two of the three principal stresses as follows

$$\sigma_i - \sigma_j = nk_BT\left(\lambda_i^2 - \lambda_j^2\right) \qquad i, j = 1,2,3 \qquad \textbf{II.1}$$

where $\sigma_i = \lambda_i \dfrac{dW}{d\lambda_i} + p \qquad i = 1,2,3$

W is the Gaussian strain energy, n is the chain density, k_B is the Boltzmann constant, T is the absolute temperature, p is the hydrostatic pressure and λ_i are the principal stretches corresponding respectively to the principal stresses σ_i.

II.1.1.2. GAUSSIAN BIREFRINGENCE

Optical properties of strained rubber or strain birefringence were successfully solved by **Kuhn and Grün (1942)**. The optical properties of elastomer can be defined as the contribution of each chain in the network to the total polarizability. Hence, as in the elastic properties at **I.3**, a single random chain of jointed links is considered and the optical properties are introduced by associating to each link an optical anisotropy defined by polarizabilities α_1 along of its length and α_2 in the transverse directions. Then, the resultant component of polarizability for the whole chain along the axes may be calculated when the directions of all links are known.

Consider a link defined by angular coordinates θ and φ (See **Figure I.14**), example, the link makes an angle θ with ox and the plane containing the angle θ makes an angle φ with the plane xoy. The components of the polarizability tensor are then given in this form:

$$\begin{aligned}
&\alpha_{xx} = \alpha_1 \cos^2\theta + \alpha_2 \sin^2\theta, \\
&\alpha_{yy} = (\alpha_1 - \alpha_2)\sin^2\theta\cos^2\varphi + \alpha_2, \\
&\alpha_{zz} = (\alpha_1 - \alpha_2)\sin^2\theta\cos^2\varphi + \alpha_2, \\
&\alpha_{xy} = \alpha_{yx} = (\alpha_1 - \alpha_2)\sin\theta\cos\theta\cos\varphi, \\
&\alpha_{xz} = \alpha_{zx} = (\alpha_1 - \alpha_2)\sin\theta\cos\theta\sin\varphi, \\
&\alpha_{yz} = \alpha_{zy} = (\alpha_1 - \alpha_2)\sin^2\theta\sin\varphi\cos\varphi.
\end{aligned} \qquad \textbf{II.2}$$

α_{ij} is the polarizability in the direction i for the field applied in the direction j. The corresponding total polarisabilities of the chain being the sum of the polarisabilities of each link and will be:

$$\gamma_{ij} = \int \alpha_{ij} dN \qquad \textbf{II.3}$$

where $dN = \frac{N\beta}{\sinh\beta} e^{\beta\cos\theta} \frac{1}{2}\sin\theta d\theta \frac{d\varphi}{2\pi}$ represents the angular distribution of link directions and $\beta = L^{-1}\left(\frac{r}{Nl}\right)$.

We obtain the following result:

$$\begin{aligned}
&\gamma_{xx} = N\left[\alpha_1 - (\alpha_1 - \alpha_2)\frac{2r/Nl}{L^{-1}(r/Nl)}\right], \\
&\gamma_{yy} = \gamma_{zz} = N\left[\alpha_2 + (\alpha_1 - \alpha_2)\frac{r/Nl}{L^{-1}(r/Nl)}\right], \\
&\gamma_{xy} = \gamma_{xz} = \gamma_{yz} = 0.
\end{aligned} \qquad \textbf{II.4}$$

For the difference of the two principal polarisabilities, we have:

$$\gamma_1 - \gamma_2 = N(\alpha_1 - \alpha_2)\left[1 - \frac{3r/Nl}{L^{-1}(r/Nl)}\right] \qquad \textbf{II.5}$$

where $\gamma_1 = \gamma_{xx}$ and $\gamma_2 = \gamma_{yy} = \gamma_{zz}$.

This can be writing in form of series:

$$\gamma_1 - \gamma_2 = N(\alpha_1 - \alpha_2)\left[\frac{3}{5}\left(\frac{r}{Nl}\right)^2 + \frac{36}{175}\left(\frac{r}{Nl}\right)^4 + \frac{108}{175}\left(\frac{r}{Nl}\right)^6 + \ldots\right] \qquad \textbf{II.5.a}$$

Like for tension, the polarisability Gaussian expression corresponds to a first term in the non-Gaussian equation **II.5.a**.

Hence:

$$\gamma_1 - \gamma_2 = N(\alpha_1 - \alpha_2)\frac{3}{5}\left(\frac{r}{Nl}\right)^2 = \frac{3}{5}(\alpha_1 - \alpha_2) \qquad \textbf{II.5.b}$$

It is interesting to remember that for free chain, we have: $r^2 = Nl^2$

The network polarizabilities β_1 and β_2 respectively parallel and perpendicular to the direction of the extension are obtained from Gaussian network assumptions from **Treloar (1975)**.

$$\beta_1 = \beta_x = n\left[\frac{N}{3}(\alpha_1 + 2\alpha_2) + \frac{1}{15}(\alpha_1 - \alpha_2)\left(2\lambda_1^2 - \lambda_2^2 - \lambda_3^2\right)\right] \qquad \textbf{II.6.a}$$

$$\beta_2 = \beta_y = n\left[\frac{N}{3}(\alpha_1 + 2\alpha_2) + \frac{1}{15}(\alpha_1 - \alpha_2)\left(2\lambda_2^2 - \lambda_3^2 - \lambda_1^2\right)\right] \qquad \textbf{II.6.b}$$

$$\beta_2 = \beta_z = n\left[\frac{N}{3}(\alpha_1 + 2\alpha_2) + \frac{1}{15}(\alpha_1 - \alpha_2)\left(2\lambda_3^2 - \lambda_1^2 - \lambda_2^2\right)\right] \qquad \textbf{II.6.c}$$

n and N are respectively the number of chains per unit volume and the number of links in the chain.

Using Lorentz-Lorenz formula in equation **I.24**, the difference between any two of the principal refractive indices resulting from Gaussian theory is:

$$\Delta\eta_{i-j} = \eta_i - \eta_j = \frac{2\pi\alpha n}{45}\frac{\left(\eta_o^2 + 2\right)^2}{\eta_o}\left(\lambda_i^2 - \lambda_j^2\right) \qquad \textbf{II.7}$$

where $\alpha = \alpha_1 - \alpha_2$ and $\eta_o = \dfrac{\eta_1 + \eta_2 + \eta_3}{3}$ is the mean refractive index.

Combining equations **II.1** and **II.7**, a linear stress–optic law is obtained:

$$\Delta\eta_{i-j} = \frac{2\pi\alpha}{45kT}\frac{\left(\eta_o^2+2\right)^2}{\eta_o}\left(\sigma_i-\sigma_j\right) \qquad \textbf{II.8}$$

According to Treloar experimental results **(Treloar 1947a, 1947b; Treloar and Riding 1979)**, it was observed that the relationship between the stress and the birefringence is not linear at large stretch. Therefore, the model described by equation **II.8** is able to predict the birefringence only in the range of moderate strains. Currently, the eight-chain model and the Gent model are two excellent predictors to describe the large stress-stretch behavior of rubbers **(Arruda and Boyce, 1993**; **Gent, 1996**; **Boyce, 1996)**. Only, the eight-chain model was used to predict birefringence by non-Gaussian statistical theory **(Arruda and Przybylo, 1995)**.

II.1.2. EIGHT-CHAIN MODEL

This model was developed by **Arruda and Boyce (1993)**. For this, they constructed a representative macromolecular network of eight-chains where each chain emanates from the center of a cube out to each corner. The cube is deformed such that each face lies along a principal stretch axis. The stress-stretch behavior of each chain is taken to be non–Gaussian and is represented with Langevin function chain statistics. The stress-stretch relations of the network are therefore given by:

$$\sigma_i-\sigma_j = \frac{nk_BT}{3}\sqrt{N}L^{-1}\left(\frac{\lambda_{chain}}{\sqrt{N}}\right)\frac{\lambda_i^2-\lambda_j^2}{\lambda_{chain}} \qquad \textbf{II.9}$$

where $\lambda_{chain}^2 = \left(\lambda_1^2+\lambda_2^2+\lambda_3^2\right)/3$

Arruda and Przybylo (1995) have extended this concept to derive a physically-based stress-optic law. For this, a non-Gaussian statistical theory is also used for birefringence. Their obtained stress–optic law is given by the following expression:

$$\Delta\eta_{i-j}^{8chain} = \frac{2\pi}{9}\frac{\alpha\sqrt{N}}{k_B T}\frac{\left(\eta_o^2+2\right)^2}{\eta_o}\left(\frac{1}{\lambda_{chain}}\right)\left[\frac{\left\{1-\frac{3\lambda_{chain}}{\sqrt{N}}\right\}}{L^{-1}\left(\frac{\lambda_{chain}}{\sqrt{N}}\right)}\right]\left(\sigma_i-\sigma_j\right) \qquad \textbf{II.10}$$

II.2. GENT MODEL AND OPTICAL ANISOTROPY

II.2.1. GENT MODEL

Elastomers exhibit complex mechanical behavior, which includes non linear elasticity at large strain, hysteresis, time dependent response, stress-softening or Mullins effect. Some constitutive models **Arruda and Boyce, (1993)**, **Hart-Smith, (1966)**, **Marckmann et al, (2002)**, **Gent, (1996)**, **Qi and Boyce, (2005)** focus on one or more phenomenon observed experimentally like large strain elasticity, hysteresis, time dependent response, stress-softening or Mullins effect. Currently, strain energy potential W are proposed for elastomers material to capture these behaviors. Assuming that elastomers are isotropic and incompressible, a strain energy is generally given as function of the two first invariants of the left Cauchy-Green stretch tensor B.

$$W = W\left(I_1, I_2\right) \qquad \textbf{II.11}$$

The true stress tensor is defined by the differentiation of W with respect to B:

$$\sigma = -pI + 2B\frac{\partial W}{\partial B} = -pI + 2\left(\frac{\partial W}{\partial I_1} + I_1\frac{\partial W}{\partial I_2}\right)B - 2\frac{\partial W}{\partial I_2}B^2 \qquad \textbf{II.12}$$

Considering the proposed **Gent (1996)** model in equation **I.23**, and taking into account that W is in function of I_1 and independent of I_2 the associated Cauchy stress is in the following form:

$$\sigma = -pI + \frac{E}{3}\frac{J_m}{J_m - J_1}B \qquad \textbf{II.13}$$

where: $J_1 = I_1 - 3$

As shown by **Boyce (1996)**, **Chagnon et al (2004)**, **Horgan and Saccomandi (2002)**, the parameters E and J_m in the Gent model are rather related to well established parameters for elastomers deformation behaviour, namely the rubbery modulus and the locking stretch. To show this equivalence for the modulus E, Gent strain energy can be expressed in a series of polynomial form:

$$W_G = \frac{E}{6}\sum_{n=0}^{\infty}\frac{1}{n+1}\frac{J_1^{n+1}}{J_m^n} \qquad \textbf{II.14.a}$$

For small strains, the expression **II.14.a** is reduced to the first term:

$$W_G = \frac{E}{6}J_1 = \frac{E}{6}(I_1 - 3) \qquad \textbf{II.14.b}$$

The equivalence of this equation **II.14.b** with the Neo-Hookean strain energy $W_{NH} = \frac{\mu}{2}J_1 = \frac{\mu}{2}(I_1 - 3)$, which is valid in the range of small strains, implies:

$$E = 3\mu = 3nk_BT \qquad \textbf{II.15}$$

where μ is the shear modulus.

The relation between the parameter J_m and other parameters can be obtained by the use of the current chain stretch expression (λ_{chain}) **(Arruda and Boyce, 1993)** and its limited value (lock chain) at full stretch condition. The locking stretch is given by $\lambda_{chain}^{lock} = N^{1/2}$, where N is the number of statistical links in the chain between two chemical crosslinks. Let's introduce the average stretch as $\lambda_{chain}^2 = \frac{1}{3}(\lambda_1^2 + \lambda_2^2 + \lambda_3^2)$. Then, we obtain:

$$\lambda_{chain} = \frac{I_1^{1/2}}{\sqrt{3}} = \frac{(J_1+3)^{1/2}}{\sqrt{3}} \qquad \textbf{II.16}$$

At full stretch condition the parameter J_1 tends to its limiting value J_m and equivalently the chain stretch tends to the locking one:

$$J_1 \to J_m \Rightarrow \lambda_{chain} \to \lambda_{chain}^{lock} = N^{1/2} \qquad \textbf{II.17}$$

From **II.16** and **II.17**, we can therefore get:

$$\frac{\left(J_m + 3\right)^{1/2}}{\sqrt{3}} = N^{1/2} \Rightarrow J_m = 3\left(N - 1\right) \qquad \textbf{II.18}$$

Horgan and Saccomandi (2002) showed that Gent model for incompressible rubber is a very good qualitative and quantitative alternative for the prediction of the stress-strain response of elastomers. They also concluded that the Gent model is a very good approximation for molecular arguments using **Kuhn and Grün (1942)** non–Gaussian probability distribution function.

The difference between two principal stresses using Gent strain energy is given by:

$$\sigma_i - \sigma_j = \frac{J_m E}{3\left(J_m - J_1\right)}\left(\lambda_i^2 - \lambda_j^2\right) \qquad \textbf{II.19}$$

where: $\sigma_i = \lambda_i \dfrac{\partial W}{\partial \lambda_i} + p$

The combination of equation **II.7** for the birefringence based on the Gaussian network theory and equation **II.19** for the stress-stretch relations based on the Gent model yields the stress-optic law in the following form:

$$\Delta\eta_{i-j}^{GG} = \frac{2\pi}{15}\frac{\alpha n\left(\eta_o^2 + 2\right)^2}{J_m E \eta_o}\left(J_m - J_1\right)\left(\sigma_i - \sigma_j\right) \qquad \textbf{II.20}$$

When we introduce equation **II.15** into equation **II.20**, the stress-optic law becomes:

$$\Delta\eta_{i-j}^{GG} = \frac{2\pi}{45}\frac{\alpha\left(\eta_o^2 + 2\right)^2}{J_m k_B T \eta_o}\left(J_m - J_1\right)\left(\sigma_i - \sigma_j\right) \qquad \textbf{II.21}$$

Finally, one can compare equations **II.10** and **II.21** where the number of material parameters is the same. However, stress-optic law in equation **II.10** based on the eight-chain model use

the inverse Langevin function which is not the case for our stress-optic model in equation **II.21**. To directly compare the expressions of the birefringence $\Delta\eta_{i-j}$ using the eight-chain model and our proposed Gent-based relationship, we introduce the Padé approximation for the inverse of Langevin function: $L^{-1}(x) \approx x\dfrac{3-x^2}{1-x^2}$ **(Cohen, 1991; Richeton et al., 2007)**. By inserting this approximation in equations **II.9** and **II.10**, after some rearrangements, we can write the birefringence based on the eight-chain model, Δ_{i-j}^{8chain}, as follows:

$$\Delta\eta_{i-j}^{8chain} = \frac{4}{9}\frac{\pi\alpha}{k_BT}\frac{\left(\eta_o^2+2\right)^2}{\eta_o}\frac{N}{\left(3N-\lambda_{chain}^2\right)^2}\left(N-\lambda_{chain}^2\right)\left(\sigma_i-\sigma_j\right)$$
$$= A\frac{\pi\alpha}{k_BT}\frac{\left(\eta_o^2+2\right)^2}{\eta_o}\left(N-\lambda_{chain}^2\right)\left(\sigma_i-\sigma_j\right) \qquad with \qquad A=\frac{4}{9}\frac{N}{\left(3N-\lambda_{chain}^2\right)^2} \qquad \textbf{II.22.a}$$

where

$$\sigma_i-\sigma_j = nk_BT\frac{1}{N-\lambda_{chain}^2}\left(N-\frac{\lambda_{chain}^2}{3}\right)\left(\lambda_i^2-\lambda_j^2\right) \qquad \textbf{II.22.b}$$

Equation **II.22.a** can be compared to the birefringence expression obtained using our proposed model that combines the Gaussian–birefringence with the Gent model ($\Delta\eta_{i-j}^{GG}$). Since $J_1 = 3\left(\lambda_{chain}^2-1\right)$, $J_m = 3(N-1)$ and $E = 3nk_BT$, we can also write equations **II.21** and **II.19** in the following form:

$$\Delta\eta_{i-j}^{GG} = \frac{2}{15}\frac{\pi\alpha}{k_BT}\frac{\left(\eta_o^2+2\right)^2}{\eta_o}\frac{1}{3(N-1)}\left(N-\lambda_{chain}^2\right)\left(\sigma_i-\sigma_j\right)$$
$$= B\frac{\pi\alpha}{k_BT}\frac{\left(\eta_o^2+2\right)^2}{\eta_o}\left(N-\lambda_{chain}^2\right)\left(\sigma_i-\sigma_j\right) \qquad with \qquad B=\frac{2}{15}\frac{1}{3(N-1)} \qquad \textbf{II.23.a}$$

where

$$\sigma_i-\sigma_j = nk_BT\frac{1}{N-\lambda_{chain}^2}(N-1)\left(\lambda_i^2-\lambda_j^2\right) \qquad \textbf{II.23.b}$$

As we can obtain, both equations **II.22.a** and **II.23.a** for stress-optic relationship and the two expressions have some similarities. However, we should note that the Arruda-Przyblyo model is based on non-Gaussian eight-chain. However, the Gent model is based on using the stress induced principal stretch differences in the Gent stress stretch formulation to scale the stretch induced principal birefringence in the Gaussian network model.

In what follows, the results from equations **II.22.a.** and **II.22.b.** will be referred to as the AP (Arruda-Przyblyo) model and the AB (Arruda-Boyce) model, respectively. Results from equations **II.23a.** and **II.23.b.** will be referred to as the proposed model and the Gent model, respectively.

II.2.2. RESULTS

We implemented the Gent model to predict the stress-stretch response and birefringence evolution as a function of the stretch for both uniaxial tension and compression. The results from the proposed Gent model are compared to those of the non-Gaussian eight-chain model and also to experimental data from the literature. The selected rubbers are those used by **Arruda and Przybylo (1995)** where they compared the eight-chain model to experimental data.

The experimental data are those from **Flory and Erman (1982)** and **Erman and Flory (1982, 1983a, 1983b)** for two Polydimethylsiloxanes (Name here: PDMS(A) and PDMS(B)), as well as those from **Von Lockette and Arruda (1999)** for two other polydimethylsiloxanes (Name here: PDMS(C), PDMS(D)) and also on natural rubber. The molecular weights for PDMS(C) PDMS(D) are 2600g/mol and 21500g/mol respectively. The molecular weights for PDMS(A) and PDMS(B) were not given but they were reported to differ in their mechanical and optical properties **(Arruda and Przybylo, 1995)** since they were synthesized under different conditions. The material parameters for both models are those used by **Arruda and Przybylo (1995)** and **Von Lockette and Arruda (1999)** and are shown in **Table II.1**.

Table II.1: Parameters of the materials used for simulation.

	Fig.1. PDMS(A)*	**Fig.2. PDMS(B)***	**Fig.3. PDMS(C)****	**Fig.4. PDMS(D)****	**Fig.5. Rubber***
η_o	**1.4074**	**1.4074**	**1.4074**	**1.4074**	**1.5205**
α (m^3)	$5.4\ 10^{-31}$	$5.4\ 10^{-31}$	$8.5\ 10^{-31}$	$4.66\ 10^{-31}$	$51.1\ 10^{-31}$
n(m^{-3})	$2.25\ 10^{25}$	$4.55\ 10^{25}$	$1.42\ 10^{25}$	$2.12\ 10^{25}$	$7.25\ 10^{25}$
$Jm=3(N-1)$	**147**	**72**	**29.67**	**297**	**72**
$E=3nk_BT$(MPa)	**0.278**	**0.56**	**0.175**	**0.262**	**0.895**

*** Arruda and Przybylo (1995)**

**** Von Lockette and Arruda (1999)**

Figures II.1. shows the results for PDMS(A) under uniaxial tensile (in $\vec{X}_1$ direction). **Figure II.1.a.** gives the evolution of the nominal stress versus the uniaxial stretch and **Figure II.1.b**. shows the evolution of the birefringence ($\Delta\eta_{1-2} = \Delta\eta_{1-3}$ and $\Delta\eta_{2-3} = 0$). From these results, we observe that the two models predict exactly the same stress-stretch response which slightly deviates from the experimental results of **Flory and Erman (1982)** and **Erman and Flory (1982, 1983a, 1983b)** at large stretches. However, the birefringence results from the proposed model yield a relative error of 10% from the experimental results of **Flory and Erman (1982)** and **Erman and Flory (1982, 1983a, 1983b)**.

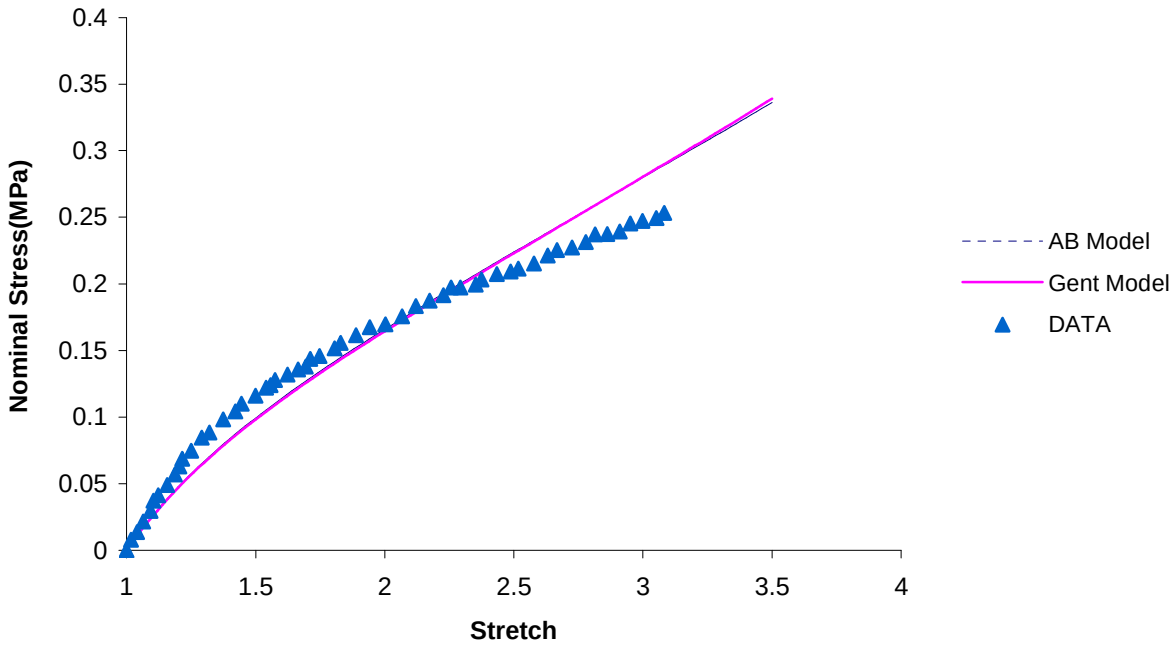

Figure II.1.a: PDMS (A) Stress–stretch response in uniaxial tension.

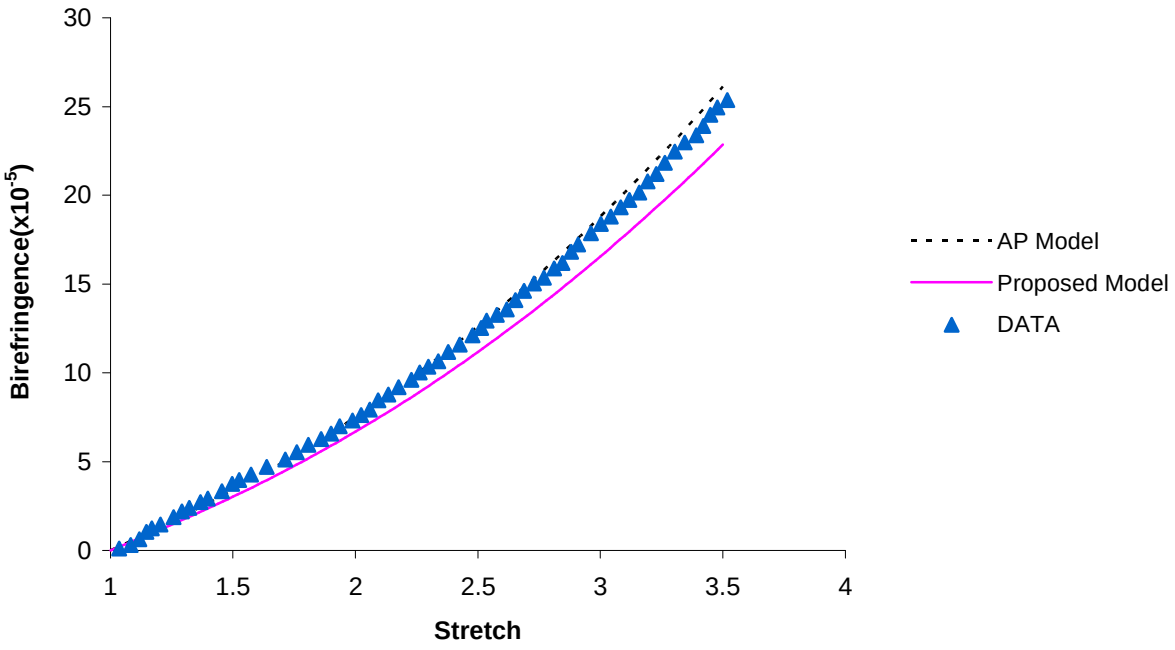

Figure.II.1.b: PDMS (A) Birefringence–stretch response in uniaxial tension

$$\Delta\eta_{1-2} = \Delta\eta_{1-3}.$$

Figures II.2. shows the results for PDMS(B) under uniaxial tension. **Figure II.2.a.** shows a good accord between the predicted results by both models and the experimental results of **Flory and Erman (1982)** and **Erman and Flory (1982, 1983a, 1983b)** for the stress-stretch response. **Figure II.2.b.** exhibits the birefringence stretch as predicted by the two models where we observe a small deviation (about 10% at a stretch of 1.8) between the predictions of the AP model and the experimental results of **Flory and Erman (1982)** and **Erman and Flory (1982, 1983a, 1983b)**.

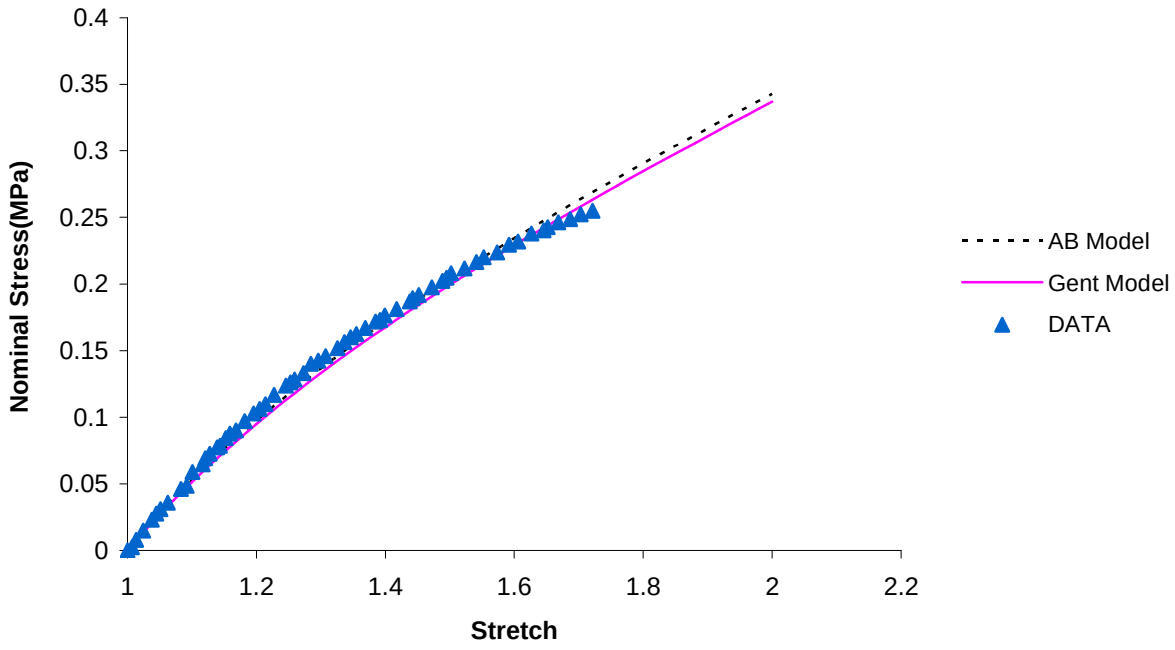

Figure II.2.a: PDMS (B) Stress–stretch response in uniaxial tension.

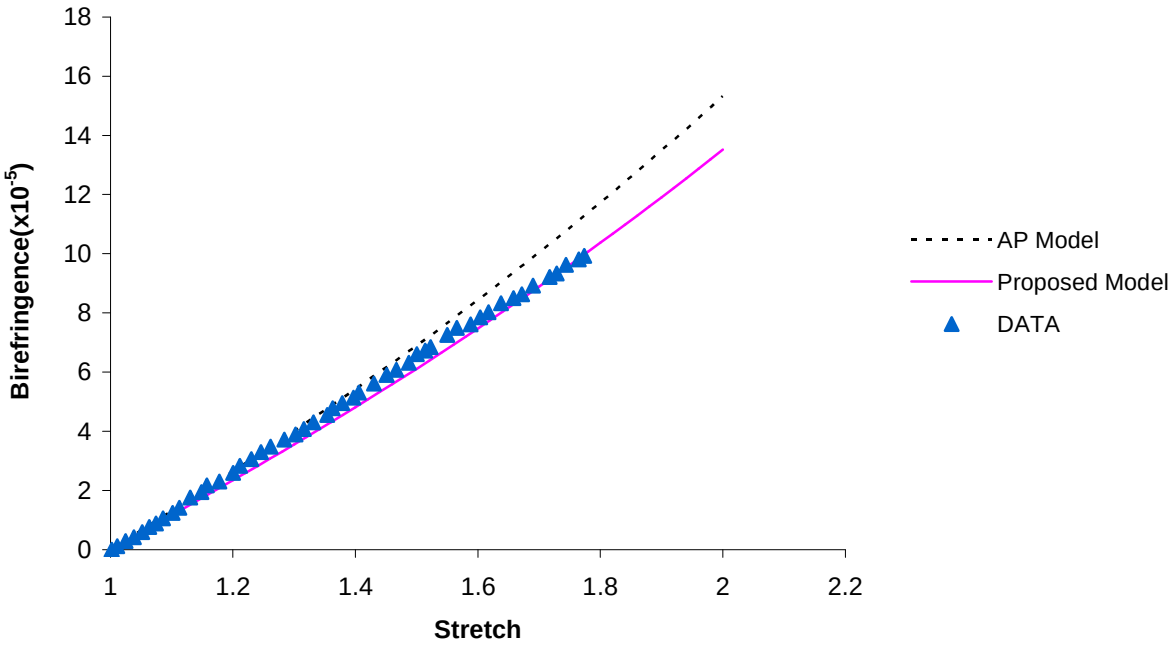

Figure II.2.b: PDMS (B) Birefringence–stretch response in uniaxial tension $\Delta\eta_{1-2} = \Delta\eta_{1-3}$.

Figures II.3 and **Figures II.4** show results for PDMS(C) and PDMS(D) respectively. **Figures II.3.a** and **II.4.a** depict the stress-stretch responses under uniaxial compression (in $\overrightarrow{X_1}$ direction) predicted by the two models in comparison with the experimental results. This comparison shows that the two models predict very close results which are in a good agreement with the experimental data. The similarity of the stress-stretch results from the two models was reported previously by **Boyce (1996)**. **Figures II.3.b** and **II.4.b** show the predicted birefringence evolution with the compressive stretch. We note that the difference between the two models prediction diverge slightly with compressive stretching. In the first stage of compressive stretching, the experimental results seem to be closer the predicted results by our model. As the compressive stretching increases, the prediction of Arruda and Przybylo (AP model) numerical results tend to get closer to the experimental data.

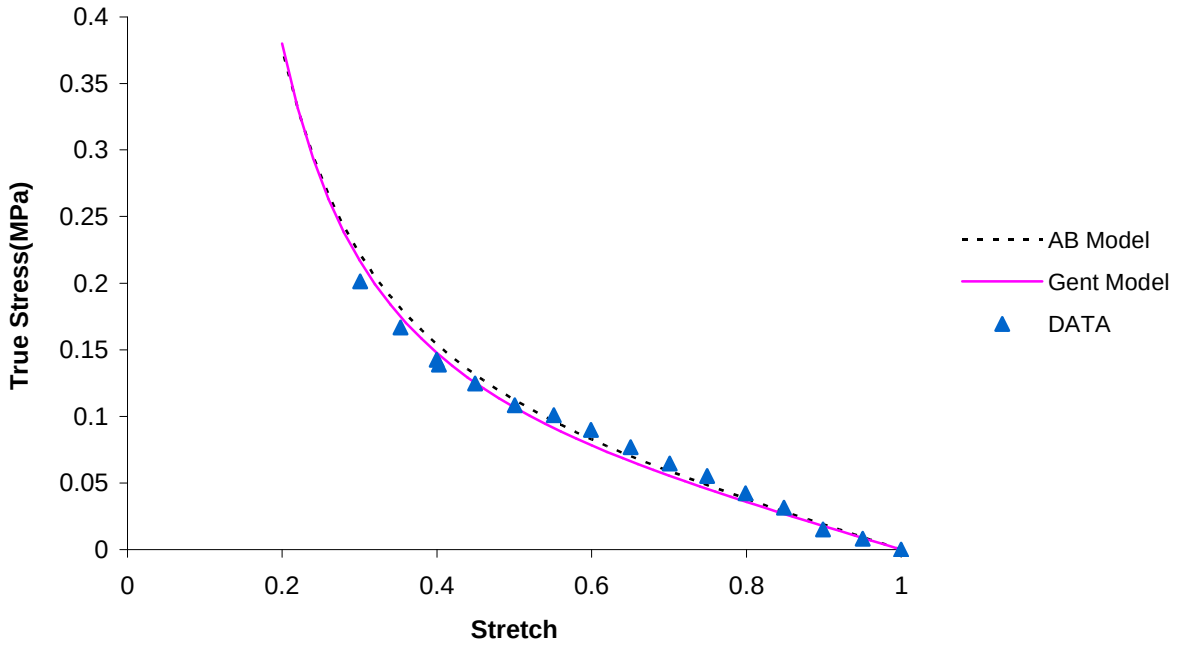

Figure II.3.a: PDMS (C) Stress–stretch response in uniaxial compression.

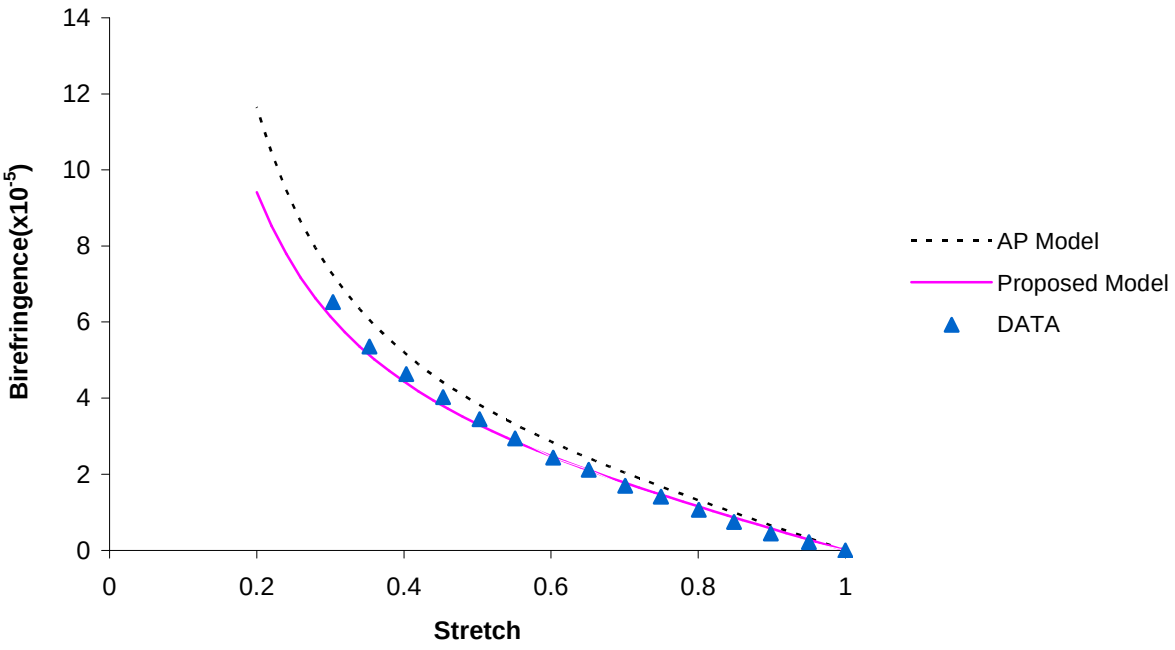

Figure II.3.b: PDMS(C) Birefringence–stretch response in uniaxial compression

$$\Delta\eta_{i-j} = \Delta\eta_{i-j}.$$

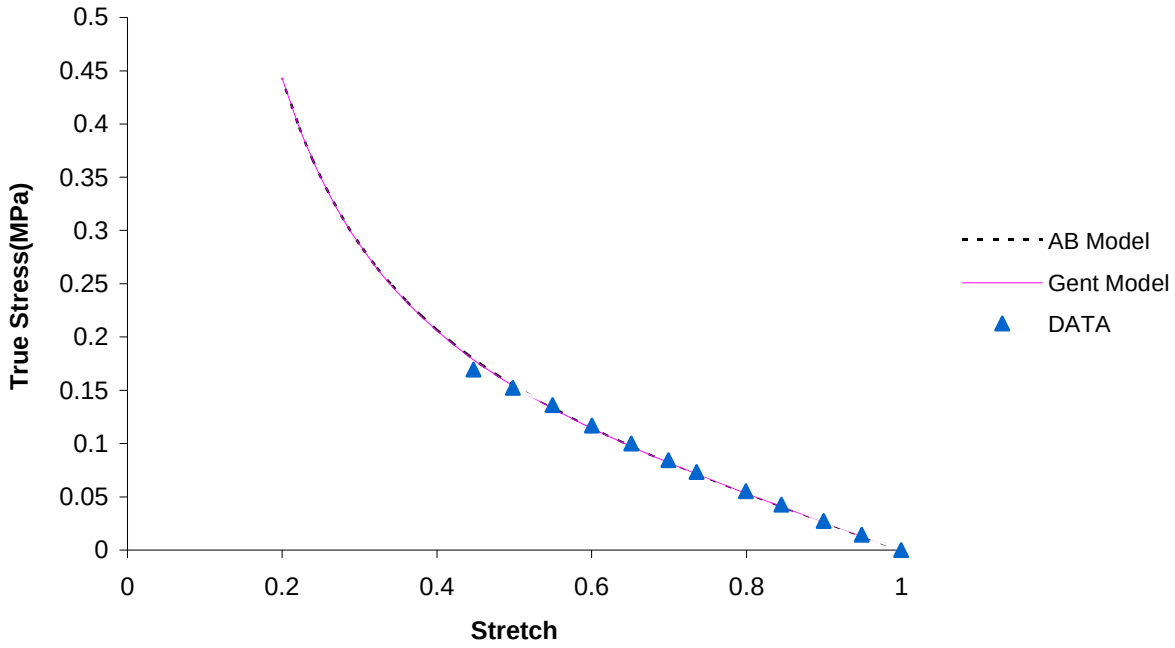

Figure II.4.b: PDMS (D) Stress–stretch response in uniaxial compression.

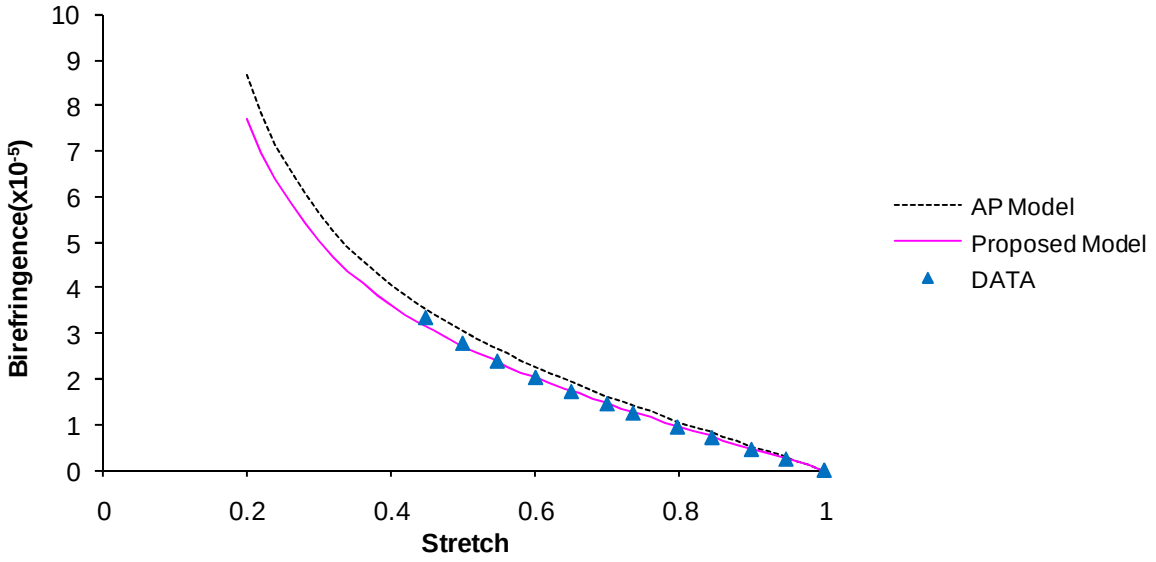

Figure II.4.b: PDMS (D) Birefringence–stretch response in uniaxial compression

$$\Delta\eta_{i-j} = \Delta\eta_{i-j}.$$

Figures II.5 shows the results for natural rubber. **Figure II.5.a** depicts the stress-stretch response and **Figure II.5.b** depicts the birefringence evolution under uniaxial tension (in $\overrightarrow{X_1}$ direction). As shown on these figures, predicted numerical results for the two models show good agreement with experimental data for stretch value below 3.5. For larger stretches, some divergences between these results are obtained where the models seem to slightly overestimate the stress-stretch response and the birefringence evolution data seems to be comprised between the two models predictions.

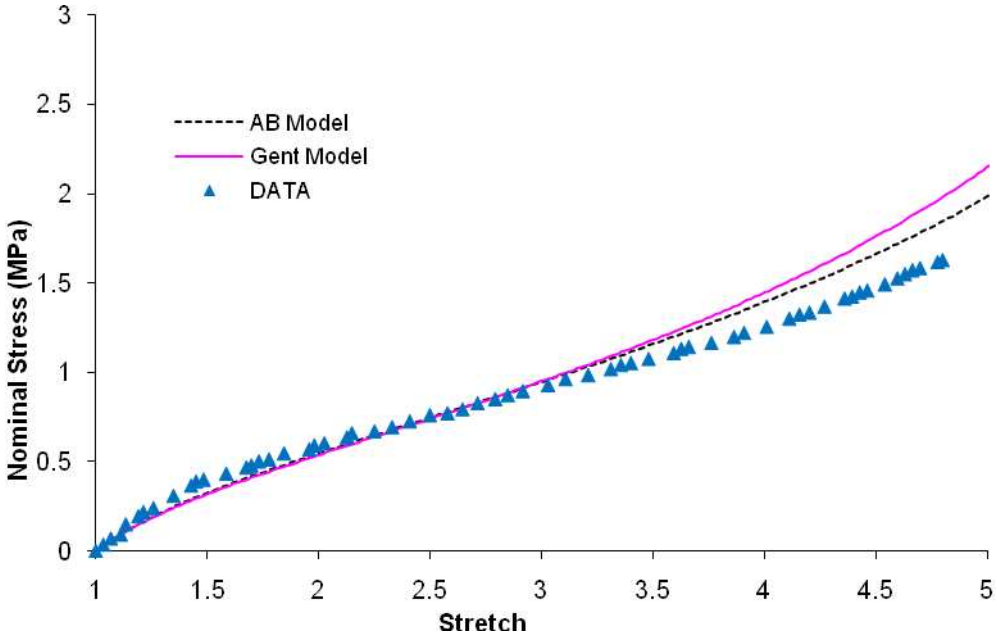

Figure II.5.a: Natural rubber Stress–stretch response in uniaxial tension

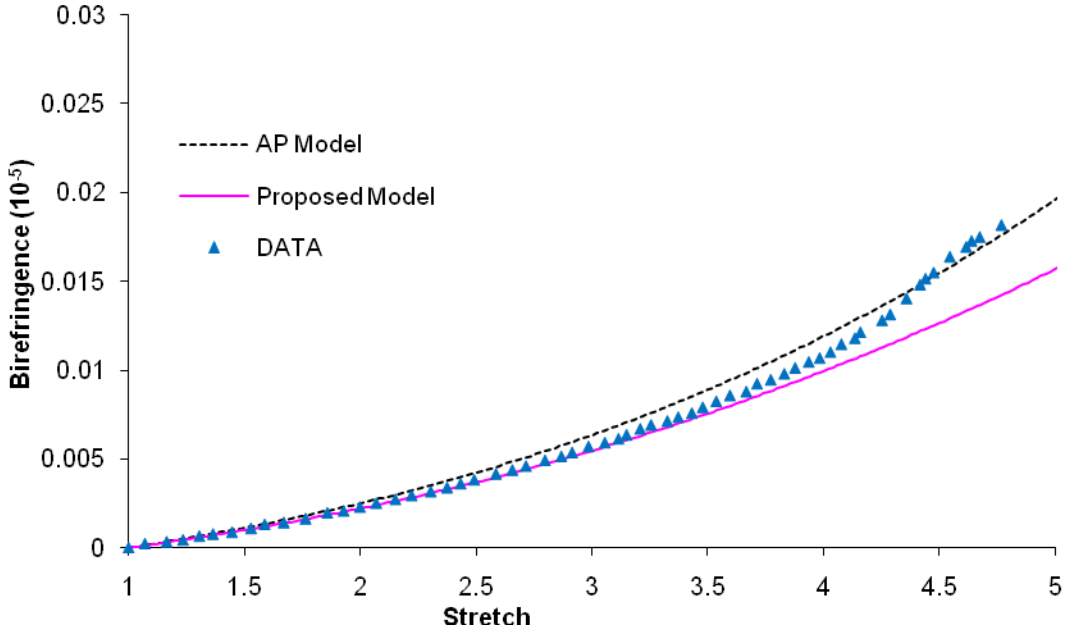

Figure II.5.b: Natural rubber Birefringence–stretch response in uniaxial tension

$$\Delta\eta_{i-j} = \Delta\eta_{i-j}$$

Another way for comparing the birefringence predictions by the two models consists of a comparison of the terms in equations **II.22.a** and **II.23.a** The second terms of the right hand sides of these two equations are similar and yield exactly the same results since the stress evolutions in the two models are shown to be similar. Therefore, the difference resides only in the evolution of the first terms, A and B, of the right hand sides of these two equations. The evolution of A and B under tensile stretching is plotted for a fixed value of N in **Figures II.6** and **II.7.** It is clear that A is constant, B varies with stretching and $A > B$. **Figures II.6** and **II.7** show the evolution of A and B as well and the evolution of their difference $A-B$ for $N=10.89$ and $N=50$, respectively. These curves show that A increases and starts to noticeably deviates from B when the stretch extends to locking stretch which equal to $\sqrt{N}$. The two figures also show that the value of N affects the difference between A and B which decreases when N increases. The difference between A and B is less than 2.10^{-3} and 4.10^{-4} at locking stretch for respectively $N=10.89$ and $N=50$. Therefore, the difference between the two models prediction for birefringence is very small for stretches less than the locking stretch but this difference increases as the stretch extends to the locking stretch.

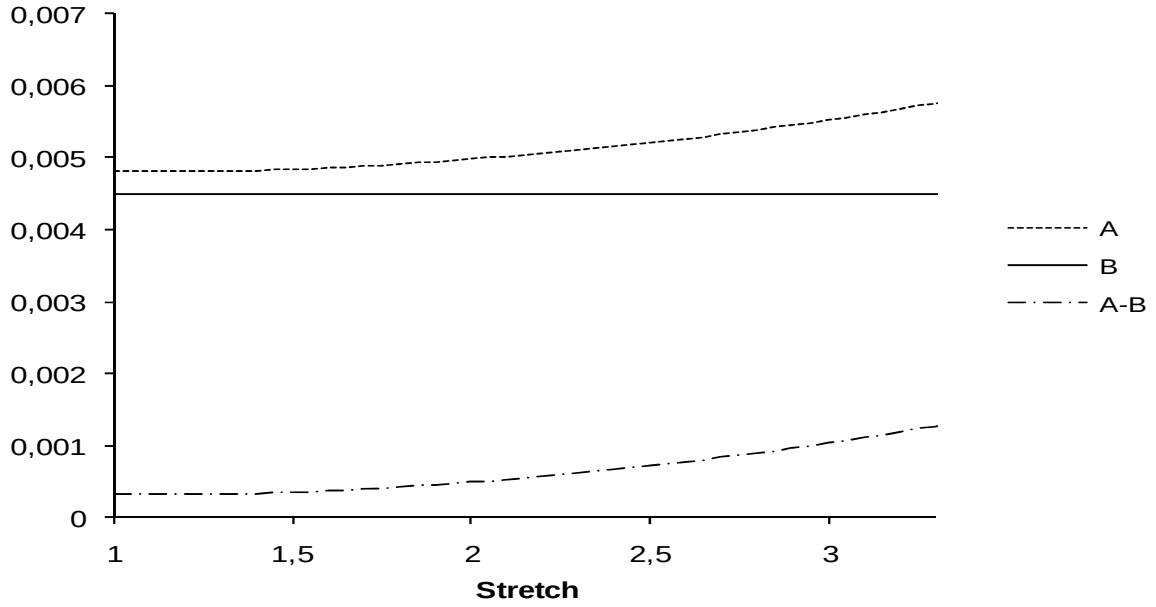

Figure II.6: The difference between expressions A and B for $N=10.89$ or $J_m=29.67$.

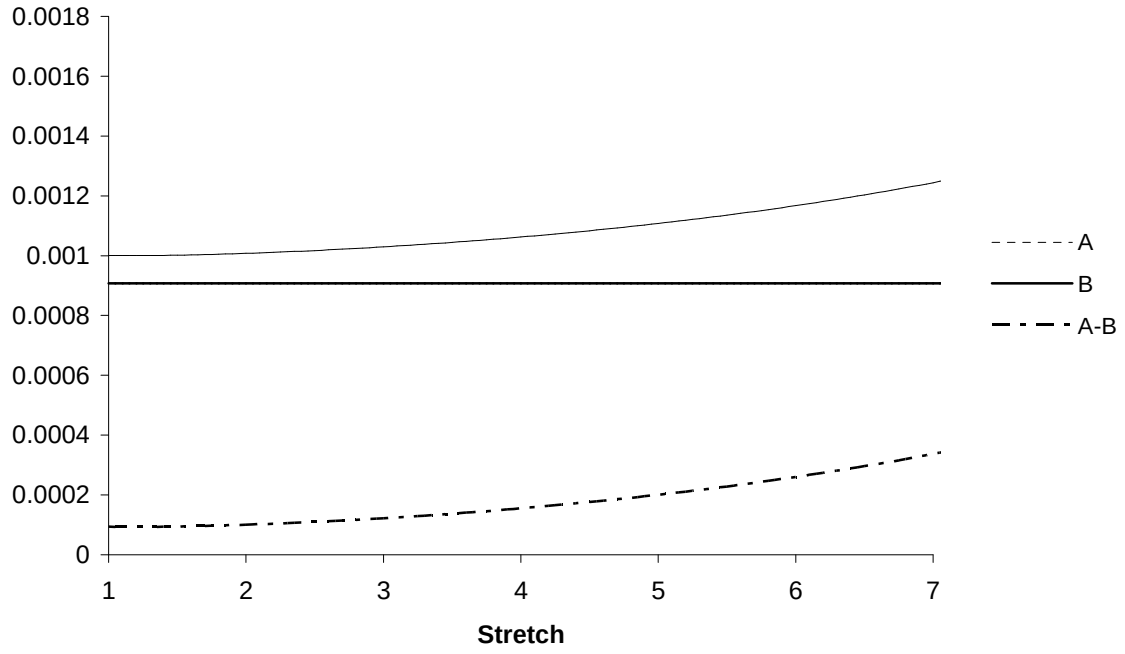

Figure II.7: The difference between expressions A and B for $N = 50$ or $J_m = 147$.

II.3. CONCLUSION

We proposed the formulation of a simplified stress-optic relationship for rubbers. This formulation is based on combining the simpler stress-stretch relationship from the phenomenological Gent model with a Gaussian network theory for birefringence. The obtained stress-optic law is valid for large strains and also includes the non linear behavior. Our results show a fairly good agreement with the experimental data from the literature for the PDMS and natural rubber. Thus, we conclude that our simplified formulation basing on Gent model; can be used to predict optical anisotropy evolution under large strains. These numerical results are nearly equivalent to the predictions from physically-based formulations using the eight-chain model.

Although, Arruda and Przybylo model is physically based of **Arruda and Boyce (1993)** Eight-chain model but Gent model is rather phenomenological; their numerical results are mainly controlled by two parameters N, $\mu = nk_BT$ for Arruda and Przybylo model and J_m, E for Gent model. These parameters are related as shown in equations **II.15** and **II.18** which

leads to similarities in the physics represented by these parameters in the two models and to similar stress-strain response as well as to the closeness of the birefringence results from both models.

CHAPTER III

A CONSTITUTIVE MODEL FOR STRESS-STRAIN RESPONSE WITH MULLINS EFFECT IN FILLED ELASTOMER

For many industrial applications, elastomers have been charged by different kind of fillers like carbon-black in order to improve the material mechanical properties such as stiffness, rupture energy, tear strength, tensile strength, cracking resistance, durability, owed to filler-filler and filler-elastomer interactions. Filled and unfilled elastomers show differences in their stress-strain response under loading. Particularly, strain-induced stress softening phenomenon during cyclic tension, known as Mullins effect (See **Figure III.1**), is more pronounced in filled elastomers. For unfilled elastomers, **Mullins (1947)** experimental data showed that previous stretching has little effect on the stress-strain properties, this implies neglected softening. This phenomenon was observed first by **Bouasse and Carrière (1903)** and several subsequent authors' studies showed that the phenomenon doesn't have one single interpretation. **Blanchard and Parkinson (1952)** and **Bueche (1960, 1961)** suggested that increase in stiffness obtained in filled rubber to be a result of rubber-filler attachments providing additional restrictions on the cross linked rubber network and Mullins effect resulted from the breakdown of macromolecular chains rubber or loosing their links with filler particles.

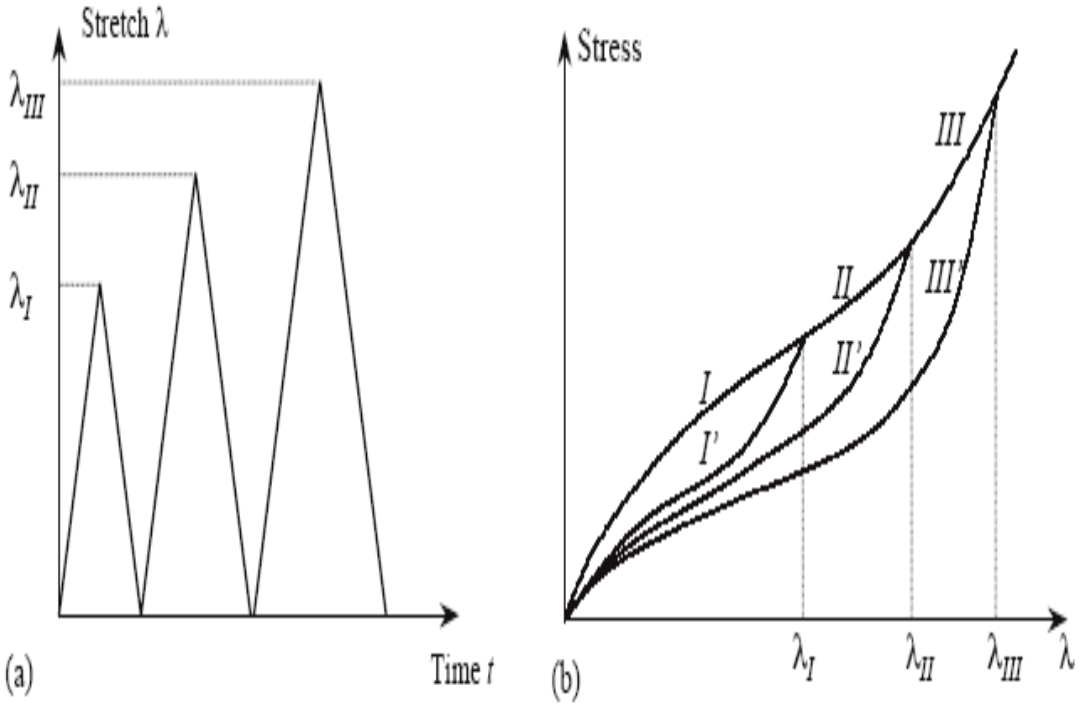

First cycle: $\lambda \to \lambda_I \Rightarrow Loading\ correspond \quad to: I \quad \lambda \to 0 \Rightarrow unloading\ correspond \quad to: I'$

Second cycle: $\lambda \to \lambda_{II} \Rightarrow Loading\ correspond \quad to: I' + II \quad \lambda \to 0 \Rightarrow unloading\ correspond \quad to: I\,I'$

Third cycle: $\lambda \to \lambda_{III} \Rightarrow Loading\ correspond \quad to: I\,I' + III \quad \lambda \to 0 \Rightarrow unloading\ correspond \quad to: III'$

Figure III.1: Macroscopic description of the Mullins effect: (a) Stretching history, (b) stress-stretch. Marckmann et al. (2002).

This idea was extended by other authors like **Simo (1987), Govindjee and Simo (1991, 1992)** by considering chains breakdown in the material network (See **Figure III.2**). Based on this idea of damage induced softening, **Klüppel and Schramm (2000)** also proposed a model for rubber elasticity and stress softening which combines generalized tube model of rubber elasticity with a damage model of stress-induced filler cluster breakdown. **Miehe and Keck (2000)** also developed a superimposed phenomenological material model with damage at large deformation. The constitutive model is decomposed into nonlinear elastic, nonlinear viscoelastic and nonlinear plastoelastic over-stresses which are in parallel (See **Figure III.3**). In this model, the damage is assumed to act isotropically on each branch and their stresses are

in the form $S^b = (1-d)S_0^b\left(C;G^b\right)$ for $b = e, v, p$ and $C = F^tF$ is the current metric. The inelastic stress response is governed by evolution equations for the two reference metric tensors G^v, G^p and the scalar damage variable evolution $\dot{d} = \frac{1}{\eta^d}\left(d^\infty - d\right)\dot{z}$ where η^d is a material parameter, $\dot{z}$ is a rate of the arc length and d^∞ is the saturation.

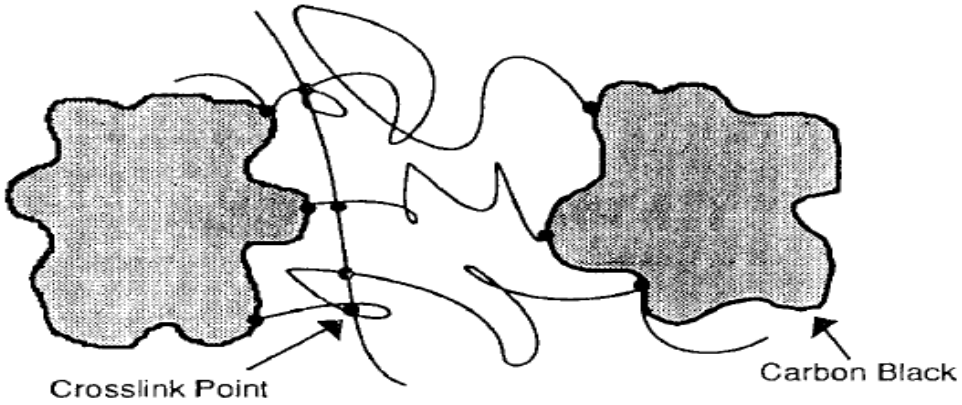

(a)

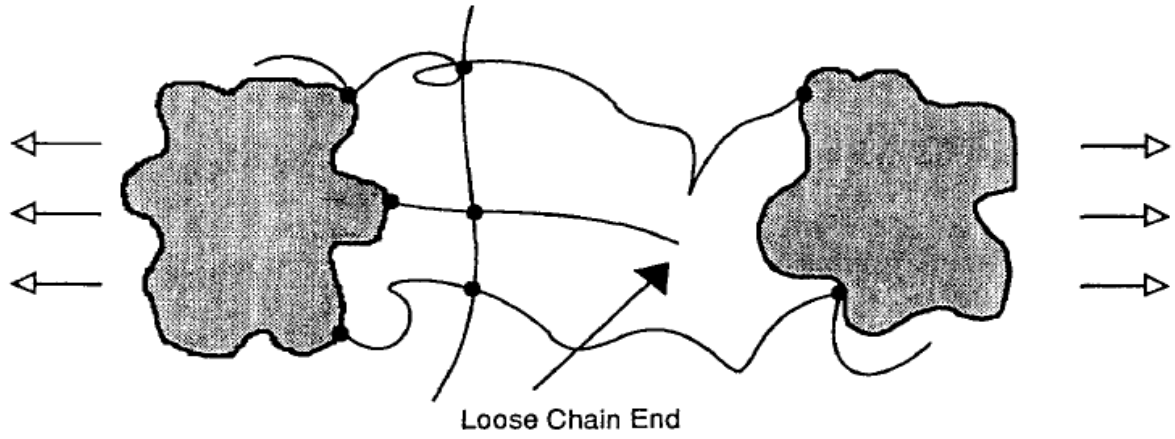

(b)

Figure III.2: Local schematic of two particles in the rubber matrix (a) in the reference state and strained state (b). Govindjee and Simo (1991).

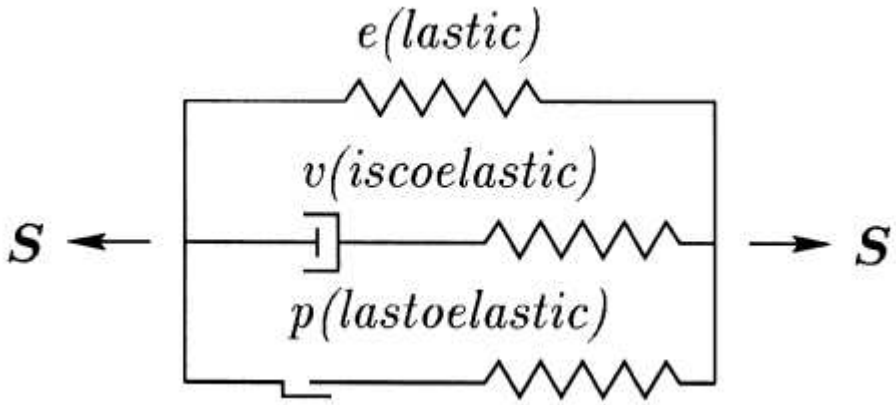

Figure III.3: Superimposed stress response $S = S^e + S^v + S^p$ **with damage. Miehe and Keck (2000).**

Recently, **Marckmann et al. (2002)** proposed a theory of network alteration to explain the Mullins effect (See **Figure III.4**). They assumed that breakdown of chain interactions in the material network decreases macromolecular chains density and increase their length.

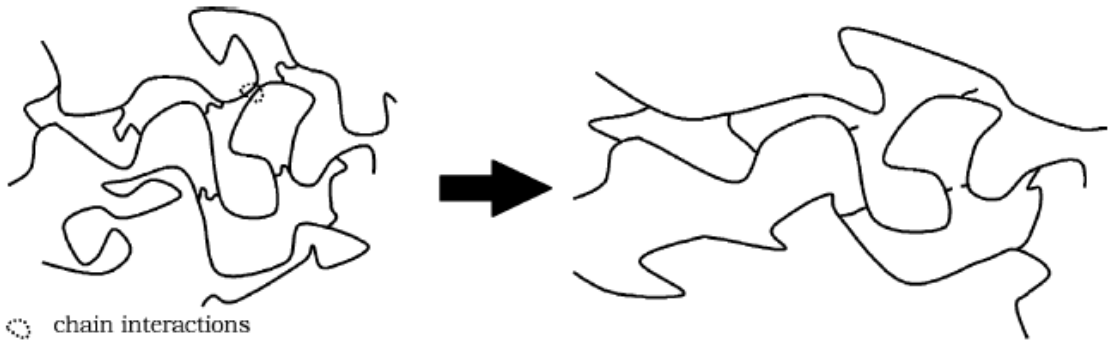

Figure III.4: Weak links and cross-links breakdown. Marckmann et al (2002).

However, for **Mullins and Tobin (1957, 1965)**, **Mullins (1969)** filled rubber is composed of two domains: one hard and another soft. During the application of stress, most deformation happens in the soft domain and the hard one makes neglected contribution to the deformation and may be broken down to form soft domain by the application of stresses in excess of those previously applied. Hence, the soft domain volume increases when stretch becomes high.

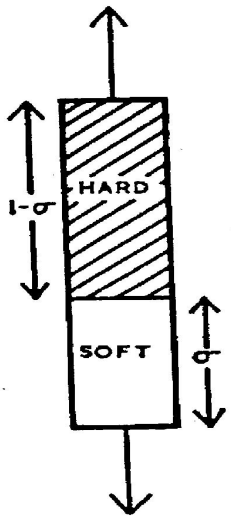

Here, σ is soft domain volume fraction.

Figure: III.5 Mullins and Tobin (1957) model for filled elastomer.

Mullins (1947, 1969) also showed that the samples of filled rubber which were previously stretched have their stress-strain properties approach those of pure rubber due to the destruction of some substantially hard domain which increased the stiffness. In addition, it was also observed a recovery of partially or totally their original stiffness very slowly, several days at room temperature after cyclic loading-unloading. This recovery is accelerated when the temperature is high, **Bueche (1960)**. Hard and soft domain concept is used by **Johnson and Beatty (1993)** where they considered hard domain like cluster of macromolecular chains held together by short chain segments entanglements or intermolecular forces. Hence, during material stretching, chains are pulled from clusters and hard domain is transformed into soft domain. Other observations from **Mullins (1948)**, **James and Green (1975)** showed that softening is not identical in all directions. It is less in perpendicular direction of the stretch than stretch direction.

Based on **Miehe and Keck (2000)** model, **Qi and Boyce (2004)** proposed a constitutive approach using the eight-chain stress-strain response to predict Mullins effect.

The rate of the soft domain evolution is in the following form:

$$\dot{v}_s = A\left(v_{ss} - v_s\right)\frac{\lambda_{chain}^{lock} - 1}{\left(\lambda_{chain}^{lock} - \Lambda_{chain}^{\max}\right)^2}\dot{\Lambda}_{chain}^{\max} \text{ where } \dot{\Lambda}_{chain}^{\max} = \begin{cases} 0, & \Lambda_{chain} < \Lambda_{chain}^{\max} \\ \dot{\Lambda}_{chain} & \Lambda_{chain} \geq \Lambda_{chain}^{\max} \end{cases}$$

and the associated eight-chain stress-strain response is given in the following equation:

$$\sigma = \frac{v_s X \mu}{3}\frac{\sqrt{N}}{\Lambda_{chain}} L^{-1}\left(\frac{\Lambda_{chain}}{\sqrt{N}}\right)B - pI\,.$$

Here, $\Lambda_{chain} = \left[X\left(I_1/3 - 1\right) + 1\right]^{1/2}$, $X = 1 + 3.5\left(1 - v_s\right) + 18\left(1 - v_s\right)^2$ is the amplified factor, $\lambda_{chain}^{lock} = N^{1/2}$ is the locking chain, I_1 is the first invariant of the macroscopic B tensor, v_s is the soft volume fraction, v_{ss} is the saturation value of v_s, $\mu = nk\theta$ is the soft domain modulus, N is the number of rigid links between crosslinks of the soft domain region and A is a fitting parameter.

In addition to filler particle volume fraction, other parameters of fillers can influence their contribution in filled elastomers mechanical response: fillers size, type and shape **(Harwood et al 1965, Mullins 1950)** or the fillers aggregate **(Smallwood 1944, Meinecke and Taftaf 1988)**. These are not generally included in most developed models. Here, the aim of this work is to develop a theory based on filled elastomers microstructure evolution to explain softening phenomena.

III.1. MICROSTRUCTURE BEHAVIOR

Several authors like **Morozov et al. (2010)**, **Heinrich et al. (2002)**, **Vilgis et al. (2009)** showed that filler volume concentration in filled rubber affect the material microstructure. In the microstructure, particles are present in the following states: individual dispersion of primary particle with length scales 20nm-50nm for small concentrations, their cluster gives a filler aggregate with length scales 100nm-200nm, from filler aggregates clustering we obtain filler agglomerate which can build a continuous network of particles.

The microstructure of elastomers reinforced by carbon black can be represented as a system composed of soft and hard domains like in Mullins and Tobin (1957) concept. Here, the volume of the hard domain includes total volume of the filler and the occluded matrix volume which is formed in aggregates of the carbon black particles. The occluded matrix is immobilized by particles within the carbon black agglomerates and increases effectively the initial volume fraction of the hard domain φ_h^0 as: $\varphi_h^0 = \varphi_{oc}^0 + \varphi_f^0$. The terms φ_f^0 and φ_{oc}^0 are the initial volume fractions of the filler and the occluded matrix, respectively. The soft domain corresponds to the elastomeric matrix no occluded by the carbon black agglomerates and aggregates. Its initial volume fraction is denoted by φ_s^0. The occluded volume does not contribute to the deformation of the composite until rupture of the agglomerates or aggregates. So, the released occluded matrix contributes to the deformation as an additional part of the elastomeric matrix. Hence, the transformation of hard to soft domain which implies softening in reinforced elastomers.

Medalia (1970) showed that effective volume occupied by clustering carbon black in a rubber can be obtained by: $\varphi_h^0 = \varphi_{oc}^0 + \varphi_f^0 = \varphi_f^0 p$ with $p = (1 + 0.02139 DBP_{Abs})/1.46$ where $(p > 1)$.

DBP_{Abs} is dibutyl phthalate absorption, where small amounts of DBP are added to dry fillers

until saturation. The DBP_{Abs} is expressed in cm^3 of DBP per 100g filler (cm^3/100g) for each type of carbon filler.

We can therefore get the volume fraction of the occluded domain by:

$$\varphi_{oc}^0 = (p-1)\varphi_f^0 \qquad \textbf{III.1}$$

In unstretched state, the material composition is defined by the following relationships:

$$\begin{aligned} &\varphi_h^0 + \varphi_s^0 = 1, \\ &\varphi_h^0 = \varphi_{oc}^0 + \varphi_f^0, \\ &\varphi_{oc}^0 = (p-1)\varphi_f^0. \end{aligned} \qquad \textbf{III.2.a}$$

During deformation, the composition evolution can be written in the following form:

$$\begin{aligned} &\varphi_h + \varphi_s = 1, \\ &\varphi_h = \varphi_{oc} + \varphi_f, \\ &\varphi_s \geq \varphi_s^0, \\ &\varphi_h \leq \varphi_h^0. \end{aligned} \qquad \textbf{III.2.b}$$

where $\varphi_s, \varphi_h, \varphi_f$ and φ_{oc} are soft domain, hard domain, particles and occluded matrix volume fractions respectively, $\varphi_s^0, \varphi_h^0, \varphi_f^0$ and φ_{oc}^0 correspond to initial values.

We assume that the decrease of the hard domain in the filled elastomers is caused by the deformation during loading but not during unloading or a reloading under previous deformation. We assume that hard domain volume fraction evolution as function of kinematical transformation is given by the following equation during loading:

$$\frac{d\varphi_h}{d\varepsilon} = -K_{hs}\varphi_h + K_{sh}\varphi_s \qquad \textbf{III.3}$$

where K_{hs} and K_{sh} are kinetic coefficients defined by **Oshmyan et al. (2006)** which are the transformation from hard-to-soft and soft-to-hard domains. They are defined by:

$$\begin{cases} K_{hs} = k_{hs}^{0} \exp\left(-\dfrac{U_{hs} - \gamma\sigma_h}{k_B T} \right) = b_{hs} \exp\left(\beta\sigma_h\right) \\ K_{sh} = k_{sh}^{0} \exp\left(-\dfrac{U_{sh} + \gamma\sigma_s}{k_B T} \right) = b_{sh} \exp\left(-\beta\sigma_s\right) \end{cases} \quad with \quad \beta = \frac{\gamma}{k_B T} \qquad \textbf{III.4}$$

where, σ_h, σ_s are stress in the hard and soft domain, U_{hs}, U_{sh} are activation energies, k_{hs}^{0}, k_{sh}^{0} are pre-exponential coefficients and γ an activation volume. In fact, **Mullins (1969)** observed that several days are needed to recover very slowly the stiffness which is decreased by the softening.

Using the condition of $b_{sh} = 0$, because the recovery time constant is far greater than the time period of interest here. We obtain a simplification of equation **III.3** in as follows :

$$\frac{d\varphi_h}{d\varepsilon} = -K_{hs}\varphi_h \qquad \textbf{III.5.a}$$

After integration of equation III.5.a we get:

$$\varphi_h = \varphi_{oc} + \varphi_f = \varphi_h^{0} \exp\left(-K_{hs}\varepsilon\right) \qquad \textbf{III.5.b}$$

The following expressions are also deduced:

$$\varepsilon \to 0 \Rightarrow \varphi_h \to \varphi_h^{0} \qquad \textbf{III.5.c}$$

$$\varepsilon \to \infty \Rightarrow \varphi_h \to 0 \qquad \textbf{III.5.d}$$

The last two equations **III.5.c** and **III.5.d** show that hard domain volume fraction is bounded by upper and lower bound estimates. However, experimental conditions do not permit the transformation of entire hard domains, particularly in the case of non-deformable particles like carbon black for the applied stress. In this case, $\varphi_f = \varphi_f^{0}$, and only the occluded matrix becomes soft. Then:

$$\varepsilon \to \infty \Rightarrow \varphi_h \to \varphi_f \qquad \textbf{III.5.e}$$

Using equations **III.2.b** and **III.5.b**, we obtain the soft domain evolution in the following form:

$$\varphi_s = 1 - \varphi_h^0 \exp\left(-K_{hs}\varepsilon\right) \qquad \textbf{III.6}$$

where $\varepsilon \to \infty \Rightarrow \varphi_s \to 1 - \varphi_f$

Equations **III.5.b** and **III.6** describe the filled elastomer microstructures evolution during deformation and also explain the softening phenomena produced in the material. In the next part, filled elastomers mechanical behaviors are treated with a reformulated Gent's strain energy which takes into account filler effect and microstructure evolution.

Figure III. 6: Difference of microstructure aggregate before (a) and after (b) deformation.

III.2. MECHANICAL BEHAVIOR

Here, reinforcing fillers effect is taken into account for reformulation of Gent strain energy which is limited to unfilled elastomers, in order to extend this model into reinforced ones. Hence, the microstructure evolution which happens during deformation is introduced in the stress-strain relationship. The strain energy, W^*, of reinforced elastomers which present soft and hard domain is found from the strain energy of the deformable domain, W_s, corresponding to the soft domain.

Then:

$$\left.\begin{array}{l} W^* = \varphi_s W_s + \varphi_h W_h \\ here \qquad \varepsilon_h = 0 \end{array}\right\} \Rightarrow W^* = \varphi_s W_s \qquad \textbf{III.7}$$

Using Gent model for the soft domain which is elastomeric material, we obtain the following equation:

$$W_G^* = \varphi_s W_{GS} = -\varphi_s \frac{E_m}{6} J_m \ln\left[1 - \frac{I_{1m} - 3}{J_m}\right] \qquad \textbf{III.8}$$

where W_{GS} is the Gent strain energy for the soft domain and I_{1m} is the average first invariant stretch of this domain.

In filled elastomers, the matrix is prevented from deforming uniformly by adhesion of the rubber to the surface of the particles. Thus, macromolecule deformation is more complex than in unfilled elastomers.

Mullins and Tobin (1965) introduced the notion of strain amplification strain to estimate the uniaxial strain in the matrix for filled elastomers. This relation can be shown when the stress-strain relationship for filled elastomers, $\sigma = E\varepsilon = E(\lambda - 1) = E_m X(\lambda - 1)$, and unfilled elastomers, $\sigma = E_m(\Lambda - 1)$, is considered for the same average stress. Where E and E_m are respectively filled and unfilled elastomer modulus. The amplified stretch expression is therefore deduced as: $\Lambda = X(\lambda - 1) + 1$, where λ is the apparent macroscopic axial stretch in filled rubber and X the amplification factor.

Whereas, **Govindjee and Simo (1991)** proposed amplifying the total deformation gradient in order to obtain the relation between the average volume strain quantities and the matrix quantities. This can be written in the following form: $F_m = (F - \varphi_f R)/(1 - \varphi_f)$ where $F = RU$, F and F_m are respectively the average volume deformation gradients in the material and in the matrix, R the rotation tensor and U the right stretching tensor.

As in the work of **Bergstrom and Boyce (1999)** or **Qi and Boyce (2004)**, we propose to use the amplification of the first invariant stretch I_1 which corresponds to Mullins and Tobin stretch amplification with an extension to a general three-dimensional deformation state:

$$I_{1m} = X\left(I_1 - 3\right) + 3 \qquad \textbf{III.9}$$

where I_1 is the average first invariant stretch in the overall macroscopic of the composite material. Using equation **III.9** in the reinforced elastomers strain energy of equation **III.8**, we can deduce our proposed extension of the Gent strain energy for filled elastomers in this form:

$$W_G^* = -\varphi_s \frac{E_m}{6} J_m \ln\left[1 - \frac{X\left(I_1 - 3\right)}{J_m}\right] \qquad \textbf{III.10}$$

where, $X = 1 + 3.5\left(1 - \varphi_s\right) + 18\left(1 - \varphi_s\right)^2$ is amplification factor used by **Qi and Boyce (2004)** for filled elastomers. From the proposed strain energy for filled elastomers in equation **III.10**, we get the corresponding Cauchy stress tensor:

$$\sigma_G^* = -pI + \varphi_s \frac{E_m X}{3} \frac{J_m}{J_m - X\left(I_1 - 3\right)} B \qquad \textbf{III.11}$$

Where I and B are the unit tensor and the left Cauchy-Green stretch tensor $\left(B = FF^t\right)$.

In summary, the proposed constitutive model for stress-strain behavior of filled elastomers can be summarized by the following constitutive relations:

$$\begin{aligned}
&\sigma_G^* = -pI + \varphi_s \frac{E_m X}{3} \frac{J_m}{J_m - X\left(I_1 - 3\right)} B \\
&X = 1 + 3.5\left(1 - \varphi_s\right) + 18\left(1 - \varphi_s\right)^2 \\
&\varphi_s = 1 - \varphi_h^0 \exp\left(-K_{hs}\varepsilon\right) \\
&\varphi_h^0 = \varphi_f^0 p
\end{aligned} \qquad \textbf{III.12}$$

p was defined at page 67.

III.3. RESULTS

Equations **III.12** which represent the constitutive model are used to predict numerical results for stress-strain response of filled elastomers including soft domain evolution. In the first application, we simulated loading-unloading in cyclic tension. The predicted stress-strain response is shown in **Figure III.7.a**, the corresponding soft domain volume fraction evolution

is shown in **Figure III.7.b.** The selected material parameters are also shown in these figures. **Figure III.7.a** corresponds to the stress-strain behavior with cyclic loading-unloading. The first cyclic shows loading until $\varepsilon = 2$ and unloading to $\varepsilon = 0$. In the second cyclic, we have reloading until $\varepsilon = 3$ and unloading to $\varepsilon = 0$. The third cyclic corresponds to reloading until $\varepsilon = 4$ and also unloading to $\varepsilon = 0$.

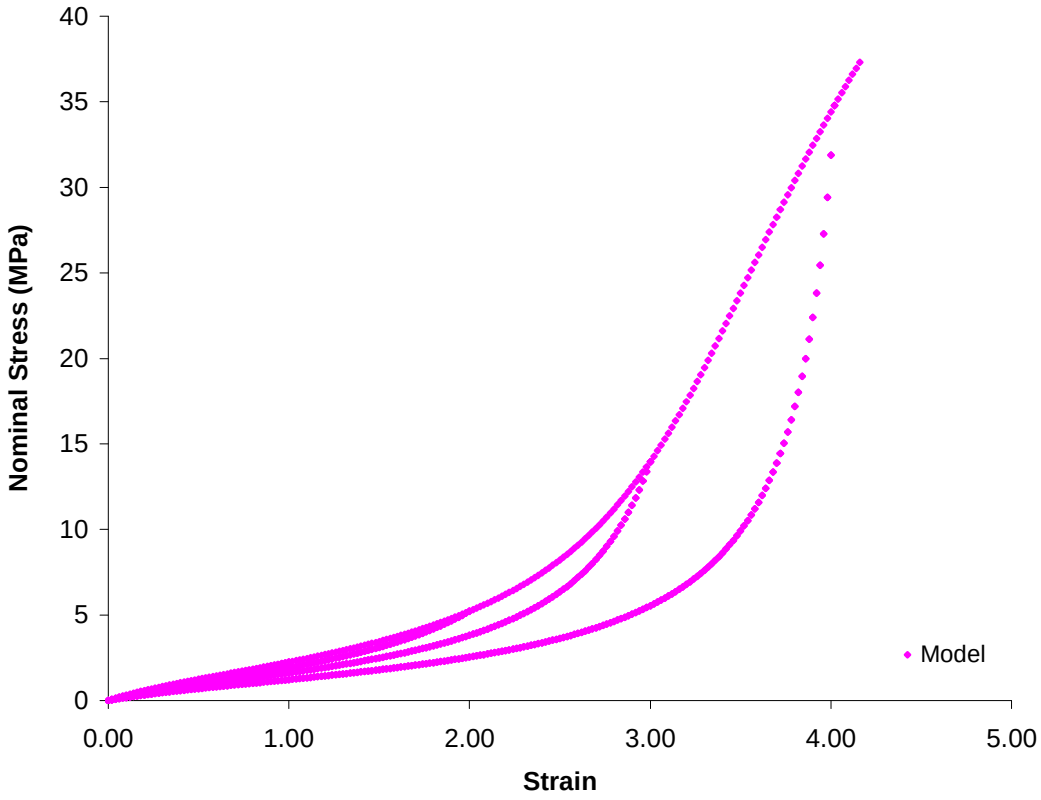

$b_{hs}=0.15s^{-1}$, $\varphi_f=0.19$, $\beta=2.10^{-3}MPa^{-1}$, $E=1MPa$, $J_m=60$, $DBP_{Abs}=120\ cm^3/100g$

Figure III.7.a: Loading-unloading-reloading cyclic for the new constitutive model.

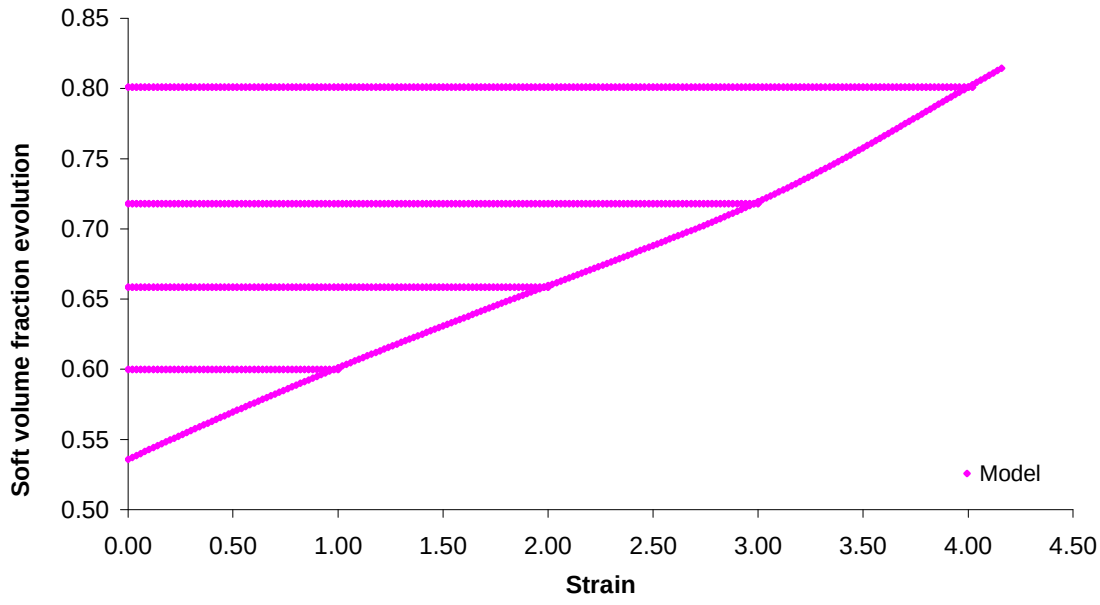

Figure III.7.b: Corresponding soft volume evolution for the new constitutive model during stretching.

In order to validate this model, it is compared to **Mullins and Tobin (1957)** vulcanized materials data for GRS and natural rubbers filled with carbon black S301. DBP_{Abs} for carbon black S301 equal to $113cm^3/100g$ **(Roychoudhury and De (1993))**. These comparisons are reported on **Figure III.8.a** for GRS (Government Rubber Styrene) and **Figure III.9.a** for filled natural rubber. These comparisons show a fairly good agreement between the model predictions and the experimental stress-strain response; their soft volume fraction evolutions are given respectively in **Figure III.8.b** and **Figure III.9.b.**

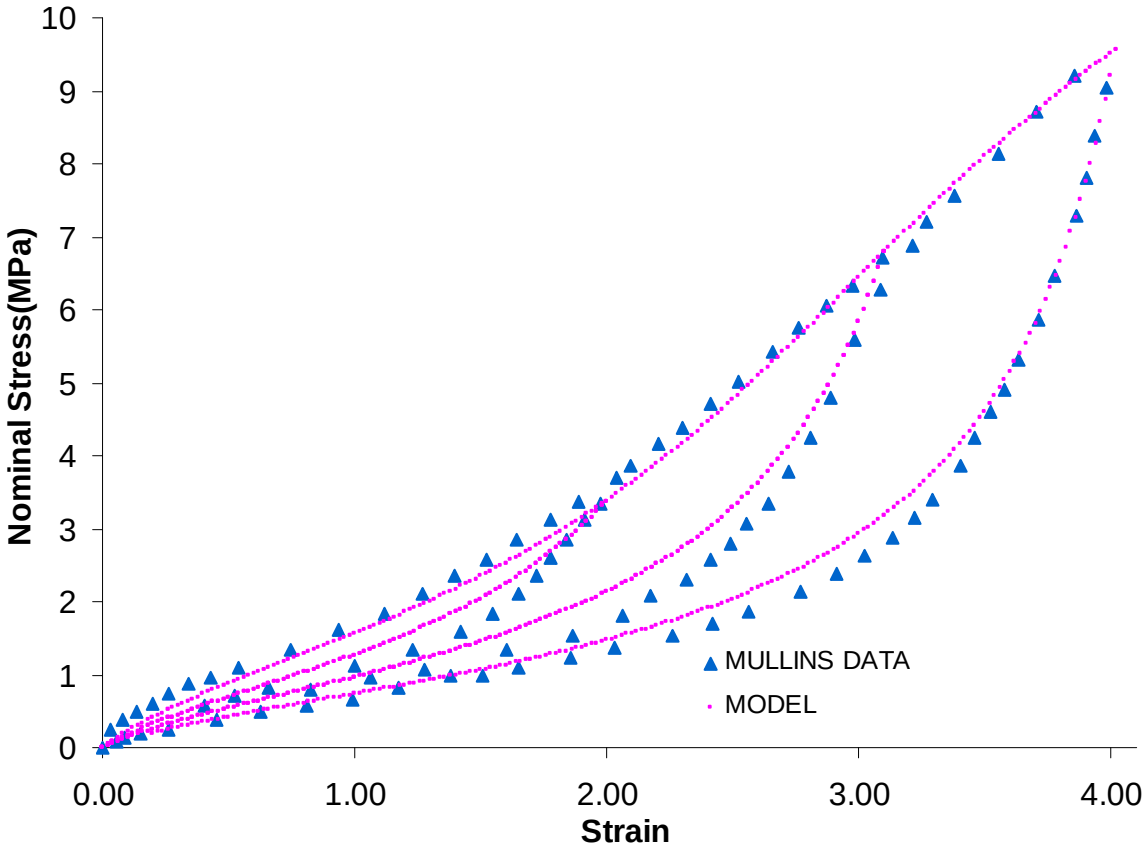

Figure III.8.a: Model compared to Mullins and Tobin (1957) experimental data where GRS is filled by carbon black S301.

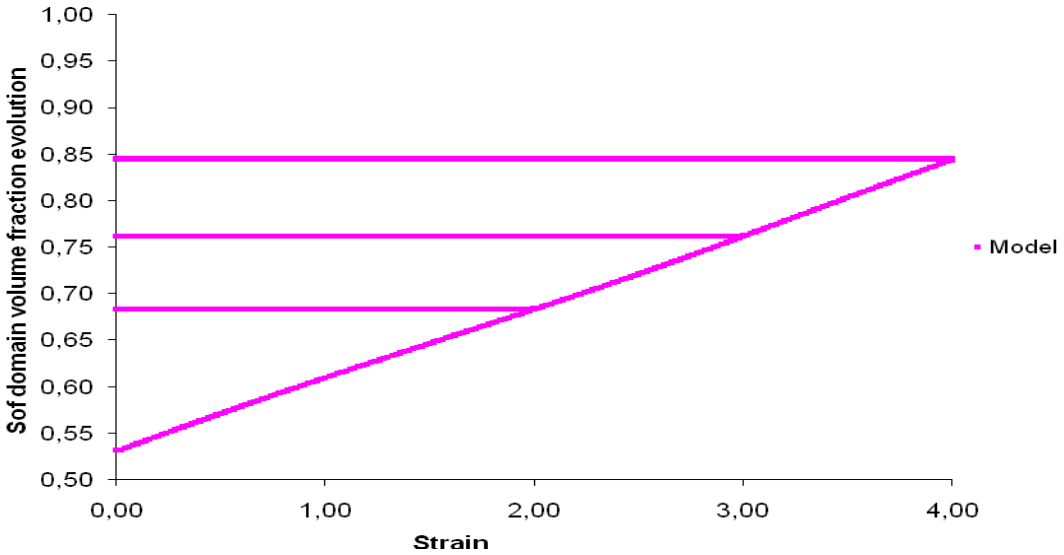

Figure III.8.b: Corresponding soft volume evolution for the constitutive model during stretching.

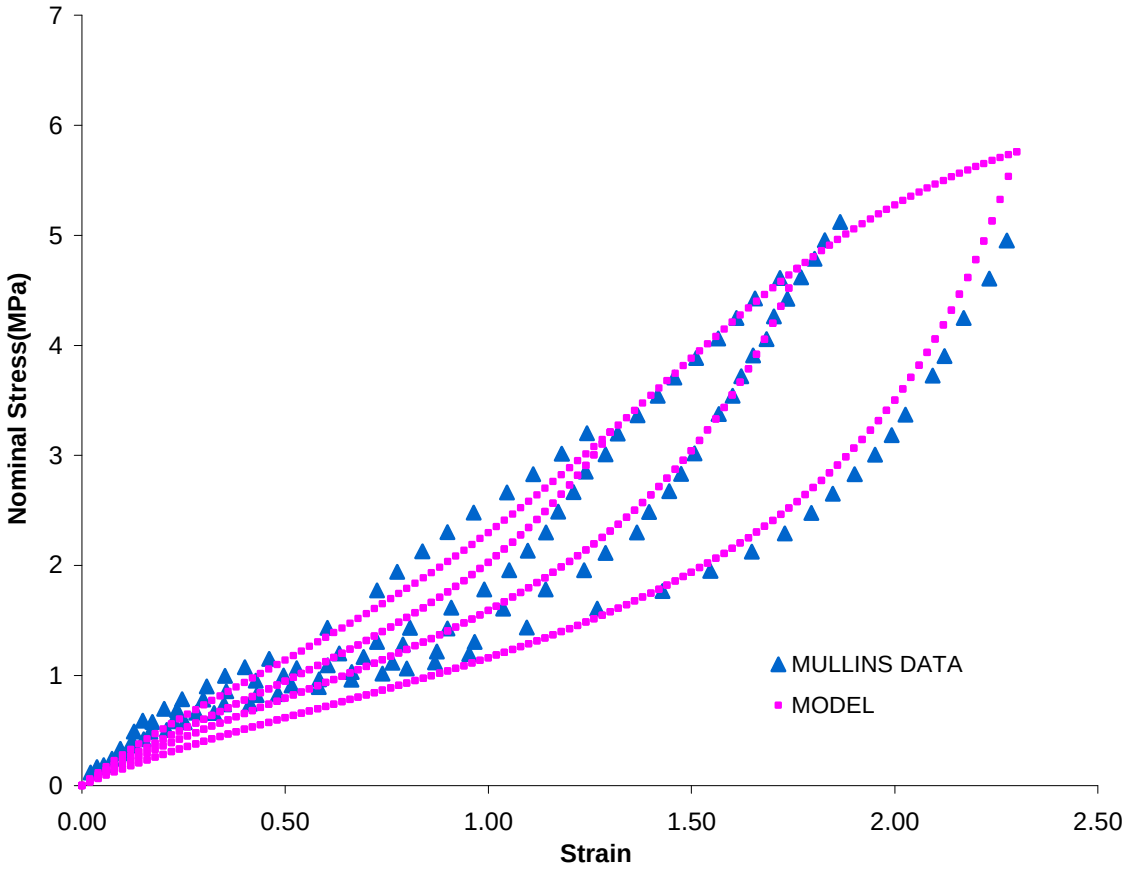

$b_{hs}=0.18s^{-1}$, $\varphi_f=0.19$, $\beta=4.10^{-2}MPa^{-1}$, $E=0.9MPa$, $J_m=28$, $DBP_{Abs}=113\ cm^3/100g$

Figure III.9.a: Model compared to Mullins and Tobin (1957) experimental data where natural rubber is filled by carbon black S301.

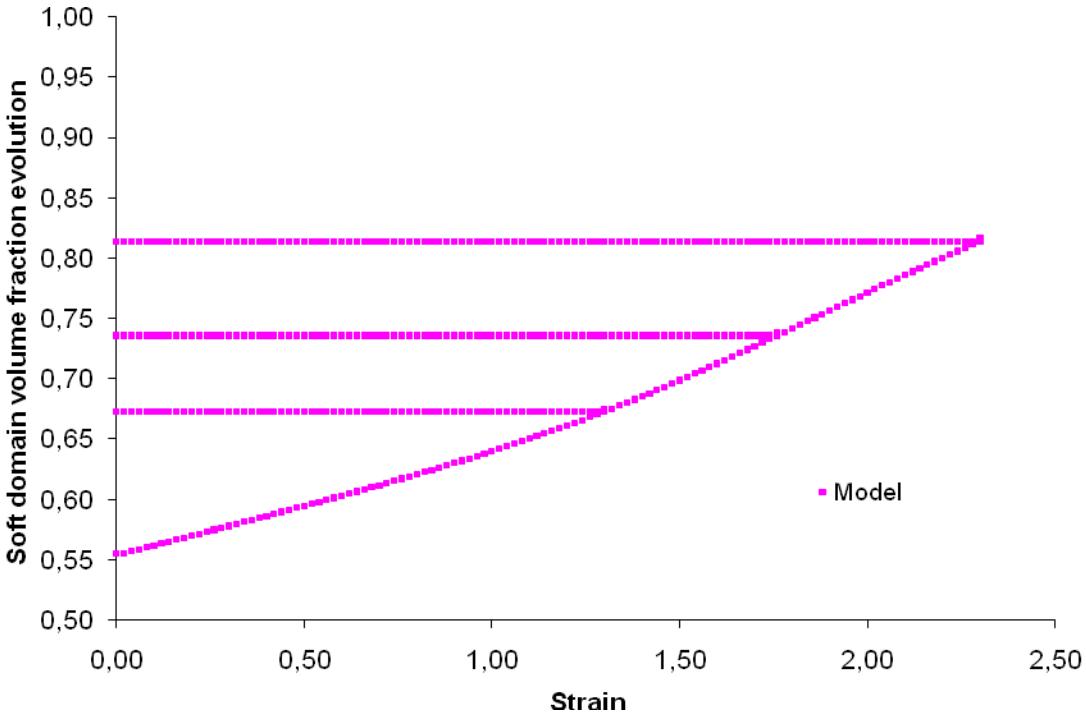

Figure III.9.b: Corresponding soft volume evolution for the constitutive model during stretching.

In our model, the two parameters that characterize the filler particles in the composite are their volume fraction and DBP_{Abs}. In **Figure III.10**, the effect of filler volume fraction is shown by changing its value, 0.1, 0.15 and 0.20. As expected, we can observe in this **Figure III.10** that the higher filler volume fraction leads to a stiffer stress-strain response. In **Figure III.11**, three types of carbon black (N660 (DBP_{Abs}=91 $cm^3/100g$), N550 (DBP_{Abs}=120 $cm^3/100g$), N330 (DBP_{Abs}=101 $cm^3/100g$)) are used for the same filler volume fraction. In this figure, the type of the carbon black affects the stress-strain response. Stiffer response is obtained for carbon black with higher DBP which implies higher volume fraction of the hard domain.

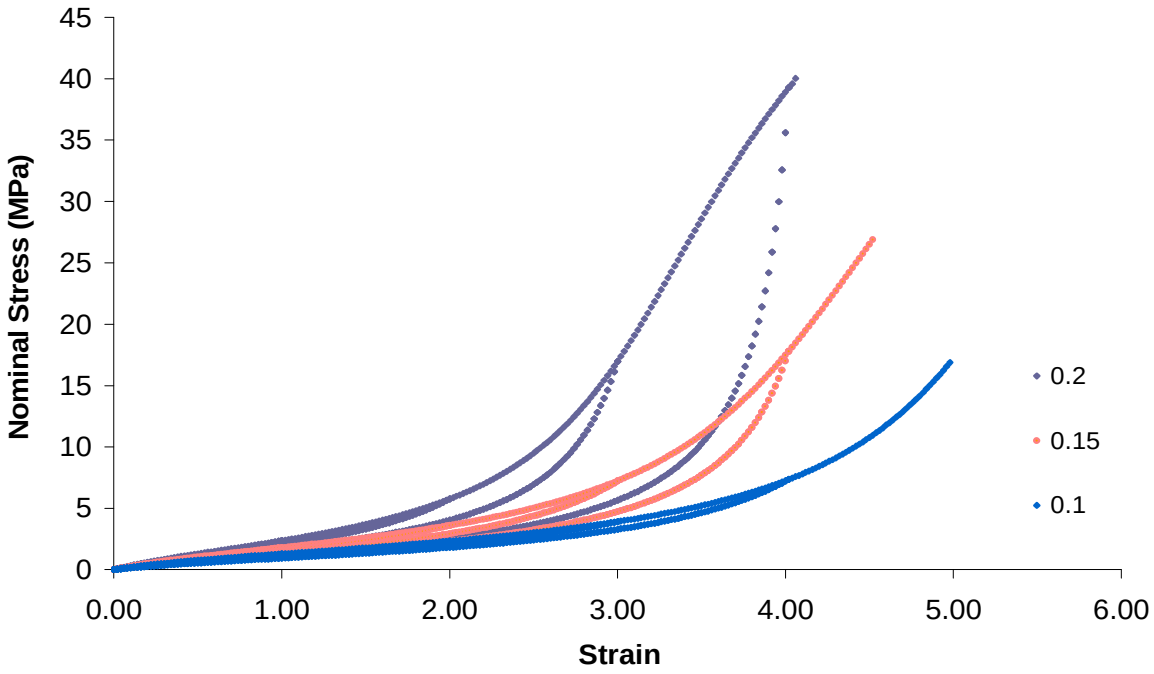

$b_{hs}=0.15s^{-1}$, $\beta=2.10^{-3}MPa^{-1}$, $E=1MPa$, $J_m=60$, $DBP_{Abs}=120\ cm^3/100g$

Figure III.10: Effect of filler volume fraction on the mechanical behavior.

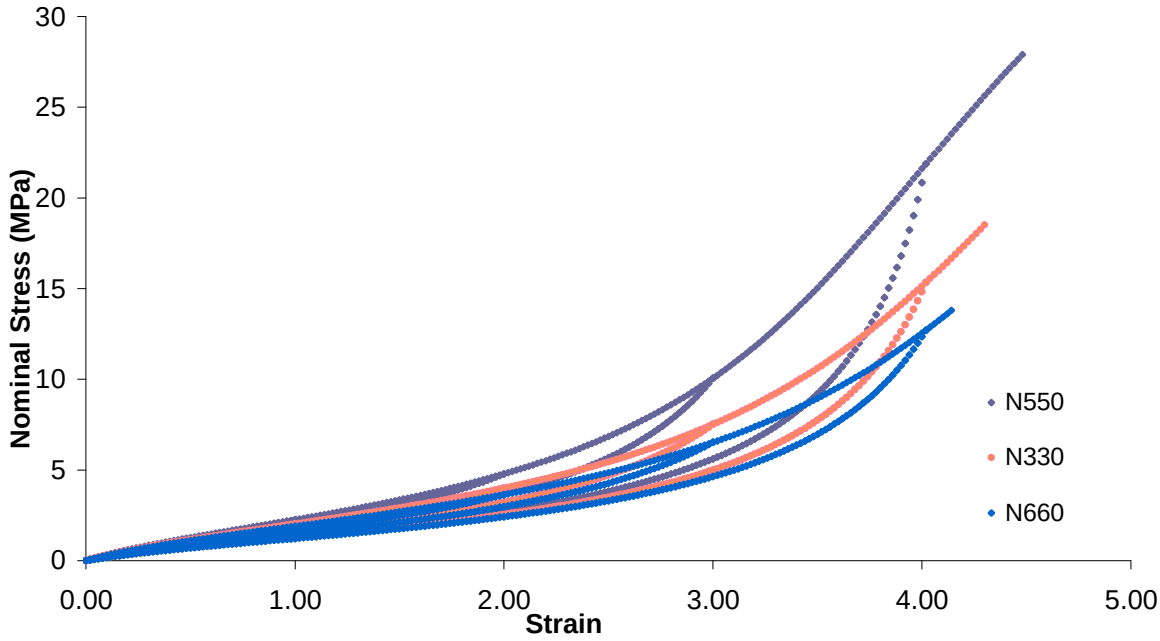

$b_{hs}=0.15s^{-1}$, $\varphi_f=0.20$, $\beta=2.10^{-3}MPa^{-1}$, $E=1MPa$, $J_m=75$, $N660/DBP_{Abs}=91\ cm^3/100g$,

$N330/DBP_{Abs}=101\ cm^3/100g$, $N550/DBP_{Abs}=120cm^3/100g$

Figure III.11: Effect of the type of carbon black on the mechanical behavior.

To verify our model's ability to predict the stress-strain response under different cyclic states of deformation, **Figures III.12.a**, **III.12.b** and **III.12.c** are the predicted results for uniaxial tension where the chains extend in one direction $\left(\lambda_1 = \lambda, \quad \lambda_2 = \lambda^{-1/2}, \quad \lambda_3 = \lambda^{-1/2}\right)$, equi-biaxial tension offers two principal tensile stretching $\left(\lambda_1 = \lambda, \quad \lambda_2 = \lambda, \quad \lambda_3 = \lambda^{-2}\right)$ and plane strain tension $\left(\lambda_1 = \lambda, \quad \lambda_2 = 1, \quad \lambda_3 = \lambda^{-1}\right)$. The corresponding soft domains volume fraction evolutions are shown in **Figure III.12.d**. Our predicted stress-strain response under different cyclic stretching conditions is in accord with the results obtained by **Qi and Boyce (2004)**

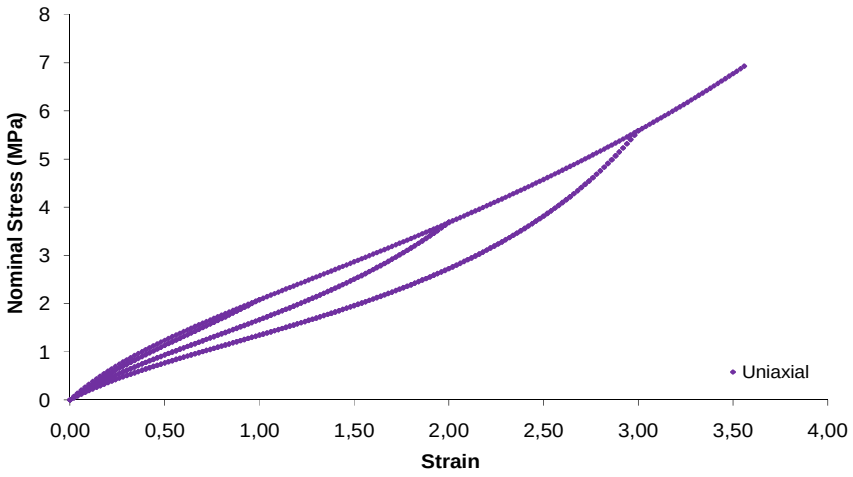

b_{hs}=0.24s^{-1}, φ_f=0.2, β=2.$10^{-3}$$MPa^{-1}$, E=1MPa, J_m=75, DBP_{Abs}=120cm^3/100g

Figure III.12.a: Numerical results under uniaxial tension.

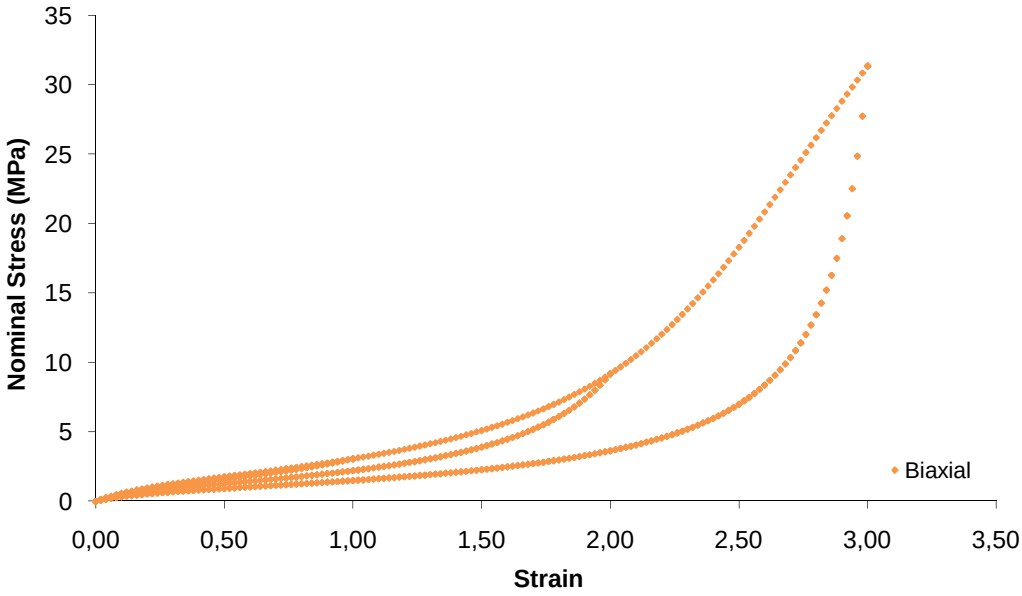

$b_{hs}=0.24s^{-1}$, $\varphi_f=0.2$, $\beta=2.10^{-3}MPa^{-1}$,$E=1MPa$, $J_m=75$, $DBP_{Abs}=120cm^3/100g$

Figure III.12.b: Numerical results under equi-biaxial tension.

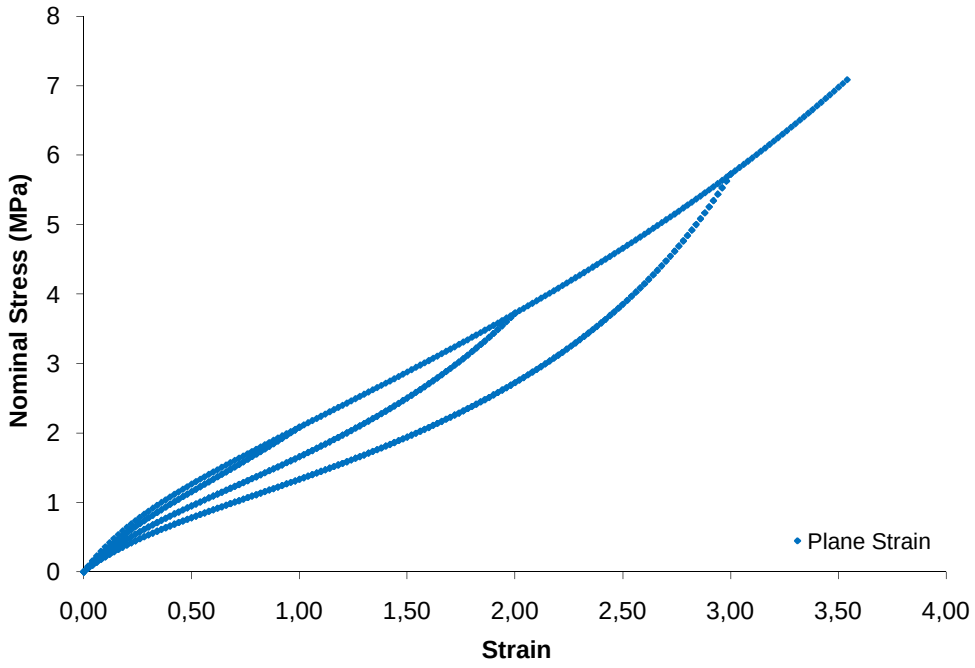

$b_{hs}=0.24s^{-1}$, $\varphi_f=0.2$, $\beta=2.10^{-3}MPa^{-1}$, $E=1MPa$, $J_m=75$, $DBP_{Abs}=120cm^3/100g$

Figure III.12.c: Numerical results under plane strain tension.

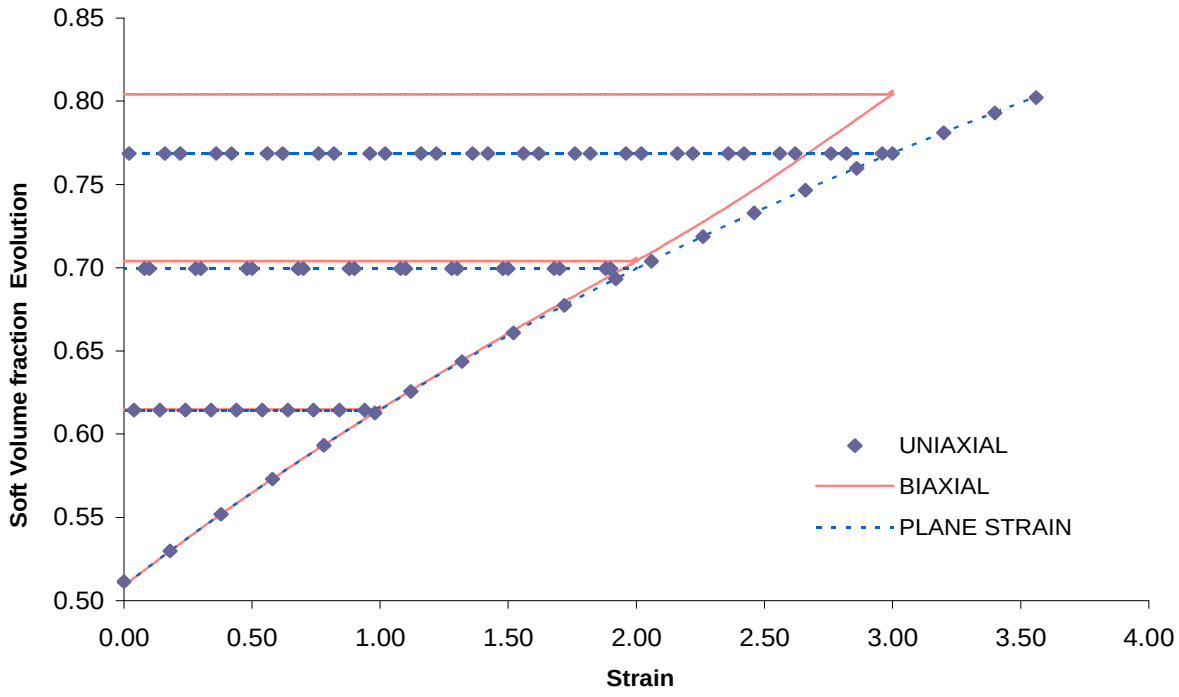

Figure III.12.d: States deformation effect on the soft volume evolution in the microstructure.

III.4. CONCLUSION

The combination of the extended Gent model with a new kinematic model for phase transformation leads to a simple and original approach that correctly predicts the stress-strain behavior which takes into account Mullins effect for filled elastomers. The proposed model takes into account the type of carbon black via the DBP_{Abs}. Although neglected here, this model has the ability to predict stiffness increase which happens slowly by setting b_{sh} different to zero. This is not possible with damage theories based only on the breakdown of elastomers links of **Govindjee and Simo (1991)** or **Marckmann et al. (2002)**. For isotropic softening, the approach can also be easily implemented in computational codes such as FEM. The constitutive model gives a fairly good agreement with experimental data from the literature and also proves its ability to be applicable on different states of deformation.

CHAPTER IV

THERMOPLASTIC ELASTOMERS

Thermoplastic elastomers (TPEs) are an interesting class of polymeric materials. They are a copolymer with hard and soft segments like thermoplastic polyurethane elastomer (See **Figure IV.1**) or another class of composite materials made of thermoplastic homopolymer and elastomer (See **Figure IV.2**). For the last case, the thermoplastic polypropylene (PP) and ethylene-propylene diene monomer (EPDM) elastomer composite is an example like in the work of **Boyce et al. (2001)**. Then, thermoplastic elastomers are biphasic materials; they possess the properties of glassy or semi-crystalline thermoplastics like processability and properties of cross-linked elastomers like hyper-elasticity. This elasticity comes from the structure of the macromolecules which contain soft segments for copolymers or a dispersed soft phase elastomer forming microscopic droplets in a continuous phase of a hard thermoplastic for TPEs. Thermoplastic elastomers find use in many applications. Advantages offered by TPEs over thermoset elastomers include the following points: Processing is simpler and requires fewer steps, TPEs need little or no mixing with other particles in opposition of thermoset elastomers which must be mixed with curatives, stabilizers, processing aids and others, TPE scrap may be recycled which is not the case for thermoset elastomers scrap which is often discarded, causing environmental problems.

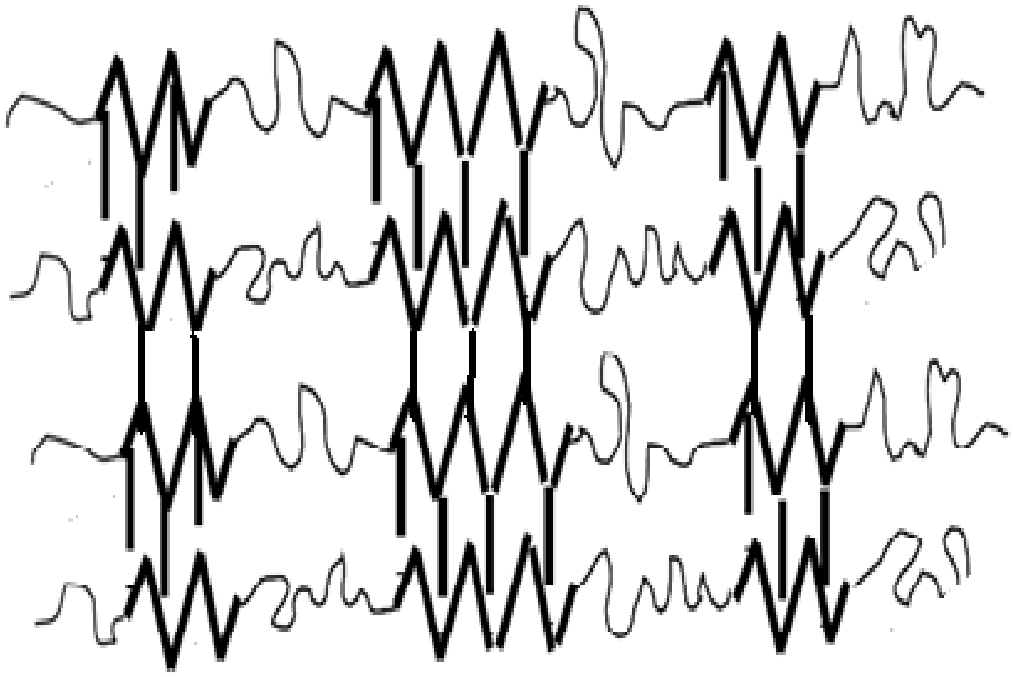

Figure IV.1: Schematic structure of copolymer with hard segments arranged in domains.

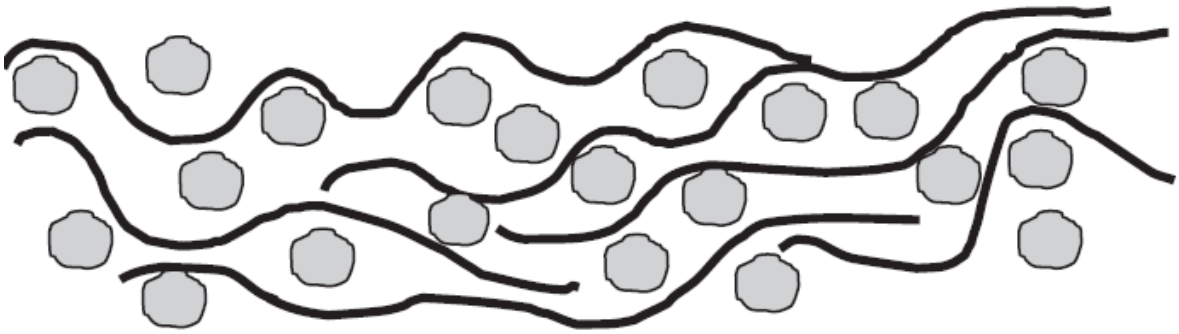

Figure IV.2: Schematic structure compound of rubber particles dispersed in thermoplastic.

IV.1. THERMOPLASTIC POLYURETHANES

Thermoplastic polyurethanes (TPUs) elastomers are copolymer thermoplastic elastomers consisting of urethane monomer which is obtained from the reaction of two molecules containing isocyanate (See **Figure IV.3.a**) and hydroxyl (See **Figure IV.3.b**) functional groups. Bayer-Farbenfabriken established the first commercial thermoplastic polyurethanes in Germany. Their general structure is **–A-B-A-B-** (See **Figure IV.4**), where **A** represents a hard

segment obtained from chain extension of a diisocyanate with a glycol and **B** is a soft segment and originates from either polyester or polyether. The hard segment possess a high glass transition temperature (Tg) or high melting temperature (Tm) like for glassy polymers and a low transition temperature (Tg) for soft segments like in the case of rubbers. The nature of the soft segments affects the final TPUs elastic behavior and low-temperature performance. TPUs based on polyester soft segments have excellent resistance for non polar fluids, high tear strength and abrasion resistance and high resilience, thermal stability or hydrolytic stability for those based on polyether soft segments. The properties of TPUs are largely defined by the ratio between hard and soft phases, hard segments length and their distribution. TPUs are also known for their outstanding abrasion resistance and low coefficient of friction on other surfaces. For these properties, thermoplastic polyurethanes are used for a wide range of applications but still limited by their relatively high mechanical hysteresis in comparison with other elastomers.

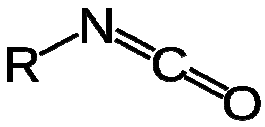

Figure IV.3.a: Isocyanate functional group.

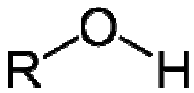

Figure IV.3.b: Hydroxyl functional group.

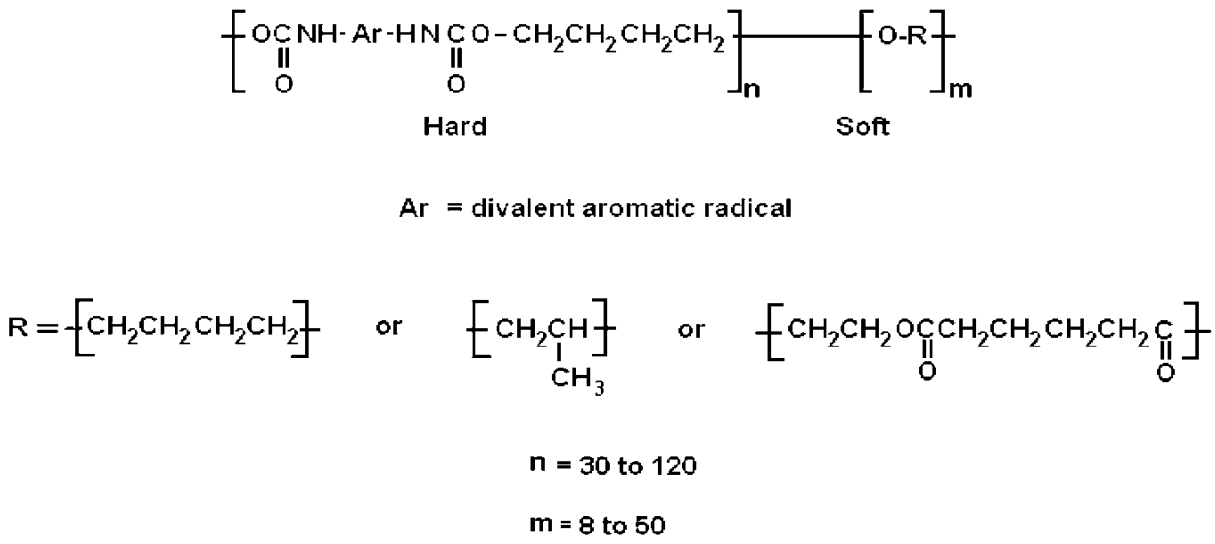

Figure IV.4: TPUs chemical representation.

It has been established by **Ryan et al (1991, 1992)** and **Elwell et al (1994)** that hard segments phase separate in spinodal mechanism or micro phase separation and form hard domains. These domains render TPUs behavior similar to a composite with nanoscale fillers **(Petrovic and Ferguson, 1991)**. From the work of **Aneja and Wilkes (2003)**, **Schneider et al. (1975)**, **Chen-Tsai et al. (1986)**, **Garrett et al. (2001)**, **Halary et al.(2008)**, **O'Sickey et al. (2002)**, it is shown that mesophase separation of hard and soft domains in TPUs is responsible for the versatile properties of this kind of polymer. Several authors **(Qi and Boyce 2005, Yi et al. 2006, Buckley et al. 2010)** studied the thermoplastic polyurethane mechanical behavior. Among them, **Russo and Thomas (1983)** studied a series of polyurethanes with different percent of hard segments. They found that the increase of hard segments in samples implies an increase in both initial modulus and ultimate strength. This shows that hard segments improve mechanical strain-stress response and behave like stiff particles.

IV.2. THREE-DIMENSIONAL CONSTITUTIVE MODEL

IV.2.1. KINEMATICS OF FINITE STRAIN

Currently, finite deformation or transformation method is used for computation of polymer mechanical behavior at large deformation. The deformed configuration state is described by the deformation gradient tensor F, obtained by:

$$F = \nabla x = \frac{\partial x}{\partial X} \qquad \textbf{IV.1}$$

where x are the coordinates of a point in the current configuration state and X are coordinates of a point in the initial configuration state. This deformation gradient can be the combination of plastic and elastic deformation gradients (See **Figure IV.5**) in isothermal conditions.

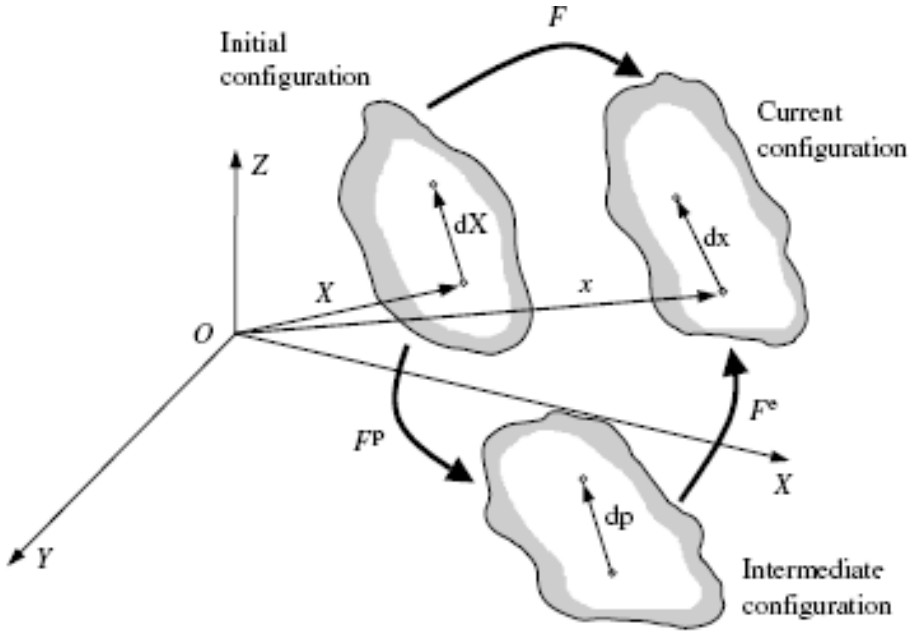

Figure IV.5: F decomposition in plastic F^p and elastic F^e deformation gradient.

In this work, the thermal deformation gradient F^{th} is taken equal to identity I.

$$F = F^e F^{th} F^p = F^e F^p \qquad \textbf{IV.2}$$

where $F^{th} = I$.

The deformation gradient tensor can also be given in polar decomposition which implies that any non-singular second-order tensor can be decomposed uniquely into the product of an orthogonal tensor (rotation) and a symmetric tensor (stretch). Hence, the elastic deformation gradient F^e is decomposed in terms of the elastic stretch tensors V^e or U^e respectively left or right and the elastic rotation tensor R^e in order to separate out stretch and rotation.

$$F^e = V^e R^e = R^e U^e \qquad \textbf{IV.3}$$

The velocity field of the material varies spatially. The increment in velocity dv, occurring over an incremental change in position dx and can be written in the deformed configuration as:

$$dv = \frac{\partial v}{\partial x} dx \qquad \textbf{IV.4}$$

The velocity gradient tensor describes the spatial rate of change of the velocity and is given in the following form:

$$L = \frac{\partial v}{\partial x} \qquad \textbf{IV.5}$$

The velocity gradient can be also written in function of the time rate and the inverse of the deformation gradient:

$$\dot{F} = \frac{\partial}{\partial t}\left(\frac{\partial x}{\partial X}\right) = \frac{\partial v}{\partial X} = \frac{\partial v}{\partial x}\frac{\partial x}{\partial X} = LF \qquad \textbf{IV.6}$$

Hence:

$$L = \dot{F}\, F^{-1} \qquad \textbf{IV.7}$$

The velocity gradient can be decomposed into symmetric and anti-symmetric part:

$$L = D + W \qquad \textbf{IV.8}$$

The symmetric part is called the rate deformation D and the anti-symmetric part the continuum spin W. These tensors are written in function of velocity gradient in the following form:

$$D = \frac{1}{2}\left(L + L^T\right) \qquad \textbf{IV.9}$$

$$W = \frac{1}{2}\left(L - L^T\right) \qquad \textbf{IV.10}$$

IV.2.2. CONSTITUTIVE MODEL

In TPEs or TPUs network structure, we have a rubbery and glassy phase in the same material. The glassy phase, which is hard, is also acting like reinforcing fillers where the increase of hard segments produces modulus rise **(Petrovic and Ferguson, 1991)**. Then, a constitutive model for these materials must take into account behavior of the two phases and also the relationship between them. Hence, we propose a constitutive model with parallel branches corresponding to hyperelastic and elastic-viscoplastic behaviors. A one dimensional model which is constituted by a linear elastic spring $\left(E_2\right)$ for the hyperelasticity behavior part and spring $\left(E_0\right)$ in series with Kelvin model (See **Figure I.6**) for the elastic-viscoplastic part. In this Kelvin model, a nonlinear viscoplastic dashpot $\left(\mu_1\right)$ capturing the rate and temperature is in parallel with a spring $\left(E_1\right)$. The stresses across the two branches are σ_1 for the hyperelastic and σ_2 for elastic-viscoplastic branch and the overall stress in the rheological model is σ (See **Figure IV.6**).

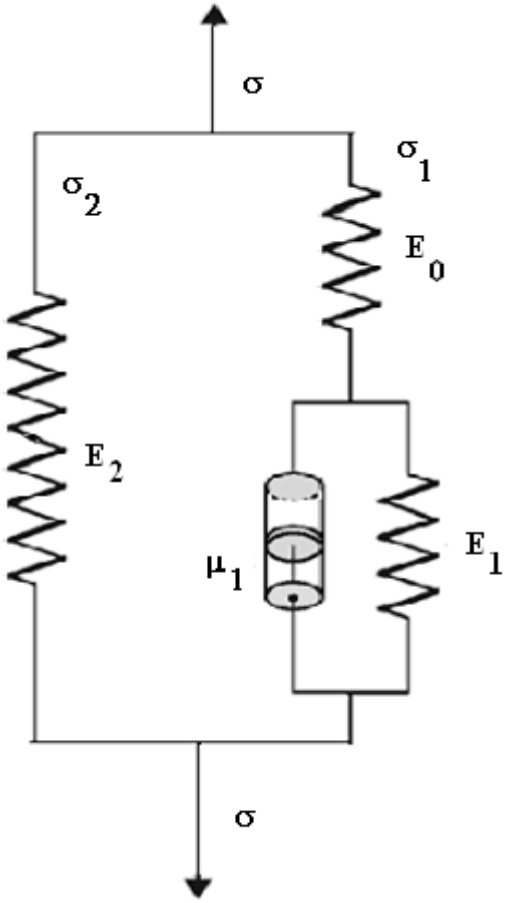

Figure IV.6: Schematic representation of the mechanical model.

The parallel arrangement of the components implies:

$$F_1 = F_2 = F \qquad \textbf{IV.11}$$

where F is the macroscopic deformation gradient, F_1 and F_2 are respectively the glassy network with elastic-viscoplastic behavior and rubbery network with hyperelastic behavior deformation gradient.

The Cauchy stress is given by the following form:

$$\sigma = \sigma_1 + \sigma_2 \qquad \textbf{IV.12}$$

where σ_1 and σ_2 originate respectively from the glassy and rubbery portions whose behaviors are elastic-viscoplastic and hyperelastic.

IV.2.2.1. ELASTIC-VISCOPLASTIC OF THE GLASSY NETWORK BEHAVIOR

Cauchy stress σ_1 in the hard domain is obtained in the following form:

$$\sigma_1 = \frac{\varphi_h}{\det V_1^e} L^e \left[\ln V_1^e\right] \qquad \textbf{IV.13}$$

where L^e is the fourth-order tensor modulus of elastic constants. V_1^e is the left stretch tensor of the elastic deformation gradient tensor F_1^e and φ_h the current hard domain volume fraction in the thermoplastic polyurethane. It decreases during stress and is given by equation **III.5.b** $\left(\varphi_h = \varphi_h^0 \exp\left(-K_{hs}\varepsilon\right)\right)$.

The elastic-viscoplastic deformation gradient F_1 can be decomposed into contribution of elastic F_1^e and viscoplastic F_1^p deformation gradient.

Then:

$$F_1 = F_1^e F_1^p \qquad \textbf{IV.14}$$

The corresponding decomposition of the velocity gradient is:

$$L_1 = \dot{F}_1 F_1^{-1} = \dot{F}_1^e F_1^{e-1} + F_1^e \dot{F}_1^p F_1^{p-1} F_1^{e-1} \qquad \textbf{IV.15}$$

The velocity of the viscoplastic element is obtained in this form:

$$L_1^p = \dot{F}_1^p F_1^{p-1} = D_1^p + W_1^p \qquad \textbf{IV.16}$$

Here, we take $W_1^p = 0$ with no loss in generality as shown by **Boyce et al (1988)**. The rate of deformation D^p is given in the following form:

$$D_1^p = \dot{\gamma}^p N \qquad \textbf{IV.17}$$

N is a normalized tensor aligned with the deviatoric driving stress state and $\dot{\gamma}^p$ denotes the viscoplastic shear strain rate of the viscoplastic element $\left(\mu_1\right)$. These are given in the following equations:

$$N = \frac{1}{\sqrt{2}\tau}\sigma^{*\prime} \qquad \textbf{IV.18}$$

where τ is the equivalent shear stress and $\sigma^{*\prime}$ is the deviatoric form of the driving stress.

Argon and cooperative model are used separately for the viscoplastic shear strain rate evolution to show our model ability for the two:

$$\dot{\gamma}^{p} = \dot{\gamma}_0^{p} \exp\left[-\frac{\Delta G}{k_B T}\left\{1-\left(\frac{\tau}{S}\right)\right\}\right] \textbf{(Argon's model)} \text{ Argon, (1973a, 1973b)} \qquad \textbf{IV.19.a}$$

$$\dot{\gamma}^{p} = \dot{\gamma}_0^{p} \exp\left(-\frac{\Delta H}{k_B T}\right)\sinh^{n}\left[\frac{(\tau - S)V}{2k_B T}\right] \textbf{(Cooperative model)} \text{ Richeton et al (2005)} \qquad \textbf{IV.19.b}$$

where $\dot{\gamma}_0$ is the pre-exponential shear rate factor, ΔG is the zero stress level activation energy, τ is the effective equivalent shear stress, ΔH is the activation energy of the secondary relaxation of mechanical significance, V is the shear activation volume and S is the internal stress which evolves in the following form:

$$\dot{S} = h\left(1-\frac{S}{S_{ss}}\right)\dot{\gamma}^{p} \qquad \textbf{IV.20}$$

The effective equivalent shear stress τ is obtained from the tensorial difference between the Cauchy stress σ_1 and the network stress σ^{N} from the spring (E_1).

$$\tau = \left[\frac{1}{2}\sigma^{*\prime}\cdot\sigma^{*\prime}\right]^{1/2} \qquad \textbf{IV.21}$$

where:

$$\sigma^{*} = R_1^{eT}\left[\sigma_1 - \frac{1}{J}F^{e}\sigma^{N}F^{eT}\right]R_1^{e} \qquad \textbf{IV.22}$$

where σ^{*} is the driving stress state. This portion of the Cauchy stress σ_1 continues to activate the plastic flow and $\sigma^{*\prime}$ corresponds to its deviatoric part. σ^{N} is the network stress. This portion of the Cauchy stress σ_1 captures the effect of orientation-induced strain hardening:

$$\sigma^N = \frac{E_1}{3}\frac{J_{1m}}{J_{1m} - (I_1 - 3)}\overline{B} \qquad \textbf{IV.23}$$

where $\overline{B} = F^p F^{pT} - \frac{I_1}{3} I$

IV.2.2.2. HYPERELASTIC OF THE RUBBERY NETWORK BEHAVIOR

For the hyperelastic network mechanical behavior, we use Gent model for filled elastomers which is developed in chapter III. Because the hard segments act as stiff filler, the material can be considered as composite **(Petrovic and Ferguson, 1991, Qi and Boyce, 2005)**. Then, TPU can be modeled as elastomer reinforced by stiff particles. This implies the introduction of amplified stretch and softening effect in the TPU network behavior. Hence, we have the following expression for the stress in rubbery network:

$$\sigma_2 = (1 - \varphi_h)\frac{E_2 X}{3}\frac{J_{m2}}{J_{m2} - X(I_1 - 3)}B - pI \qquad \textbf{IV.24}$$

where $B = FF^T$

IV.2.2.3. NUMERICAL IMPLEMENTATION

At time zero, the deformation gradient tensors are all unit tensor I and the velocity gradient L is given as a deformation constraint. The stress and strain of the material are equal to zero. The update of the model between the time t and $t + \Delta t$ is presented in **Figure IV.7**.

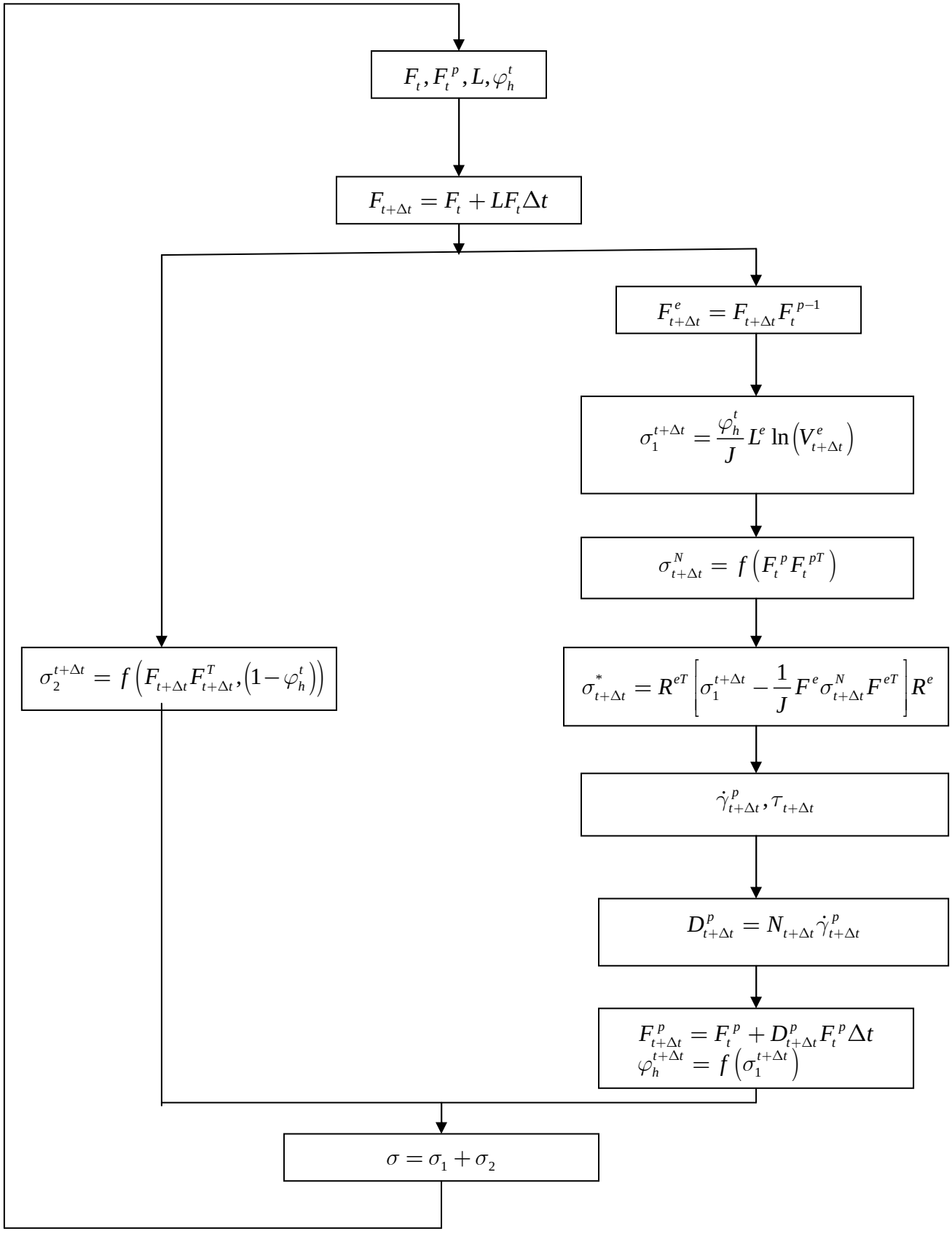

Figure IV.7: Numerical implementation of the constitutive model.

The evolving internal stress S is given by an implicit differential equation **IV.20**. **Figure IV.8** shows a numerical method to get an approximate solution for S at time $t+\Delta t$ by iteration. When $\Delta S = \left| \frac{S_{t+\Delta t} - S_t}{S_t} \right|$ is small than error, we obtain $S_{t+\Delta t}$.

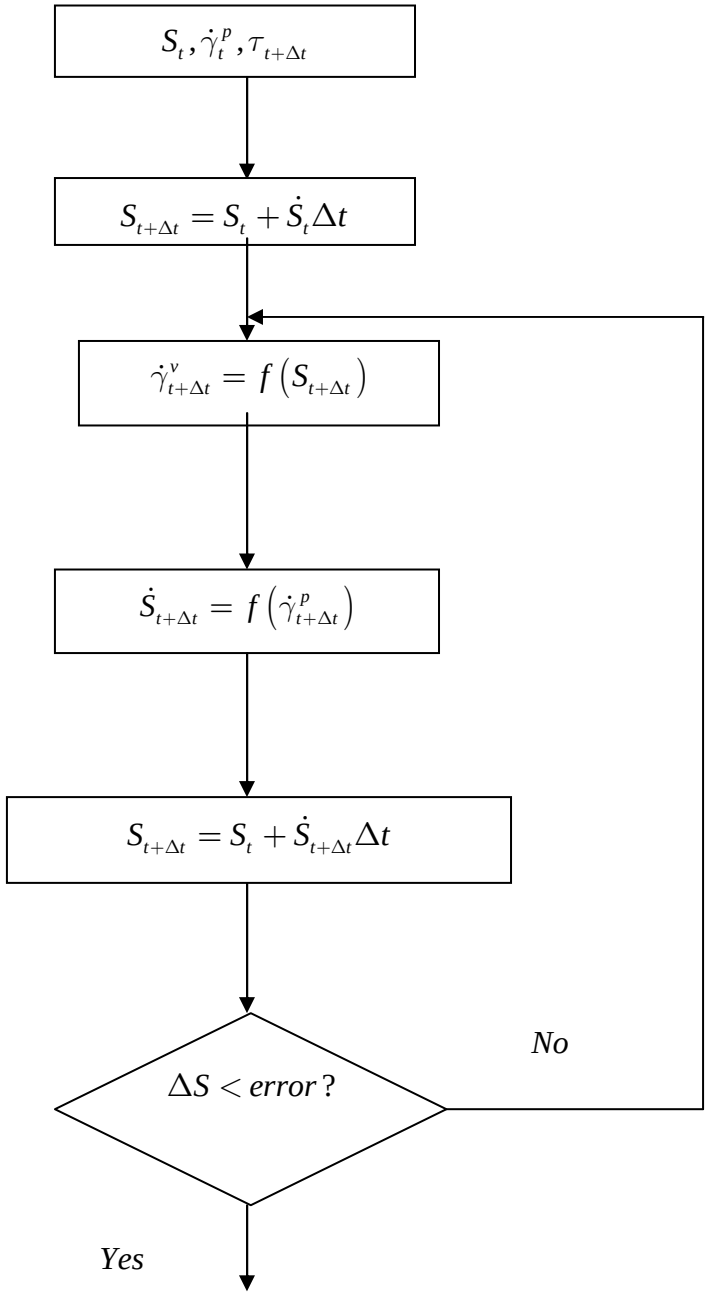

Figure IV.8: Numerical method to solve the implicit Equation IV.20.

IV.3. RESULTS

The three-dimensional constitutive model is implemented to predict stress-strain response as function of the microstructure evolution. The results from the constitutive model are compared to two TPUs experimental data from the literature. The selected data are from the work of **Yi and al. (2006)**. TPUs (TPU(A), TPU(B)) were based on diphenylmethane diisocyanate (MDI, ISONATE) and poly(tetramethylene ether) glycol, mixed with chain extender respectively 1,4-butanediol (BDO) for TPU(A) and 2,2-dimethyl-1,3-propanediol (DMPD) for TPU(B). These materials properties are shown in **Table IV.1**. The experimental data correspond to uniaxial compression at strain rate $\dot{\varepsilon} = 1s^{-1}$. In **Figure IV.9.a** and **Figure IV.10.a** using Argon shear rate evolution and **Figure IV.11.a** and **Figure IV.12.a** using cooperative shear rate evolution, it shows a good agreement with experimental data. The corresponding soft domain evolutions are also shown respectively in **Figure IV.9.b**, **Figure IV.10.b** and **Figure IV.11.b**, **Figure IV.12.b**. During unloading, the soft domain evolution does not return back to strain 0 because we have a viscoplastic deformation in the material.

Table IV.1: Thermoplastic polyurethane samples properties.

Sample	Density (g/mm^3)	Hard segment (wt%)	Chain extender	Tg (°C) DSC	Tg (°C) DMA (1Hz)	Tg shift (°C/decade Strain rate)	T_β(°C)	T_γ(°C)
TPU(A)	1.128	55	DMPD	12	24	4.7	-80	-146
TPU(B)	1.133	44	1,4-BDO	-37	-25	4.6	-80	-144

DMA: Dynamic Mechanical Analysis T_β: Temperature of transition β

DSC: Differential Scanning Calorimetry T_γ: Temperature of transition γ

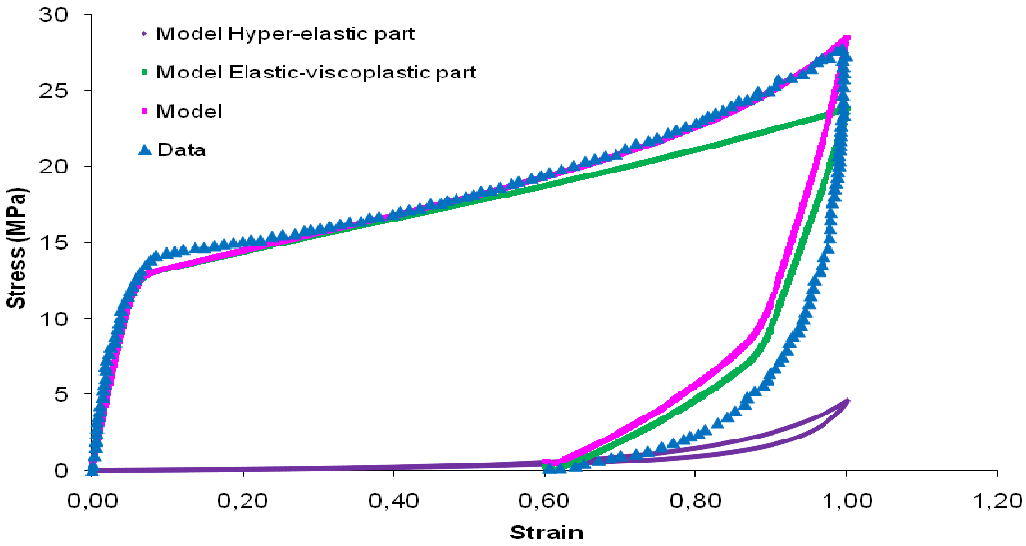

Figure IV.9.a: TPU(A).uniaxial compression response at strain rate $\dot{\varepsilon} = 1s^{-1}$ with Argon shear rate evolution.

$$E_2 = 0.1MPa,\ J_{m2} = 42,\ E_1 = 16,\ J_{m1} = 16,\ \mu = 0.499999,\ \dot{\gamma}_0^p = 1.94.10^5\, s^{-1},$$
$$\Delta G = 0.77.10^{-19}\, J,\ E_{Young} = 300MPa,\ S_0 = 30MPa,\ S_{ss} = 26MPa,\ h = 100MPa,\ \varphi_h^0 = 0.80,$$
$$\beta = 8.10^{-3}\, MPa^{-1},\ b_{hs} = 1.10^{-3}\, s^{-1},\ T = 298.15K.$$

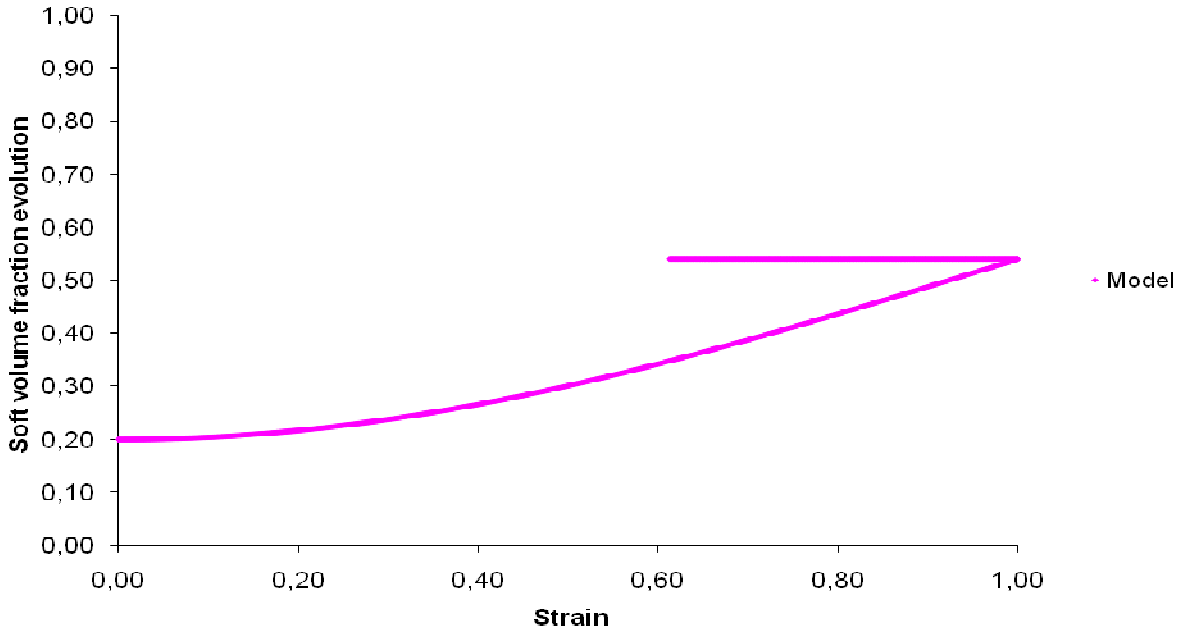

Figure IV.9.b: TPU(A) soft volume fraction evolution for the constitutive model during stretching. $(\varphi_s = 1 - \varphi_h)$

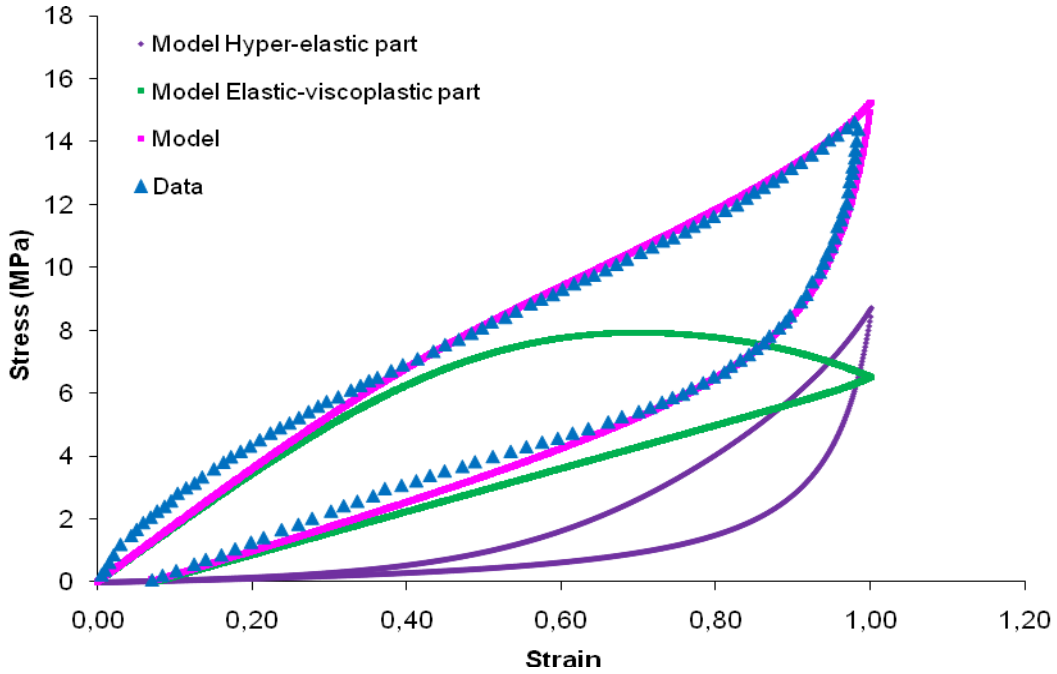

Figure IV.10.a: TPU(B).uniaxial compression response at strain rate $\dot{\varepsilon} = 1s^{-1}$ with Argon shear rate evolution.

$E_2 = 0.2MPa,\ J_{m2} = 21.5,\ E_1 = 0.2MPa,\ J_{m1} = 16,\ \mu = 0.499999,\ \dot{\gamma}_0^p = 1.94.10^{-2}\,s^{-1},$
$\Delta G = 0.77.10^{-19}\,J,\ E_{Young} = 22MPa,\ S_0 = 30MPa,\ S_{ss} = 10MPa,\ h = 100MPa,\ \varphi_h^0 = 0.80,$
$\beta = 0.1MPa^{-1},\ b_{hs} = 1.10^{-3}\,s^{-1},\ T = 298.15K.$

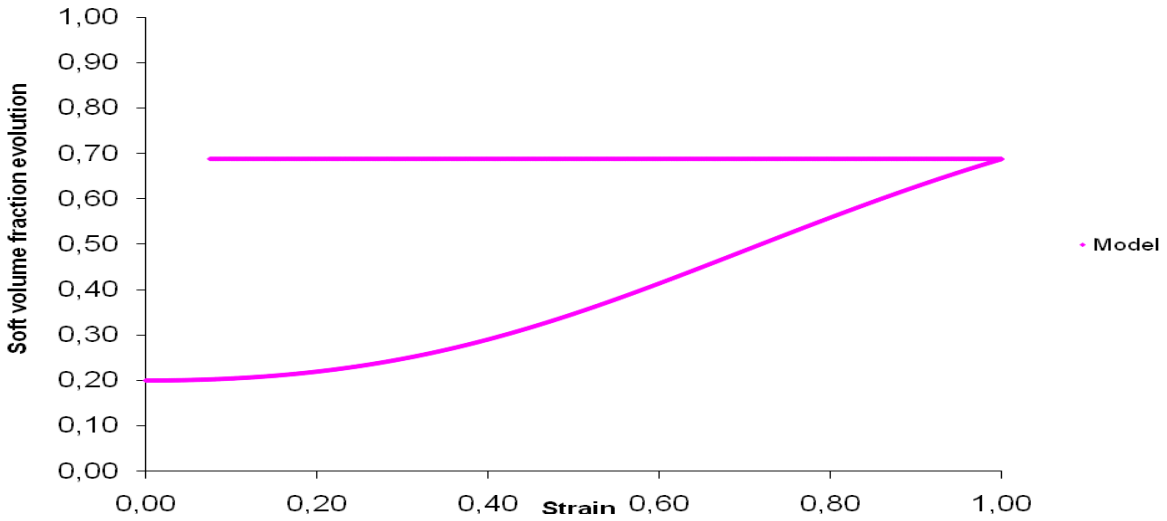

Figure IV.10.b: TPU(B) soft volume fraction evolution for the constitutive model during stretching. $(\varphi_s = 1 - \varphi_h)$

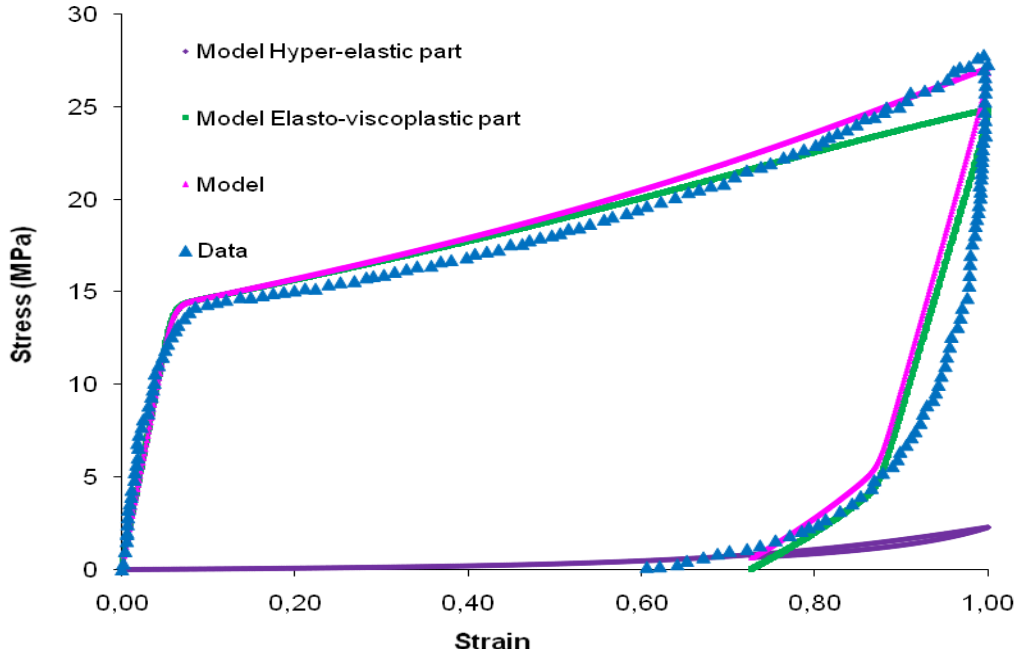

Figure IV.11.a: TPU(A).uniaxial compression response at strain rate $\dot{\varepsilon} = 1s^{-1}$ with cooperative shear rate evolution.

$E_2 = 0.1MPa$, $J_{m2} = 65$, $E_1 = 12$, $J_{m1} = 16$, $\mu = 0.499999$, $\dot{\gamma}_0^p = 1.94.10^{30}\, s^{-1}$,
$\Delta H = 90.10^3\, J$, $E_{Young} = 300MPa$, $S_0 = 5MPa$, $S_{ss} = 1MPa$, $h = 0MPa$, $\varphi_h^0 = 0.80$,
$\beta = 1.10^{-1} MPa^{-1}$, $b_{hs} = 1.10^{-4}\, s^{-1}$, $T = 298.15K$, $n = 8$, $V = 1.10^{-19}\, m^3$.

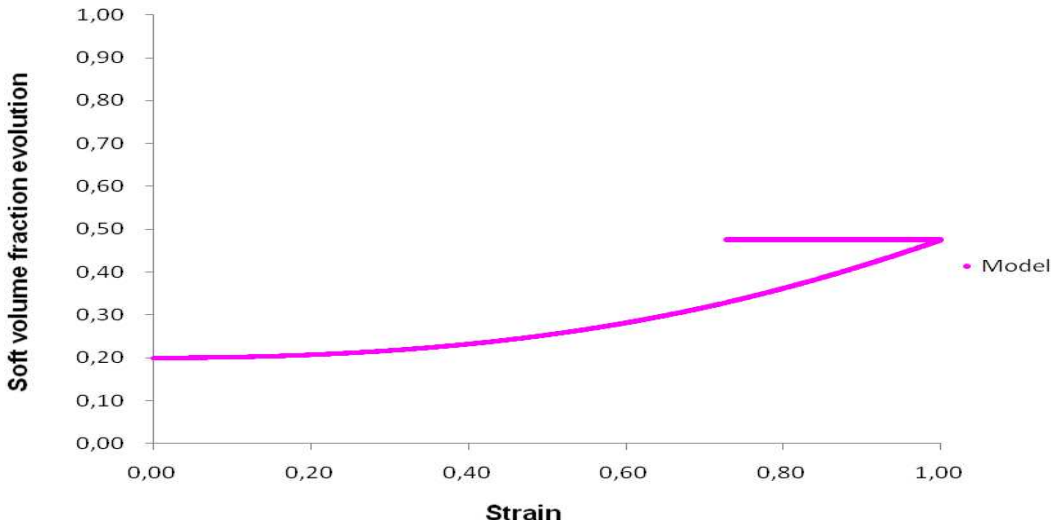

Figure IV.11.b: TPU(A) soft volume fraction evolution for the constitutive model during stretching. $\left(\varphi_s = 1 - \varphi_h\right)$.

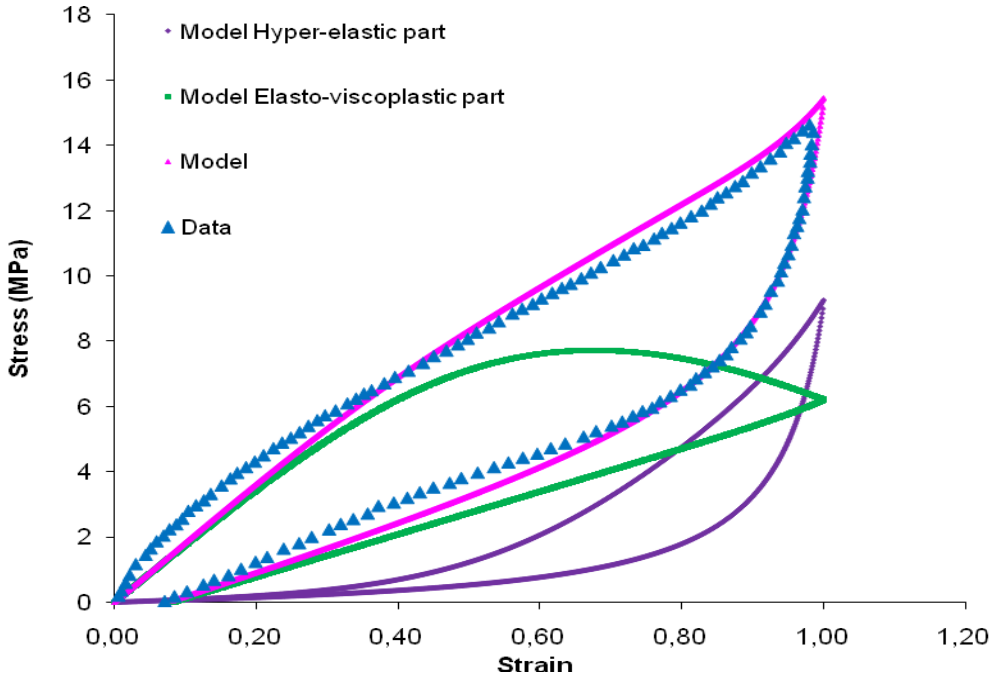

Figure IV.12.a: TPU(B).uniaxial compression response at strain rate $\dot{\varepsilon} = 1s^{-1}$ with cooperative shear rate evolution.

$E_2 = 0.25MPa,\ J_{m2} = 22.25,\ E_1 = 1MPa,\ J_{m1} = 16,\ \mu = 0.499999,\ \dot{\gamma}_0^p = 1.94.10^{29}\, s^{-1},$
$\Delta H = 90.10^3\, J,\ E_{Young} = 22MPa,\ S_0 = 30MPa,\ S_{ss} = 1MPa,\ h = 0MPa,\ \varphi_h^0 = 0.80,$
$\beta = 0.1MPa^{-1},\ b_{hs} = 1.10^{-3}\, s^{-1},\ T = 298.15K,\ n = 8,\ V = 1.10^{-29}\, m^3$

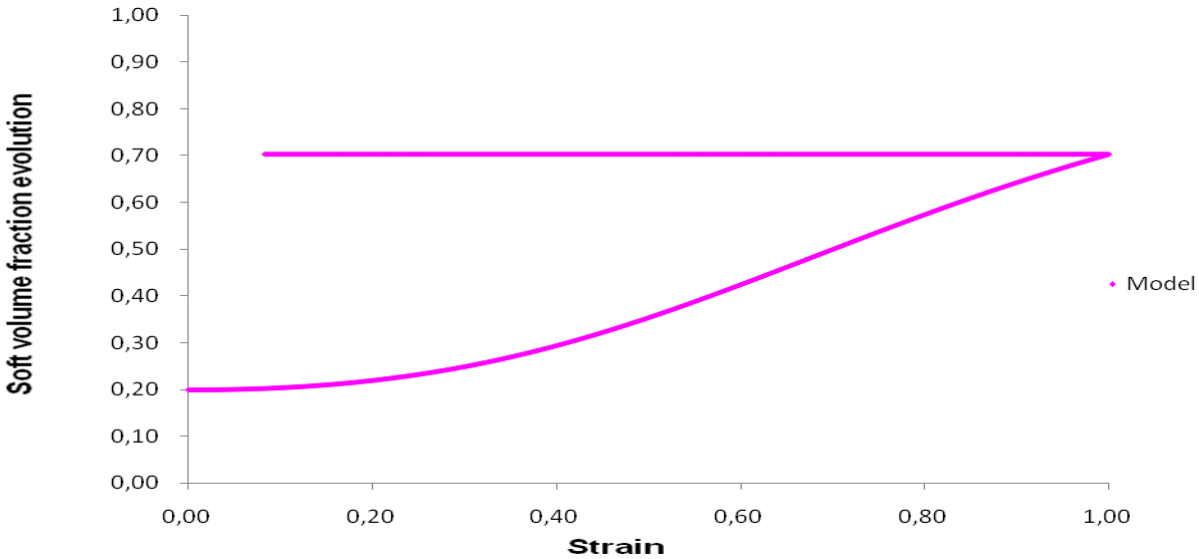

Figure IV.12.b: TPU(B) soft volume evolution for the constitutive model during stretching. $\left(\varphi_s = 1 - \varphi_h\right)$.

IV.4. CONCLUSION

This constitutive model for thermoplastic elastomers is based on microstructure evolution and mechanical behavior. The thermoplastic polyurethane chains are consisted by hard segments which are separated in spinodal mechanism and form nanoscale hard domains acting like fillers. It also implies nanoscale soft domains. However, the hard segments are considered to be deformable and present an elastic-viscoplastic behavior. Hence, the rheological model proposed in **Figure IV.6** takes into account the two domains behavior during mechanical deformation. The numerical results are obtained for two viscoplastic shear strain rate evolutions which are Argon and cooperative model. These numerical results are also in good agreement with different thermoplastic polyurethane experimental data. The model also shows its ability to predict thermoplastic polyurethanes whose behavior is more elastomeric or more thermoplastic.

V. CONCLUSIONS AND FUTURE WORK

In this thesis, we propose three constitutive models for elastomeric materials under stress. The first is on stress-birefringence-stretch and the two others are on biphasic elastomers stress-strain behavior in relationship with microstructure evolution. Here, the biphasic elastomers are elastomers filled by carbon black or thermoplastic elastomers with hard segments and soft segments. The second constitutive model has the ability to predict only filled elastomers behavior because it does not include plasticity. However, the third is extended to include the plasticity behavior which happens in thermoplastic elastomers.

For stress-birefringence-stretch, the constitutive model is based on the well know Gaussian model for birefringence-stretch response and Gent model for stress-stretch response. The stress-optical law obtained from these models predicts results in good agreement with experimental data from the literature for the PDMS and natural rubber. Our stress-optical law is also compared with the non-Gaussian birefringence-stretch coupled with the eight-chain model in order to show the difference between the two approaches. The results are controlled by the two parameters in these approaches, N and $\mu = nk_BT$ for the non-Gaussian model and J_m and E for the Gent model. These parameters also show some similarities in their representation for the two models. Similar Stress-strain response as well as to the closeness of the birefringence results from both models confirm the relation between models parameters.

The constitutive model for filled elastomers includes microstructure evolution and mechanical behavior. The microstructure of the filled elastomers is considered to be composed of soft and hard domains where the hard domain includes fillers and occlude matrix. Under stress, the

filler aggregates break down leads to the transformation of the immobilized occlude matrix to deformable matrix (hard-to-soft domain transformation). Hence, the soft domain volume fraction increases during loading and the hard one decreases. This is what induces the softening or Mullins effect. The soft domain evolution controls the relationship between microstructure and mechanical behavior because the applied stress generates deformation only in filled elastomers soft part (the fillers are assumed non-deformable). The model takes into account the carbon black volume fraction and its type via the DBP_{Abs}. It also gives explanation to stiffness increase by soft-to-hard domains transformation which happens slowly after experimental test, this is not the case in other models based on damage theories. For isotropic softening, the approach can also be easily implemented in computational codes. The constitutive model gives good agreement with experimental data from the literature and also proves its ability to be applicable on different states of deformation.

The third constitutive model for thermoplastic elastomers is also based on microstructure evolution and mechanical behavior. The thermoplastic polyurethane chains are consisted by hard segments and soft segments. The hard segments phase separate in spinodal mechanism and form nanoscale hard domains acting like fillers However, the hard segments are considered to be deformable and present an elastic-viscoplastic behavior. Hence, unlike the case of filled elastomers, here the stress generates deformation in the two domains of the materials. Hence, the rheological model proposes taking into account the two domains behavior during mechanical deformation. The numerical results are obtained for two viscoplastic shear strain rate evolutions which are Argon and cooperative model. These numerical results are also in good agreement with different thermoplastic polyurethane experimental data. Then, our model shows is ability to predict thermoplastic polyurethanes whose behavior is more elastomeric or more thermoplastic.

For future work, Mullins effect model should be compared to experimental data for different states of deformation. The TPU model should be applied for high strain rate tests, cyclic loading-unloading tests or on other type of thermoplastic elastomers tests.

REFERENCES

Aneja A, Wilkes G. L., 2003.

A systematic series of 'model' PTMO based segmented polyurethanes reinvestigated using atomic force microscopy, Polymer, **44**, 7221-7228, 2003.

Argon A.S., 1973a

Physical basis of distortional and dilatational plastic flow in glassy polymers, Journal of Macromolecular Science-Physics, **B8**, 573-596, 1973.

Argon A.S., 1973b

A theory for the low-temperature plastic deformation of glassy polymers, Philosophical Magazine, **28**, 839-865, 1973.

Arruda E.M., Boyce M.C., 1993.

A three–dimensional constitutive model for the large stretch behavior of rubber elastic materials, J. Mech. Phys. Solids, **41**, 389–412, 1993.

Arruda E.M., Boyce M.C., 1991.

Anisotropy and localization of plastic deformation, p.483, Elsevier/New York, 1991.

Arruda E.M., Przybylo P.A., 1995.

An investigation into the three–dimensional stress–birefringence–strain relation in elastomers, Polymer. Eng. Sci., **35**, 395–402, 1995.

Biderman V.L., 1958.

Problems of Analysing Rubbery-like Materials, Raschety na Prochnost'. Mashgiz, Moscow, 3, 1958.

Blanchard A.F., Parkinson D., 1952.

Breakage of carbon–rubber networks by applied stress, Ind. Eng. Chem., **44**, 799–812, 1952.

Bergstrom J., Boyce M.C., 1999.

Mechanical behavior of particle filled elastomers, Rubber Chem. Tech., **72**, 633–656, 1999.

Bouasse H., Carrière Z., 1903.

Courbes de traction du caoutchouc vulcanisé, Ann. Fac. Sciences de Toulouse, **5**, 257-283, 1903.

Boyce M. C., 1996.

Direct comparison of the Gent and Arruda–Boyce constitutive models of rubber elasticity, Rubber Chem. Technol., **69**, 781–785, 1996.

Boyce M. C., Kear K., Socrate S., Shaw K., 2001.

Deformation of thermoplastic vulcanizates, J. Mech. Phys. Solids, **49**, 1073-1098, 2001.

Boyce M. C., Parks D. M., Argon A. S., 1988.

Large inelastic deformation of glassy polymers Part I Rate-dependent constitutive model, Mech. Mater., **7**, 15-33, 1988.

Buckley C. P., Prisacariu C., Martin C., 2010.

Elasticity and inelasticity of thermoplastic polyurethane elastomers: Sensitivity to chemical and physical structure, Polymer, **51**, 3213-3224, 2010.

Budiansky B., 1965.

On the elastic modulus of some heterogeneous materials, J. Mech. Phys. Solids, **13**, 223–227, 1965.

Bueche F., 1960.

Molecular basis for the Mullins effect, J. Appl. Polym. Sci, **4**, 107–114, 1960.

Bueche F., 1961.

Mullins effect and rubber–filler interaction, J. Appl. Polym. Sci, **5**, 271–281, 1961.

Chagnon G., Verron E., Marckmann G., Gornet L., 2006.

Development of new constitutive equations for the Mullins effect in rubber using the network alteration theory, Int. J. Solids Struct., **43**, 6817-6831, 2006.

Chagnon G., Marckmann G., Verron E., 2004.

A comparison of the Hart–Smith model with Arruda–Boyce and Gent formulations for rubber elasticity, Rubber Chem. Technol., **77**, 724–735, 2004.

Chen-Tsai C. H Y., Thomas E. L., Macknight W. J., Schneider N. S., 1986.

Structure and morphology of segmented polyurethanes. 3. Electron microscopy and small angle X-ray scattering studies of amorphous random segmented polyurethanes, Polymer, **27**, 659-666, 1986.

Cohen A., 1991.

A Padé approximant to the inverse Langevin function, Rheologica Acta **30**, 270–273, 1991.

Einstein A., 1906.

Ann. Physik. (Leipzig) **19**, 289, 1906.

Einstein A., 1911.

Ann. Physik. (Leipzig) **34**, 591, 1911.

Elwell M. J., Mortimer S., Ryan A. J., 1994.

A synchrotron SAXS study of structure development kinetics during the reactive processing of flexible polyurethane foam, Macromolecules, **27**, 5428-5439,1991.

Erman B., Flory P.J., 1983a.

Theory of strain birefringence of amorphous polymer networks, Macromolecules, **16**, 1601–1606, 1983.

Erman B., Flory P.J., 1983b.

Experimental results relating stress and birefringence to strain in poly(dimethylsiloxane) networks. Comparisons with theory, Macromolecules, **16**, 1607–1613, 1983.

Erman B., Flory P.J., 1982.

Relationships between stress, strain and molecular constitution of polymer networks. Comparison of theory with experiments, Macromolecules, **15**, 806–811, 1982.

Flory P.J., B. Erman B., 1982.

Theory of elasticity of polymer networks.3, Macromolecules, **15**, 800–806, 1982.

Flory P.J., Rehner Jr.J., 1943.

Statistical mechanics of cross-linked polymer networks I. Rubberlike elasticity, J. Chem. Phys, **11**, 512-520, 1943.

Garrett J. T., Siedlecki C. A., Runt J., 2001.

Microdomain morphology of poly(urethane urea) multiblock copolymers, Macromolecules, **34**, 7066-7070, 2001.

Gent A.N., 1996.

A new constitutive relation for rubber, Rubber Chem. Technol., **69**, 59–61, 1996.

Gent A. N., Thomas A. G., 1958.

Forms of the stored (strain) energy function for vulcanized rubber. J. Polym. Sci., **28**, 625–637, 1958.

Goindjee S., Simo J., 1991.

A micro-mechanically continuum damage model for carbon black filled rubbers incorporating Mullins's effect, J. Mech. Phys. Solids, **39**, 87-112, 1991.

Goindjee S., Simo J., 1992.

Transition from micro-mechanics to computationally efficient phenomenology: carbon black filled rubbers incorporating Mullins' effect, J. Mech. Phys. Solids, **40**, 213-233, 1992.

Guth E., 1945.

Theory of filler reinforcement, J. Appl. Phys. **16**, 20–25, 1945.

Guth, E., Mark, H. 1934.

Internal molecular statistics, especially in chain molecules. I. Mh.Chem. **65**, 93, 1934.

Guth E., Gold O., 1938.

On the hydrodynamical theory of the viscosity of suspensions, Phys. Rev. **53**, 322, 1938.

Haines D.W., Wilson W.D., 1979.

Strain-energy density function for rubber like materials, J. Mech. Phys of Solids, **27**,345-360, 1979.

Halary J.L.,Lauprêtre F., Monnerie L. 2008.

Mécanique des matériaux polymères, Collection Echelles, Belin, (2008)

Harwood J.A.C., Mullins L., Payne A.R., 1965.

Stress softening in natural rubber vulcanizates, Part II, J. Appl. Polym. Sci. **9**, 3011–3021, 1965.

Harwood J.A.C., Payne A.R., 1966.

Stress softeningin natural rubber vulcanizates Part III., J. Appl. Polym. Sci., **10**, 315, 1966.

Hart-Smith L. J., 1966.

Elasticity parameters for finite deformations of rubber-like materials, J. App. Phys., **17**, 608–625, 1966.

Hashin, Z., Shtrikman, S., 1963.

A variational approach to the elastic behaviour of multiphase materials: J. Mech. Phys. Solids, **11**, 127-140, 1963.

Heinrich G., Klüppel M., Vilgis T. A., 2002.

Reinforcement of elastomers, Current Opinion in Solid State and Materials Science, **6**, 195-203, 2002.

Hill R., 1951.

On the state of stress in a plastic-rigid body at the yield point, Philosophical Magazine, **42**, 868-875, 1951.

Horgan C.O., Saccomandi G., 2002.

A molecular–statistical basis for Gent constitutive model of rubber elasticity, J. Elasticity, **68**, 167–176, 2002.

Isihara A., Hashitsume N., Tatibana M., 1951.

Statistical theory of rubber-like elasticity.IV. (Two-dimensional stretching) J. Chem. Phys., **19**, 1508, 1951.

James A.G., Green A., 1975.

Strain energy functions of rubber. II. Characterization of filled vulcanizates, J. Appl. Polym. Sci.**19**, 2319-2330, 1975.

James H.M., Guth E., 1943.

Theory of the elastic properties of rubber, J. Chem. Phys., **11**, 455–481, 1943.

Johnson M. A., Beatty M.F., 1993.

A constitutive equation for the Mullins effect in stress controlled uniaxial extension experiments, Continuum Mech. Thermodyn., **5**, 301-318, 1993.

Klüppel and Schramm, 2000

A generalized tube model of rubber elasticity and stress softening of filler reinforced elastomer systems, Macromolecular Theory and Simulations, 2000, **9**, 742-754

Kuhn W., 1936.

Kolloid-Z, **76**, 258, 1936.

Kuhn W., 1934.

Kolloid-Z, **68**, 2, 1934.

Kuhn W., Grün F., 1942.

Beziehungen zwischen elastischen Konstanten und Dehnungsdoppelbrechung hochelastischer Stoffe. Kolloid Z. **101**, 248–271, 1942.

Makradi A., Ahzi S., Gregory R. V., 2000.

Modeling of the mechanical response and evolution of optical anisotropy in deformed polyaniline, Poly. Eng. Sc, **40**, 1716–1723, 2000.

Marckmann G., Verron E., Gornet L., Chagnon G., Charrier P., Fort P., 2002.

A theory of network alteration for the Mullins effect, J. Mech. Phys. Solids, **50**, 2011-2028, 2002.

Maxwell J.C., 1873.

Treatise on electricity and magnetism, Clarendon Press, Oxford, 1873.

Medalia A.I., 1970.

Morphology of aggregates VI. Effective volume of aggregates of carbon black from electron microscopy; application to vehicle absorption and to die swell of filled rubber, Journal of Colloid and Interface Science, **32**, 115–131, 1970.

Meinecke E. A., Taftaf M.I., 1988.

Effect of Carbon Black on the Mechanical Properties of Elastomers, Rubber Chem. Technol., **61**, 534, 1988.

Miehe C., Keck J., 2000.

Superimposed finite elastic-viscoelastic-plastoelastic response with damage in filled rubbery polymers. Experiments, modeling and algorithmic implementation, J. Mech. Phys. Solids, **48**, 323-365, 2000.

Mooney M.J., 1940.

A theory of large elastic deformation, J. Appl. Phys., **11**, 582–592, 1940.

Mori T., Tanaka K., 1973.

Average stress in matrix and average elastic energy of materials with misfitting inclusions, Acta Metall, **21**, 571–574, 1973.

Morozov I., Lauke B., Heinrich G., 2010.

A new structural model of carbon black framework in rubbers, Computational Materials Science, **47**, Issue 3, 817–825, 2010.

Mullins L., 1947.

Effect of stretching on the properties of rubber, J. Rubber Res., **16**, 275–289, 1947.

Mullins L., 1948.

Effect of stretching on the properties of rubber, Rubber Chem. Technol., **21**, 281-300, 1948.

Mullins L., 1950.

Thixotropic behavior of carbon black in rubber, Rubber Chem. Technol., **23**,733, 1950.

Mullins L., 1969.

Softening of rubber by deformation, Rubber Chem. Technol., **42**, 339-362, 1969.

Mullins L., Tobin N.R., 1957.

Theoretical model for the elastic behavior of filler–reinforced vulcanized rubber, Rubber Chem. Technol., **30**, 555–571, 1957.

Mullins L., Tobin N.R., 1965.

Stress softening in natural rubber vulcanizates, Part I. J. Appl. Sci., **9**, 2993–3010, 1965.

Ogden R.W., 1972.

Large deformation isotropic elasticity–On the correlation of theory and experiment for incompressible rubbelike solids, Proc. R. Soc. London. A **326**, 565–584, 1972.

Oshmyan V. G., Patlazhan S. A., Remond Y., 2006.

Principles of structural-mechanical modeling of polymers and composites, Polymer Science, Series A, **48** (9), 1004–1013, 2006.

O'Sickey M. J., Lawrey B. D., Wilkes G. L., 2002.

Structure-property relationships of poly(urethane urea)s with ultra-low monol content poly(propylene glycol) soft segments: I. Influence of soft segment molecular weight and hard segment content, Journal of Applied Polymer Science, **84**, 229-243, 2002.

Petrovic Z., Ferguson J., 1991

Polyurethane elastomers, Progress in Polymer Science, **16**, 695-836, 1991.

Ponte Castañeda P., 1989.

The overall constitutive behaviour of nolinear elastic composite, Proc. R. Soc. London, Ser. A **A422**, 147-171, 1989.

Qi H. J., Boyce M. C., 2005.

Stress-strain behavior of thermoplastic polyurethanes, Mechanics of Materials, **37**, 817–839, 2005.

Qi H.J., Boyce M.C., 2004.

Constitutive model for stretch–induced softening of the stress–stretch behavior of elastomeric materials, J. Mech. Phys. Solids, **52**, 2187–2205, 2004.

Rayleigh L., 1892.

On the influence of obstacles arranged in a rectangular order upon the properties of medium. Philosophical Magazine **34**,481-502, 1892.

Reuss A., 1929.

Berechnung der fliessgrenze von mischkristallen auf grund der plastizitatsbedingung fur einkristalle, Zeitung Angewandte Mathematik und Mechanik **9**, 49-58, 1929.

Richeton J., Ahzi S., Vecchio K.S., Jiang F.C., Makradi A., 2007.

Modeling and validation of the large deformation inelastic response of amorphous polymers over a wide range of temperatures and strain rates, International Journal of Solids and Structures, **44**, 7938–7954, 2007.

Richeton J., Ahzi S., Daridon L., Rémond Y., 2005.

A formulation of the cooperative model for the yield stress of amorphous polymers for a wide range of strain rates and temperatures, Polymer, **46**, 6035-6043, 2005.

Rivlin R. S., 1948.

Large elastic deformation of isotropic materials-IV. Further developments of the general theory, Phil. Trans. Roy. Soc. London. A. **241**, 379, 1948.

Rivlin R.S., Saunders D.W., 1951.

Large elastic deformations of isotropic materials-VII. Experiments on the deformation of rubber, Phil. Trans. Roy. Soc. A243, 251, 1951.

Roychoudhury A., De P.P., 1993.

Reinforcement of epoxidized natural rubber by carbon black: Effect of surface oxidation of carbon black particles, J. Applied Polymer Science, **50**,181–186, 1993.

Russo R., Thomas E., 1983.

Phase separation in linear and cross-linked polyurethanes, Journal of Macromolecular Science-Physics, **B22**, 553-575, 1983.

Ryan A. J., Macosko C. W., Bras W., 1992.

Order-disorder transition in a block copolyurethane, Macromolecules, **25**, 6277-6283, 1992.

Ryan A. J., Stanford J. L., Still R. H., 1991.

Thermal, mechanical and fracture properties of reaction injection-moulded poly(urethane-urea)s, Polymer, **32**, 1426-1439, 1991.

Schneider N. S., Desper C. R., Illinger J. L., King A. O., Barr D., 1975.

Structural studies of crystalline MDI-based polyurethanes, J. Macromol. Sci. Phys, B11, 527-552, 1975.

Simha R., 1940.

The influence of Brownian movement of the viscosity of solutions, J. Phys. Chem., **44**, 25–34, 1940.

Simo J., 1987.

On a fully three-dimensional finite-strain viscoelastic damage model: formulation and computational aspects, Comput. Methods Appl. Mech. Eng., **60**, 153-173, 1987.

Smallwood H.M., 1944.

Limiting law of the reinforcement of rubber, J. Appl. Phys., **15**, 758–766, 1944.

Stepto R.F.T., 1986.

In advances in Elastomers and Rubber Elasticity, J. Lal and J.E. Mark, eds., Plenum Press, New York, 1986.

Suquet P., 1997.

Effective properties of nonlinear composites, In: Suquet P., (Ed.), Continuum Micromechanics, Springer–Wien, New York, 1997.

Treloar L.G.R., 1975.

The physics of rubber elasticity. Oxford University Press, Oxford 1975.

Treloar. L. R. G., 1954.

The photoelastic properties of short-chain molecular networks, Trans. Faraday Soc., **50**, 881, 1954.

Treloar L.G.R., 1947a.

The photo–elastic properties of rubber. Part I: Theory of the optical properties of strained rubber, Trans. Faraday. Soc., **43**, 277–284, 1947.

Treloar L.G.R., 1947b.

The photo–elastic properties of rubber. Part II: Double refraction and crystallization in stretched vulcanized rubber, Trans. Faraday Soc., **43**, 284–293, 1947.

Treloar L. R. G., 1946.

The statistical length of long chain molecules, Trans. Faraday Soc., 42:77–83, 1946.

Treloar L.G.R., Riding G., 1979.

A non–Gaussian theory for rubber in biaxial strain. I. Mechanical properties, Proc. Roy. Soc. London. A **369**, 261–280, 1979.

Tschoegl N. W., 1971.

Constitutive equation for elastomers, J. Polymer Sci., A1, **9**, 1959, 1971.

Ullman, 1986.

Advances in Elastomers and Rubber Elasticity, J. Lal and J.E. Mark, eds., Plenum Press, New York (1986).

Valanis K.C., Landel R.F., 1967.

The strain–energy function of a hyperelastic material in terms of the extension ratios, J. Appl. Phys., **38**, 2997-3002, 1967.

Vand V., 1948.

Viscosity of solutions and suspensions. I. Theory, J. Phys. Colloid Chem., **52**, 277-299, 1948.

Vilgis T. A., Heinrich G., Klüppel, 2009.

Reinforcement of polymer nano-composites, Cambridge University Press, Cambridge, U.K. (2009).

Von Lockette P.R., Arruda E.M., 1999.

A network description of the non–Gaussian stress–optic and Raman scattering responses of elastomer networks, Acta Mechanica, **134**, 81–107, 1999.

Voigt W., 1889.

Uber die Beziehung zwischen den beiden Elastizitatskonstanten isotroper Korper, Wiedemann Annalen, **38**, 573, 1889.

Wang M.C., Guth E.J., 1952.

Satistical theory of networks of non-Gaussian flexible chains. J. Chem. Phys. **20**, 1144-1157, 1952.

Wu P.D., Van Der Giessen E., 1995.

On network descriptions of mechanical and optical properties of rubbers, Philosophical Magazine A, **71**, 1191–1206, 1995.

Wu P.D., Van der Giessen E., 1993.

On improved network models for rubber elasticity and their applications to orientation hardening in glassy polymers, J. Mech. Phys. Solids, 41, 427-456, 1993.

Wu P.D., Van der Giessen E., 1992.

On improved 3-D non-Gaussian network models for rubber elasticity, Mechanics Research Communications, 19, Issue 5, 427-433, 1992.

Yeoh O. H., 1990.

Characterization of elastic properties of carbon-black-filled rubber vulcanizates. Rubber. Chem. Technol., 63(5):792–805, 1990.

Yi J., Boyce M. C., Lee G. F., Balizer E., 2006.

Large deformation rate-dependent stress-strain behaviour of polyurea and polyurethanes, Polymer, **47**, 319-329, 2006.